8-22-2013

Topological and Isotopic Equivalence with Applications to Visualization

Ji Li
University of Connecticut, hamlet.j@gmail.com

Topological and Isotopic Equivalence with Applications to Visualization

Ji Li, Ph.D.
University of Connecticut, 2013

ABSTRACT

There is contemporary interest to preserve appropriate topological characteristics during geometric modeling. Here we focus upon topological equivalence (by homeomorphism) and isotopic equivalence (by ambient isotopy). Homeomorphism is an equivalence relation used for static images, while ambient isotopy requires a homeomorphism at each value of the time parameter, which is particularly applicable for time varying models. We provide sufficient conditions that guarantee these equivalences for geometric approximations of Bézier curves, as one of the fundamental computational representations. We also present further generalization beyond any curve approximation algorithm to establish broad criteria for a sequence of piecewise linear curves to become ambient isotopic to a given smooth curve. The criteria rely upon distance and total curvature, with upper bounds provided. Apart from the major theorems and algorithms, we investigate topological differences based on knot visualization and numerical analysis.

Topological and Isotopic Equivalence with Applications to Visualization

Ji Li

M.Sc. Mathematics, Ohio University, Athens, Ohio, 2008

A Dissertation
Submitted in Partial Fulfillment of the
Requirements for the Degree of
Doctor of Philosophy
at the
University of Connecticut

2013

APPROVAL PAGE

Doctor of Philosophy Dissertation

Topological and Isotopic Equivalence with Applications to Visualization

Presented by
Ji Li, M.Sc. Math.

Major Advisor _____
Thomas J. Peters

Associate Advisor _____
Maria Gordina

Associate Advisor _____
William Abikoff

University of Connecticut
2013

ACKNOWLEDGEMENTS

I am heartily thankful to my supervisor, Professor Thomas J. Peters for his vision, patience, support and dedication to me throughout the past few years. I would like to express my appreciation to my advisory committee members, Professor Maria Gordina and Professor William Abikoff for their kindness, insights and support. I am also grateful to the University of Connecticut Mathematics Department for their commitment to my education. I want to offer my gratitude to my professor at Ohio University, A. V. Arhangel'skii, who stimulated my interest in topology and guided me to the research in this area. I am indebted to my parents for their unflagging love and trust.

TABLE OF CONTENTS

NOTATION

- $\mathbb{R}^n$: Euclidean n-space, Section 0.1
- PL: Piecewise linear, Section 0.1
- $\mathbf{B}$: Bézier curve, Section 1.1
- $\mathbf{P}$: Control polygon, Definition 1.1.1
- $\mathcal{B}$: Simple, regular, composite, C^1 Bézier curve, Section 1.1
- $\mathcal{P}$: Control polygon of $\mathcal{B}$, Definition 1.1.1
- P^k: Sub-control polygon, Section 1.1
- $\{P_0, P_1, \cdots, P_n\}$: Control points, Definition 1.1.1
- $\mathcal{L}$: An arbitrary PL curve, Definition 1.1.3
- $\eta(\cdot, \cdot)$: Exterior angle between two vectors, Definition 1.1.3
- $\kappa(t)$: Curvature, Definition 1.1.4
- $C(t)$: Parametrized curve, Definition 1.1.4
- $T_\kappa(\cdot)$: Total curvature, Definition 1.1.4 and 1.1.5
- $||\cdot||$: Euclidean norm, Section 2.1
- $S_r(c)$: Pipe surface of radius r for curve c, Definition 2.2.5
- $D_r(t)$, Normal disc of radius r at t, Section 2.2.2
- Γ_k, Pipe section, Section 2.2.2
- Π: Plane in $\mathbb{R}^3$, Section 2.2.2
- H_1 and H_2: Half-spaces separated by Π, Section 2.2.2
- int$(\cdot)$ and $\partial(\cdot)$: Interior and boundary of a set, Section 3.2
- $\mathcal{C}$: A compact, regular, C^2, simple parametric space curve, Section 6.2
- $\{C_i\}_1^\infty$: Sequence of piecewise C^2 curves, Section 6.2
- $\{L_i\}_1^\infty$: Sequence of PL curves, Section 6.2

Introduction

This research lies properly within the broad scope of applied and computational topology and depends upon a novel integration of the 'pure mathematics' of topology with the 'applied mathematics' of scientific computing. It blends geometric topology, general topology, low-dimensional topology, and knot theory with computer graphics, visualization and simulations.

The fundamental topics include: (1) homeomorphism and ambient isotopy between smooth and piecewise linear structures; (2) applications and algorithmic efficiency; and (3) isotopic convergence criteria for curve approximation.

Admittedly, if one obtains ambient isotopy, there is no need to consider homeomorphism. But we study homeomorphism first, not only because it is a necessary condition of ambient isotopy, but also because it typically has lower computational cost than ambient isotopy, and it may be sufficient for some purposes.

0.1 Motivation

The theorems and algorithms presented were motivated by applications for dynamic visualization in high performance computing (HPC) environments, such as modeling biological molecules, for visualization synchronized to simulations of

the writhing of these molecules [36, 37, 38]. These models can be knotted and vary over time, so that ambient isotopy is a natural mathematical formalization during the visualization and simulations.

Bézier curves [11] are computational representations widely used for geometric modeling. A previous result [7] was restricted to Bézier curves of low degree (less than 4), while large molecules may have in excess of ten thousand atoms, leading to models by much higher degree Bézier curves. It is natural to consider topology for arbitrary degree Bézier curves, as we do in this dissertation.

A Bézier curve is determined by a PL curve, called a control polygon [11]. We will use the notation $\mathbf{B}$ for a Bézier curve and $\mathbf{P}$ for the control polygon. We consider the equivalence relations between $\mathbf{B}$ and $\mathbf{P}$. A homeomorphism maps a set X to a set Y, where X and Y can be considered as static images at distinct times. An ambient isotopy has further constraints upon how X can deform continuously into Y over a time interval. Specifically the permitted deformation over time requires a homeomorphism of the initial object at each instant of time. This continued equivalence over time is particularly important for visualization and simulations aided by computer graphics.

Simple closed curves form 1-dimensional knots [3], i.e. 1-dimensional manifolds embedded in $\mathbb{R}^3$ which are homeomorphic to a circle. Homeomorphism does not distinguish knot types. The finer notion of ambient isotopy is used for equivalent embeddings of knots. An ambient isotopy between two subsets X and Y is a map from the whole space to itself, while an isotopy is a map from X to Y. Ambient

isotopies send the complement of X homeomorphically to the complement of Y, but isotopies may fail to preserve the topological type of the complement [52].

However, there may be substantial topological differences between a Bezier curve $\mathbf{B}$ and its control polygon $\mathbf{P}$. First, $\mathbf{B}$ and $\mathbf{P}$ need not be homeomorphic [24]. Secondly, they are not necessarily ambient isotopic [23]. An approximation algorithm associated with Bézier curves, called subdivision [11], takes the associated control polygon and generates PL approximations that converge exponentially to a given Bézier curve in Hausdorff distance [11]. This naturally raises the question of whether this subdivision process will produce topologically reliable approximations. We present new theory and algorithms regarding this question.

Moving beyond splines, the Isotopic Convergence Theorem presented in Chapter 6 deals with a much broader class of curves, piecewise C^2 curves. It is motivated by questions about topological integrity of geometric models, but it is a general and purely theoretical result, dealing with the fundamental equivalence relation in knot theory.

0.2 Current Literature and Comparisons

The nascent field of computational topology holds great promise for science and engineering [35], while Bézier curves are popular because of the simplicity of their construction and their capability of approximating complex curves [11].

Convergence of control polygon $\mathbf{P}$ to a Bézier curve $\mathbf{B}$ under subdivision in terms of Hausdorff distance is well known [20, 21]. For a space curve, it is known how

to construct a "nice" tubular neighborhood, that is, a neighborhood bounded by a non-self-intersecting pipe surface [8]. Based on the convergence in distance, one may obtain control polygons $\mathbf{P}$ that fit in the tubular neighborhood. However, this condition is far from being sufficient for isotopy.

In Chapter 2, we present the convergence in terms of angular measure, which to the best of our knowledge, has not been previously established. We determine ambient isotopy, as well as the related local and global knot structures, based on the Angular Convergence. The proof uses a previous result showing that the discrete derivatives of $\mathbf{P}$ converge to the derivatives of $\mathbf{B}$ [6].

A previous proof [13] of existence of homeomorphism between $\mathbf{B}$ and $\mathbf{P}$ relied upon the hodograph[1] and did not provide the number of subdivision iterations. In Chapter 2, we provide a constructive geometric proof that sufficiently many subdivisions will produce $\mathbf{P}$ homeomorphic to a given $\mathbf{B}$, and the sufficient number of subdivision iterations is also established.

The previously mentioned result [7] of ambient isotopy was restricted to Bézier curves of low degree (less than 4), where a crucial unknotting condition was trivial. Deriving a comparable unknotting condition for higher degree Bézier curves is established here by significantly different arguments. In Chapter 2, we show the existence of ambient isotopy for Bézier curves of arbitrary degree. The existence result has a "convex containment" requirement, which may be computationally expensive for geometric modeling of large (petabyte) data sets, although it is

[1]The derivative of a Bézier curve is also expressed as a Bézier curve, known as the *hodograph* [11].

expected to be sufficient for many other purposes. In Chapter 3, we remove the "convex containment" requirement by explicitly constructing ambient isotopies, by relying upon much more sophisticated mathematical arguments. In Chapter 4, we give closed-form formulas to compute the sufficient number of subdivision iteration to achieve homeomorphism and ambient isotopy respectively.

Moreover, an existing result [15] has given a sufficient condition for the preservation of topological integrity when the vertices of polyhedron are perturbed. Our approaches presented in Chapters 2 3 and 4 provide more general result of sufficient condition for perturbations that do not change topological integrity.

In Chapter 5, we show two novel computational topology counterexamples. These counterexamples rely upon numerical analysis from conjectures prompted by visualization of knots. In particular, it was shown that there exists an unknotted $\mathbf{B}$ with a knotted $\mathbf{P}$ [23]. A specific dual example has also been shown [31] of a knotted $\mathbf{B}$ with an unknotted $\mathbf{P}$. However, the previous methodology [31] was a visual construction without formal proof and is not easily generalized. We find another example by using a knot visualization tool, *Knot_Spline_Vis* [30]. We also give topological and numerical proofs for a broad class of related examples.

Previous work [29] in knot visualization provides a rich set of data for equilateral PL knots, where each edge is of the same length. We used this data for an empirical study of dozens of cases using *Knot_Spline_Vis* [30], where all examples examined yielded simple curves $\mathbf{B}$ for these simple equilateral $\mathbf{P}$. This raised the question of whether the presence of equilateral edges in $\mathbf{P}$ might be a sufficient

additional hypothesis to ensure homeomorphic equivalence with $\mathbf{B}$, as the previously cited examples [24] did not have equilateral control polygons. By writing a numerical algorithm, we construct a counterexample to refute this conjecture.

The work in Chapter 6 extends to a much broader class of curves, piecewise C^2 parametric curves, and provides convergence criteria to guarantee ambient isotopy. Milnor [1] provided a proof restricted to inscribed curves. Milnor's result [1] was recently generalized to finite total curvature knots [46]. The application to graphs was also established recently [47]. We consider curves either inscribed or not.

There exist previous results [45, 46] that establish ambient isotopy between two curves using different criteria than proven here. Those earlier results use upper bounds on distance and angles between corresponding points on the two curves. There also exist several algorithms to obtain isotopic approximations on specific classes of geometric entities. The papers [48, 49] present an algorithm for implicit curves and surfaces based on interval arithmetic. The paper [50] gives an algorithm for 2D algebraic curves that relies upon the previous results [48, 49] and parameterizability, which is extended to implicit surfaces [51].

Here, after we show that isotopic approximations of Bézier curves can be obtained through subdivision algorithms, we present further generalization beyond any specific curve approximation algorithm to establish broad criteria for a sequence of piecewise linear curves to become ambient isotopic to a given smooth curve. The criteria rely upon distance and total curvature, with the upper bounds provided.

Chapter 1

Bézier Curves and Equivalence Relations

In this chapter, we introduce Bézier curves [11], and discuss topological differences and equivalence relations: topological equivalence and isotopic equivalence.

1.1 Preliminaries

Definition 1.1.1. The parameterized **Bézier curve** of degree n with control points $P_m \in \mathbb{R}^3$ is defined by

$$\sum_{m=0}^{n} \binom{n}{m} t^m (1-t)^{n-m} P_m, t \in [0,1]$$

The PL curve given by the points $\{P_0, P_1, \ldots, P_n\}$ is called its **control polygon**. When $P_0 = P_n$, the control polygon is *closed*; Otherwise when $P_0 \neq P_n$, it is *open*.

The Bézier curve of Definition 1.1.1 is typically called a **single segment Bézier curve**, while a **composite Bézier curve** is created by joining two or more single segment Bézier curves at their common end points.

Let $\mathcal{B}$ denote a simple, regular, C^1, composite Bézier curve in $\mathbb{R}^3$.

Definition 1.1.2. [4] A differentiable curve is said to be **regular** if its derivative never vanishes.

In order to avoid annoying technical considerations and to simplify the exposition, we shall restrict the class of Bézier curves considered to be regular.

Subdivision algorithms are fundamental for Bézier curves [11] and a brief overview is given here. Figure 1.1.1 shows the first step of the de Casteljau subdivision with an input value of $\frac{1}{2}$ on a single Bézier curve. For ease of exposition, the de Casteljau algorithm with this value of $\frac{1}{2}$ is assumed, but other fractional values can be used with appropriate minor modifications to the analyses presented. The initial PL approximation $\mathbf{P}$ is used as input to generate local PL approximations, P^1 and P^2. Their union, $P^1 \cup P^2$, is then a PL approximation whose Hausdorff distance is closer to the curve than that of $\mathbf{P}$.

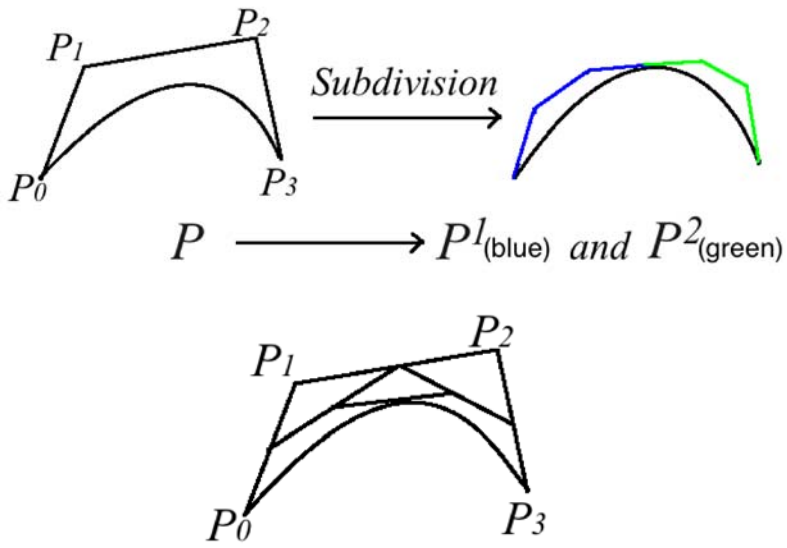

Figure 1.1.1: A subdivision with parameter $\frac{1}{2}$

A summary is that subdivision, with parameter $\frac{1}{2}$, proceeds by selecting the midpoint of each segment of $\mathbf{P}$ and these midpoints are connected to create new

segments. Recursive creation and connection of midpoints continue until a final midpoint is selected. The union of the segments from the last step then forms a PL approximation. Termination is guaranteed as $\mathbf{P}$ has only finitely many segments.

After i iterations, the subdivision process generates 2^i PL sub-curves, each being a control polygon for part of the original curve [11]. Each PL sub-curve will be referred to as a **sub-control polygon**[2], denoted by P^k for $k = 1, 2, 3, \ldots, 2^i$. Each P^k has n points and their union $(\bigcup_k P^k)$ forms a new PL curve that converges in distance to approximate the original Bézier curve. The Bézier curve defined by $(\bigcup_k P^k)$ is exactly the same Bézier curve defined by the original $\mathbf{P}$ [17]. The advantage is that $(\bigcup_k P^k)$ is a much better approximation to the Bézier curve than was the original $\mathbf{P}$.

Exterior angles were defined [1] in the context of closed PL curves, but are adapted here for both closed and open PL curves. Exterior angles unify the concept of total curvature for curves that are PL or differentiable.

Definition 1.1.3. The *exterior angle* between two oriented line segments $\overrightarrow{P_{m-1}P_m}$ and $\overrightarrow{P_mP_{m+1}}$, is the angle between the extension of $\overrightarrow{P_{m-1}P_m}$ and $\overrightarrow{P_mP_{m+1}}$, as shown in Figure 1.1.2(a). Let the measure of the exterior angle to be α_m satisfying:

$$0 \leq \alpha_m \leq \pi.$$

[2]While an original control polygon can be either closed or open, the sub-control polygons of a simple $\mathbf{B}$ must be open.

Let $\overrightarrow{v}_1 = P_m - P_{m-1}$ and $\overrightarrow{v}_2 = P_{m+1} - P_m$, then the exterior angle is the angle between $\overrightarrow{v}_1$ and $\overrightarrow{v}_2$, as shown in Figure 1.1.2(b).

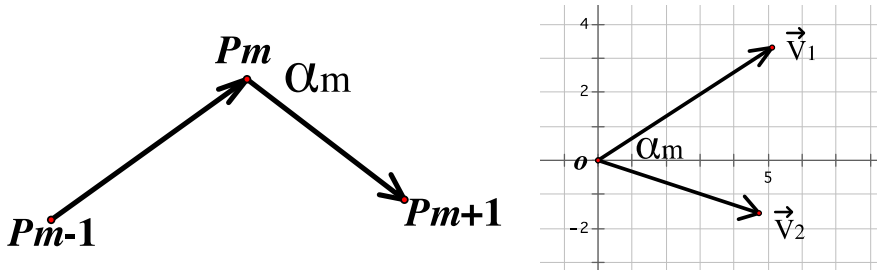

(a) Orientated lines (b) Vectors

Figure 1.1.2: An exterior angle

Definition 1.1.4. The **curvature** of a C^2 curve $C(t)$ parametrized on $[a, b]$ is given by

$$\kappa(t) = \frac{||C'(t) \times C''(t)||}{||C'(t)||^3}, \quad t \in [a, b]. \tag{1.1.1}$$

Parametrize the curve by arc length s on $[0, \ell]$. Then its **total curvature** $T_\kappa(C)$ [4] is the integral: $\int_0^\ell |C''(s)|\, ds$.

Definition 1.1.5. [1] The **total curvature** $T_\kappa(\mathcal{L})$ of a PL curve $\mathcal{L}$ is the sum of all exterior angles of $\mathcal{L}$.

Fenchel's Theorem [4] presented below is applicable both to PL curves and to differentiable curves.

Theorem 1.1.6. [4, Fenchel's Theorem] The total curvature of any closed curve is at least 2π, with equality holding if and only if the curve is convex.

Suppose that a PL curve $\mathcal{L}$ has vertices $\{v_0, v_1, \cdots, v_n\}$. Denote the uniform parametrization [6] of $\mathcal{L}$ over $[0,1]$ by $l(\mathcal{L})_{[0,1]}$. That is:

$$l(\mathcal{L})_{[0,1]}(\frac{j}{n}) = v_j \ for \ j = 0, 1, \cdots, n$$

and $l(\mathcal{L})_{[0,1]}$ interpolates linearly over all values in $[0,1]$.

Definition 1.1.7. Discrete derivatives [6] are first defined at the parameters $t_j = \frac{j}{n}$, where $l(\mathcal{L})_{[0,1]}(t_j) = v_j$ for $j = 0, 1, \cdots, n-1$. Let

$$v'_j = l'(\mathcal{L})_{[0,1]}(t_j) = \frac{v_{j+1} - v_j}{t_{j+1} - t_j}.$$

Denote $\mathcal{L}' = (v'_0, v'_1, \cdots, v'_{n-1})$. Then define the discrete derivative for $l(\mathcal{L})_{[0,1]}$ as:

$$l'(\mathcal{L})_{[0,1]} = l(\mathcal{L}')_{[0,1]}.$$

The definition given here is specialized to $\mathbb{R}^n$ as sufficient for the applications intended, but further generalizations are available [52].

Definition 1.1.8. Two subspaces of $\mathbb{R}^n$, denoted by X and Y, are said to be **ambient isotopic** if there exists a continuous function $H : \mathbb{R}^n \times [0,1] \to \mathbb{R}^n$ satisfying:

(1) $H(\cdot, 0)$ is the identity,

(2) $H(X, 1) = Y$, and

(3) $\forall t \in [0,1]$, $H(\cdot, t) : \mathbb{R}^n \to \mathbb{R}^n$ is a homeomorphism.

The map H is an **ambient isotopy** between X and Y.

Definition 1.1.9. [20] Let X and Y be two non-empty subsets of a metric space (M, d), with the Hausdorff distance defined by

$$\max\{\sup_{x\in X}\inf_{y\in Y} d(x,y), \sup_{y\in Y}\inf_{x\in X} d(x,y)\}.$$

1.2 Topological Differences

A control polygon $\mathbf{P}$ determines a Bézier curve $\mathbf{B}$ as indicated in Definition 1.1.1. The control polygon is also used as the initial approximation of $\mathbf{B}$.

However, there may be substantial topological differences between $\mathbf{P}$ and $\mathbf{B}$. Figure 1.2.1(a) displays a self-intersecting $\mathbf{P}$ and a simple $\mathbf{B}$, so that they are not homeomorphic. Figure 1.2.1(b) shows a knotted $\mathbf{P}$ and an unknotted $\mathbf{B}$ [23], which means they are not ambient isotopic. In Chapter 5, we shall show more examples with such topological differences. Other examples are available [24].

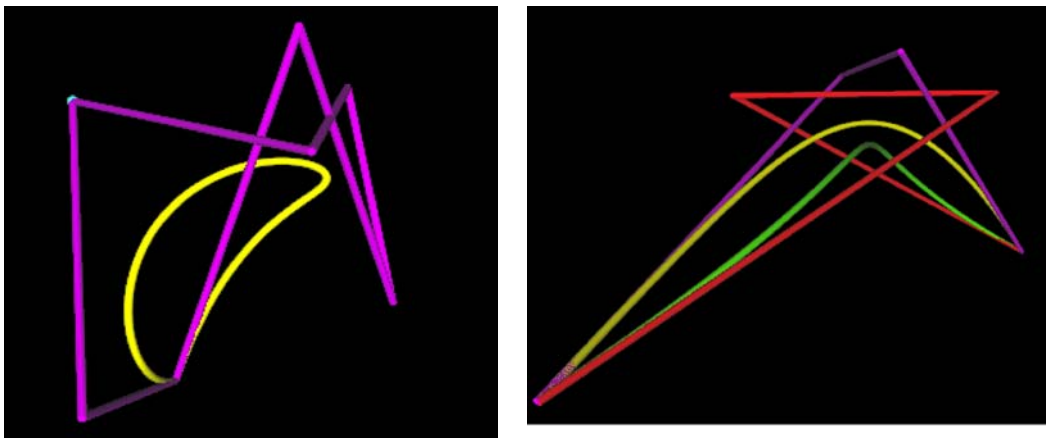

(a) Intersecting $\mathbf{P}$, Simple $\mathbf{B}$ (b) Knotted $\mathbf{P}$, Unkotted $\mathbf{B}$

Figure 1.2.1: Topological differences

1.3 Introduction to Equivalence Relations

As mentioned before, homeomorphism and ambient isotopy are desirable equivalence relations to be preserved during approximation. Since homeomorphism is not strong enough to guarantee equivalent embedding, i.e. the same knot type, we further consider the stronger equivalence relation, ambient isotopy. The 3D graphs in Figure 1.3 show the concept that a good approximation is considered to be not only homeomorphic but also ambient isotopic.

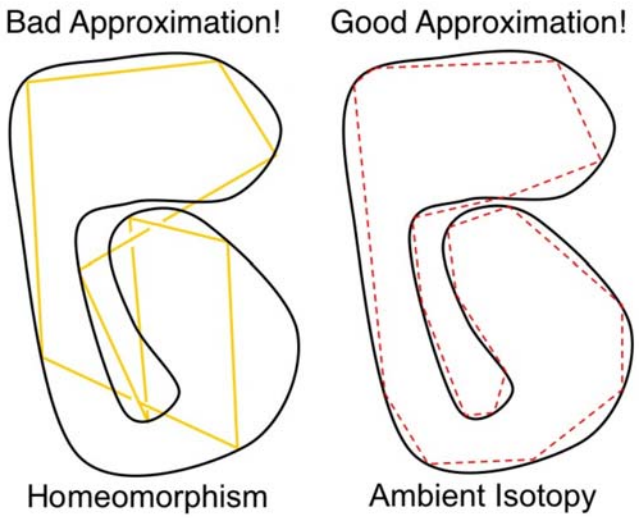

Figure 1.3.1: Homeomorphism and Ambient Isotopy

For Bézier curves, although topological differences between $\mathbf{B}$ and $\mathbf{P}$ may exist, it is natural to expect that sufficiently many subdivisions will generate new control polygons that are ambient isotopic to $\mathbf{B}$. For instance, after one subdivision, the self-intersection in the control polygon in Figure 1.2.1(a) disappears and the two curves become homeomorphic (Figure 1.3.2(a)). One subdivision generates an unknotted control polygon for the curve in Figure 1.2.1(b), and hence ambient

isotopy is obtained, as shown in Figure 1.3.2(b) [23].

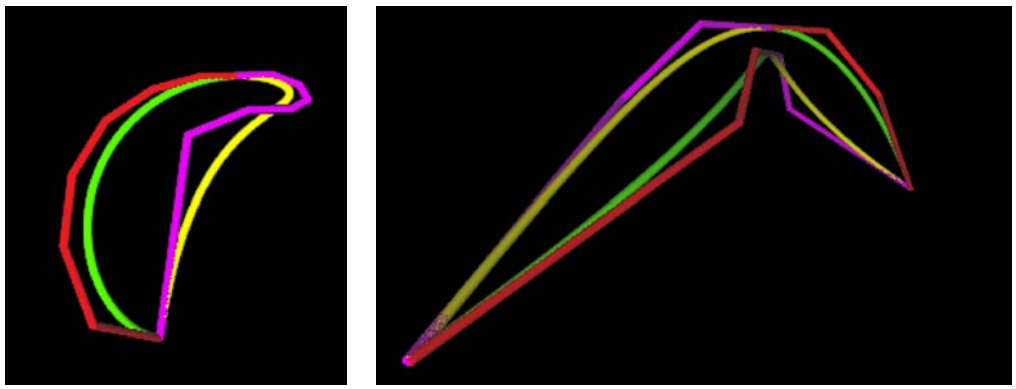

(a) Simple control polygon (b) Unknotted control polygon

Figure 1.3.2: Ambient isotopic curves

In the following chapters, we shall develop theorems and algorithms to prove and obtain homeomorphism and ambient isotopy under subdivision.

Chapter 2

Existence of Equivalence Relations

The existence of equivalence relations is based on Angular Convergence, as presented below, and convergence in terms of distance, which is well known [21].

2.1 Angular Convergence under Subdivision

We consider an arbitrary sub-control polygon P^k for the following analysis, where, for simplicity of notation, we repress the superscript and denote this arbitrary curve simply as P. Let $t_0, t_1, \cdots, t_n$ be the parameters of the control points of P. And let $l(P,i)$ be the uniform parameterization [6] of P on $[\frac{k-1}{2^i}, \frac{k}{2^i}]$ for $k \in \{1, 2, 3, \ldots, 2^i\}$. That is

$$l(P,i) = l(P)_{[\frac{k-1}{2^i}, \frac{k}{2^i}]} \quad and \quad l(P,i)(t_m) = P_m \; for \;\; m = \{0, 1, \cdots, n\},$$

where $t_m = \frac{k-1}{2^i} + \frac{m}{n2^i}$. Note from the domain of $l(P,i)$ that

$$t_n - t_0 = \frac{1}{2^i} \;\; and \;\; t_m - t_{m-1} = \frac{1}{n2^i} \;\; for \;\; m = \{1, \cdots, n\}. \tag{2.1.1}$$

Furthermore, let

$$\alpha_1, \alpha_2, \cdots, \alpha_{n-1}$$

be the corresponding measures of exterior angles of P (Definition 1.1.3). Consider the Euclidian distance between the discrete derivatives of the two consecutive segments, that is $||l'(P,i)(t_m) - l'(P,i)(t_{m-1})||$. We will show a rate of $O(\frac{1}{2^i})$ for the convergence

$$||l'(P,i)(t_m) - l'(P,i)(t_{m-1})|| \to 0 \text{ as } i \to \infty.$$

This will imply that $\cos(\alpha_m) \to 1$ with the same rate and that $\alpha_m \to 0$ at a rate of $O(\sqrt{\frac{1}{2^i}})$.

Lemma 2.1.1. For a C^1, composite Bézier curve $\mathcal{B}$, the value

$$||l'(P,i)(t_m) - l'(P,i)(t_{m-1})||$$

converges uniformly for all m and k to zero at a rate of $O(\frac{1}{2^i})$.

Proof. Note

$$\begin{aligned} &||l'(P,i)(t_m) - l'(P,i)(t_{m-1})|| \qquad (2.1.2)\\ &\leq ||l'(P,i)(t_m) - \mathcal{B}'(t_m)|| + ||\mathcal{B}'(t_m) - \mathcal{B}'(t_{m-1})|| + ||\mathcal{B}'(t_{m-1}) - l'(P,i)(t_{m-1})||. \end{aligned}$$

The first and the third terms converge to 0 at a rate of $O(\frac{1}{2^i})$, because the discrete derivative converges to the derivative of the original curve with this rate [6].

For ease of exposition in this proof, we will initially assume that $\mathcal{B}$ is C^2, but then complete the proof by extending this special case to the more general assumption that $\mathcal{B}$ is C^1. If $\mathcal{B}$ is C^2, then for the second term, the Mean Value Theorem on

$(0,1)$ provides that there exists some $s \in (t_m, t_{m-1})$ such that

$$||\mathcal{B}'(t_m) - \mathcal{B}'(t_{m-1})|| = ||\mathcal{B}''(s)|| \cdot |t_m - t_{m-1}|. \tag{2.1.3}$$

Let $\gamma = \sup_{[0,1]} ||\mathcal{B}''(t)||$, which exists because of the continuity of $\mathcal{B}''$ over $[0,1]$. It follows that

$$||\mathcal{B}'(t_m) - \mathcal{B}'(t_{m-1})|| \leq \sup_{[0,1]} ||\mathcal{B}''(t)|| \cdot |t_m - t_{m-1}| = \frac{\gamma}{n2^i}. \tag{2.1.4}$$

The second equality holds by Equation (2.1.1). So $||l'(P,i)(t_m) - l'(P,i)(t_{m-1})||$ converges to zero at a rate of $O(\frac{1}{2^i})$.

The curve $\mathcal{B}$ is only assumed to be C^1 at its junction points, so it is natural to question the validity of Equation 2.1.3 and Inequality 2.1.4 in the C^1. Note that Equations 2.1.3 is over the *open* interval $(0,1)$, so no difficulties occur relative to the junction points. However, more subtle consideration is necessary for Inequality 2.1.4. Each segment of the composite Bézier curve is a polynomial defined over $[0,1]$, so the definition of γ as a supremum over $[0,1]$ still exists. □

Theorem 2.1.2 (Angular Convergence)**.** For $\mathcal{B}$, the exterior angles of the PL curves generated by subdivision converge uniformly to 0 at a rate of $O(\sqrt{\frac{1}{2^i}})$.

Proof. Since $\mathcal{B}(t)$ is assumed to be regular and C^1, the non-zero minimum of $||\mathcal{B}'(t)||$ over the compact set [0,1] is obtained. For brevity, the notations of $u_i = l'(P,i)(t_m)$, $v_i = l'(P,i)(t_{m-1})$ and $\alpha = \alpha_m$ (measure of an arbitrary exterior angle) are introduced. The convergence of u_i to $\mathcal{B}'(t_m)$ [6] implies that $||u_i||$ has

a positive lower bound for i sufficiently large, denoted by λ.

Lemma 2.1.1 gives that $||u_i - v_i|| \to 0$ as $i \to \infty$ at a rate of $O(\frac{1}{2^i})$. This implies: $||u_i|| - ||v_i|| \to 0$ as $i \to \infty$ at a rate of $O(\frac{1}{2^i})$.

Consider the following where "$\cdot$" indicates the dot product between vectors, whereas "$*$" is for scalar multiplication:

$$\begin{aligned}
1 - \cos(\alpha) &= 1 - \frac{u_i \cdot v_i}{||u_i|| * ||v_i||} \\
&= \frac{||u_i|| * ||v_i|| - v_i \cdot v_i + v_i \cdot v_i - u_i \cdot v_i}{||u_i|| * ||v_i||} \\
&\leq \frac{||u_i|| - ||v_i||}{||u_i||} + \frac{||v_i - u_i||}{||u_i||} \\
&\leq \frac{||u_i|| - ||v_i||}{\lambda} + \frac{||v_i - u_i||}{\lambda} \\
&\leq \frac{2||v_i - u_i||}{\lambda}. \qquad (2.1.5)
\end{aligned}$$

It follows from Lemma 2.1.1 that the right hand side of Inequality 2.1.5 converges to 0 at a rate of $O(\frac{1}{2^i})$. Consequently, $1 - \cos(\alpha) \to 0$ with the same rate. It follows from the continuity of arccos that α converges to 0 as $i \to \infty$.

Taking the power series expansion of cos we get

$$\begin{aligned}
1 - \cos(\alpha) &\geq \alpha^2(\frac{1}{2} - |\frac{\alpha^2}{4!} - \frac{\alpha^4}{6!} + \cdots|) \\
&= \alpha^2(\frac{1}{2} - \alpha^2|\frac{1}{4!} - \frac{\alpha^2}{6!} + \cdots|) \qquad (2.1.6)
\end{aligned}$$

Note that for $1 > \alpha$,

$$e = 1 + 1 + \frac{1}{2!} + \frac{1}{3!} + \frac{1}{4!} + \cdots > |\frac{1}{4!} - \frac{\alpha^2}{6!} + \cdots|. \qquad (2.1.7)$$

Combining Inequality 2.1.6 and 2.1.7 we have,

$$1 - \cos(\alpha) > \alpha^2(\frac{1}{2} - \alpha^2 e).$$

For any $0 < \tau < \frac{1}{2}$, sufficiently many subdivisions will guarantee that α is small enough such that $1 > \alpha$ and $\tau > \alpha^2 e$. Thus

$$1 - \cos(\alpha) > \alpha^2(\frac{1}{2} - \alpha^2 e) > \alpha^2(\frac{1}{2} - \tau) > 0.$$

Then convergence of the left hand side implies that α converges to 0 at a rate of $O(\sqrt{\frac{1}{2^i}})$. □

2.2 Existence of Topological Equivalence

To establish a homeomorphism under subdivision, we first establish a local homeomorphism between a sub-control polygon and the corresponding sub-curve of $\mathcal{B}$, and then establish a global homeomorphism between the control polygon and $\mathcal{B}$.

2.2.1 Local Arguments for Topological Equivalence

It is likely that the following lemma is well known, possibly as a 'folk theorem', but we are unable to find a reference in the literature, so its proof is provided here, for the sake of completeness.

We use the notation $(P_0, P_1, \cdots, P_n)$ as [6] to denote a PL curve determined by a set of points $\{P_0, P_1, \cdots, P_n\}$.

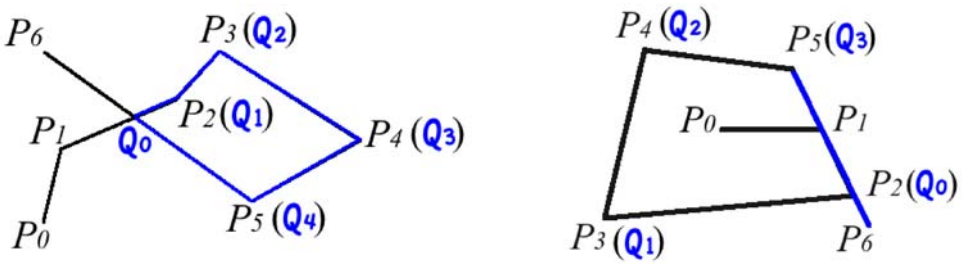

(a) Non-collinear case (b) Collinear case

Figure 2.2.1: Self-intersecting PL curves in 3D

Lemma 2.2.1 (Non-self-intersection criteria[3])**.** Let $P = (P_0, P_1, \cdots, P_n)$ be an open PL curve in $\mathbb{R}^3$. If $T_\kappa(P) = \sum_{j=1}^{n-1} \alpha_j < \pi$, then P is simple.

Proof. Assume to the contrary that P is self-intersecting. Then there must exist at least one closed loop. (The assumption $\sum_{j=1}^{n-1} \alpha_j < \pi$ precludes the case of two consecutive edges being collinear.) Arbitrarily choose such a loop. There are two cases to consider: a single point intersection as in Figure 2.2.1(a) and the collinear case as in Figure 2.2.1(b).

Case 1 (Non-collinear): Label the single intersection as Q_0 to be the first vertex of the loop (Figure 2.2.1(a)). Label the other vertices clockwise and denote this loop by

$$\bar{Q} = (Q_0, Q_1, \cdots, Q_{n'}, Q_0),$$

for an appropriately chosen value of n'. Denote the measure of the corresponding exterior angle of $\bar{Q}$ at $Q_0, Q_1, \cdots, Q_{n'}$ by $\beta_0, \beta_1, \cdots, \beta_{n'}$. Note that $\beta_0 \leq \pi$ (Definition 1.1.3). Note also that each exterior angle β_l (for $l = 1, 2, \cdots, n'$) of $\bar{Q}$

[3]A similar lemma has appeared [13] without proof.

(except the initial angle β_0) is an exterior angle of P. So

$$\sum_{l=0}^{n'} \beta_l = \beta_0 + \sum_{l=1}^{n'} \beta_l \leq \pi + \sum_{j=1}^{n-1} \alpha_j.$$

Since $\sum_{j=1}^{n-1} \alpha_j < \pi$ we get

$$\sum_{l=0}^{n'} \beta_l \leq \pi + \sum_{j=1}^{n-1} \alpha_j < 2\pi.$$

But for the closed loop $\bar{Q}$, $\sum_{l=0}^{n'} \beta_l \geq 2\pi$ (Theorem 1.1.6), which is a contradiction.

Case 2 (Collinear): The loop is formed by a subset of the vertices $\{P_0, P_1, \cdots, P_n\}$ in this case (Figure 2.2.1(b)). Pick an arbitrary point from the subset and relabel it as Q_0. Label the other vertices clockwise as $\bar{Q} = (Q_0, Q_1, \cdots, Q_{n'}, Q_0)$ and the exterior angles as $\beta_0, \beta_1, \cdots, \beta_{n'}$. Note for this case that, each exterior angle β_l of $\bar{Q}$ is an exterior angle of P. So

$$\sum_{l=0}^{n'} \beta_l \leq \sum_{j=1}^{n-1} \alpha_j.$$

And $\sum_{j=1}^{n-1} \alpha_j < \pi$, so $\sum_{l=0}^{n'} \beta_l < \pi$. But for the closed loop $\bar{Q}$, $\sum_{l=0}^{n'} \beta_l \geq 2\pi$ (Theorem 1.1.6), which is a contradiction. □

Theorem 2.2.2 (Simple sub-control polygons)**.** For $\mathcal{B}$, there exists a sufficiently large value of i, such that after i-many subdivisions, each of the sub-control polygons generated as P^k for $k = 1, 2, \ldots, 2^i$ will be simple.

Proof. For each P^k, the measures of the exterior angles of P^k converge uniformly

to zero as i increases (Theorem 2.1.2). Each open P^k has n edges. Denote the n exterior angles of each P^k by α_j^k, for $j = 1, 2, \ldots, n$ and for $k = 1, 2, \ldots, 2^i$. Then there exists i sufficiently large such that

$$\sum_{j=1}^{n-1} \alpha_j^k < \pi,$$

for each $k = 1, 2, \ldots, 2^i$. Use of Lemma 2.2.1 completes the proof.

□

2.2.2 Global Arguments for Topological Equivalence

This global homeomorphism will be proven by reliance upon non-self-intersecting pipe surfaces, which are defined in this section. Denote two generated sub-control polygons of $\mathcal{B}$ as

$$P = (P_0, P_1, \cdots, P_n) \text{ and } Q = (Q_0, Q_1, \cdots, Q_n).$$

Definition 2.2.3. The sub-control polygons P and Q are said to be *consecutive* if the last vertex P_n of P is the first vertex Q_0 of Q, that is, $P_n = Q_0$.

Remark 2.2.4. For $\mathcal{B}$, the C^1 assumption ensures that the line segments $\overrightarrow{P_{n-1}P_n}$ and $\overrightarrow{Q_0Q_1}$ are collinear, so the exterior angle at the common point $P_n = Q_0$ is either 0 or π. But the regularity assumption ensures that the exterior angle can not be π, so that the exterior angle at the common point is 0.

The global criteria will have distinct sub-control polygons being pairwise disjoint, unless they are consecutive, in which case the common end point is the only

point of intersection. We will establish these conditions with the use of *non-self-intersecting pipe surfaces.*

Pipe surfaces have been studied since the 19th century [33]. Contemporary authors [8] provided sufficient conditions for a pipe surface to be non-self-intersecting when its spine curve is regular and C^1, as is true for $\mathcal{B}$. These authors perform a thorough analysis and description of the end conditions of open curves. The junction points of $\mathcal{B}$ are merely a special case of that analysis.

Definition 2.2.5. The **pipe surface** of radius r of a parameterized curve $\mathbf{c}(t)$, where $t \in [0, 1]$ is given by

$$\mathbf{p}(t, \theta) = \mathbf{c}(t) + r[cos(\theta)\ \mathbf{n}(t) + sin(\theta)\ \mathbf{b}(t)],$$

where $\theta \in [0, 2\pi]$ and $\mathbf{n}(t)$ and $\mathbf{b}(t)$ are the normal and bi-normal vectors, as given by the Frenet-Serret trihedron. The curve $\mathbf{c}$ is called a spine curve.

Remark 2.2.6. The paper [8] provides the computation of the radius r only for rational spline curves. However, the method of computing r is similar for other compact, regular, C^2, simple curves, that is, setting

$$r < \min\{\frac{1}{\kappa_{max}}, \frac{d_{min}}{2}, r_{end}\},$$

where κ_{max} is the maximum of the curvatures, d_{min} is the minimum separation distance [8], and r_{end} is the maximal radius around the endpoints that does not yield self-intersections.

A previous ambient isotopy result [7] was restricted to cubic Bézier curves, but this will now be extended to arbitrary degree, through use of Lemma 2.2.7. Lemma 2.2.7 extends a similar result that was previously restricted to cubic Bézier curves [9].

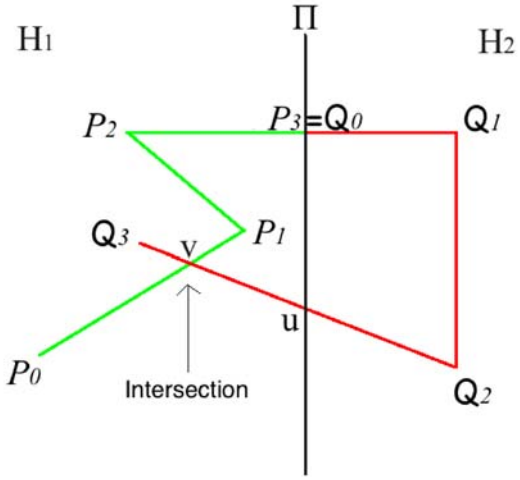

Figure 2.2.2: Intersecting consecutive sub-control polygons

Lemma 2.2.7. Let Π be the plane normal to a sub-control polygon at its initial vertex. If the total curvature of the sub-control polygon is less than $\frac{\pi}{2}$, then the initial vertex is the only point where the plane intersects the sub-control polygon.

Proof. Denote the sub-control polygon as $Q = (Q_0, Q_1, \ldots, Q_n)$, where Figure 2.2.2 shows an orthogonal projection of this 3D geometry. Assume to the contrary that $\Pi \cap Q$ contains a point u where $u \neq Q_0$. Assume without loss of generality that a segment $Q_{m-1}Q_m$ intersects Π at the point u for some $m \in \{2, 3, \cdots, n\}$. This would produce a closed PL curve denoted as

$$\bar{J} = (Q_0, Q_1, \cdots, Q_{m-1}, u, Q_0).$$

Denote the exterior angle of $\bar{J}$ at Q_0 as θ and note that $\theta = \frac{\pi}{2}$. Denote the exterior angle of $\bar{J}$ at u as γ. Then $\gamma \leq \pi$ (Definition 1.1.3). Denote the other exterior angles of $\bar{J}$ as $\beta_i, i = 1, \ldots, m-1$. By Theorem 1.1.6 we have

$$\theta + \sum_{i=1}^{m-1} \beta_i + \gamma \geq 2\pi.$$

Thus

$$\sum_{i=1}^{m-1} \beta_i \geq 2\pi - \theta - \gamma \geq \frac{\pi}{2}.$$

These β_i are also exterior angles of Q resulting in lower bound for the total curvature of Q as given by $T_\kappa(Q) \geq \sum_i^{m-1} \beta_i \geq \pi/2$, which is a contradiction to $T_\kappa(Q) < \frac{\pi}{2}$. □

Lemma 2.2.8. Recall that $\mathcal{B}$ denotes a simple, regular, C^1, composite Bézier curve in $\mathbb{R}^3$. Let w be a point of $\mathcal{B}$ where $\mathcal{B}$ is subdivided and let Π be the plane normal to $\mathcal{B}$ at w. Then there exists a subdivision of $\mathcal{B}$ such that the sub-control polygon ending at w and the sub-control polygon beginning at w intersect Π only at the single point w.

Proof. The plane Π separates $\mathbb{R}^3$ into two disjoint open half-spaces, denoted as H_1 and H_2, such that $\mathbb{R}^3 = H_1 \cup \Pi \cup H_2$ and $H_1 \cap H_2 = \emptyset$. By Remark 2.2.4, the exterior angle at $\{w\}$ is 0.

Perform sufficient many subdivisions so that the control polygon ending at w, denoted by P , and the control polygon beginning at w, denoted by Q, each have

total curvature less than $\frac{\pi}{2}$ by Theorem 2.1.2. Therefore, by Lemma 2.2.7 the only point where P or Q intersect Π is at w. $\square$

For $\mathcal{B}$ and i subdivisions with P^k for $k = 1, \ldots, 2^i$ resulting sub-control polygons, let $S_{\mathcal{B}}(r)$ be a non-self-intersecting pipe surface with spine $\mathcal{B}$ and with radius r so that $S_r(\mathcal{B})$ is non-self-intersecting. For each $k = 1, \ldots, 2^i$, denote

- the parameter of the initial point of P^k by t_0^k, and that of the terminal point by t_n^k
- the normal disc of radius r centered at $\mathcal{B}(t)$ as $D_r(t)$,
- the union $\bigcup_{t \in [t_0^k, t_n^k]} D_r(t)$ by Γ_k, called a **non-self-intersecting pipe section**.

Theorem 2.2.9 (A simple homeomorphic control polygon)**.** Sufficient subdivisions will yield a simple control polygon that is homeomorphic to $\mathcal{B}$.

Proof. By Theorem 2.1.2, we can take ι_1 subdivisions so that $T_\kappa(P^k) < \pi/2$, for each sub-control polygon P^k. By Lemma 2.2.1, this choice of ι_1 guarantees that each P^k is simple. By the convergence in Hausdorff distance under subdivision [21], we can take ι_2 subdivisions such that the control polygon generated by ι_2 subdivision fits inside the non-self-intersecting pipe surface $S_r(\mathcal{B})$. Choose $\iota = \max\{\iota_1, \iota_2\}$. By Lemma 2.2.8, this choice of ι ensures that each P^k fits inside the corresponding Γ_k. This plus the fact that P^k is simple shows that the control polygon, $\bigcup_{k=1}^{2^i} P^k$, is simple, which implies the homeomorphism. $\square$

2.3 Existence of Isotopic Equivalence

The previous section shows that each sub-control polygon will be simple. As previously noted, each sub-control polygon is an open PL curve by the subdivision process. If we connect the end points of a sub-control polygon, then we obtain a closed curve. The isotopy arguments given here depend upon each such closed curve being unknotted.

2.3.1 Locally Unkotted

Consider the sub-control polygons, P^k, defined in Theorem 2.2.2. For i subdivisions and each $k = 1, \ldots, 2^i$, denote by $\overline{P_k}$ the closed PL curve formed by adding the line segment to connect the first and last points of P^k. The following well-known theorem will be invoked.

Theorem 2.3.1 (Fary-Milnor Theorem [4])**.** The total curvature of a knotted simple closed curve is greater than 4π

Theorem 2.3.2 (Local PL Unknots)**.** For $\mathcal{B}$, there exists a sufficiently large value of i, such that after i-many subdivisions, each closed $\overline{P^k}$ for $k = 1, 2, 3, \ldots, 2^i$ will be unknotted.

Proof. Note that adding the line segment to form the closed PL curve adds exactly two exterior angles, each of which has measure no greater than π. Then by the Angular Convergence (Theorem 2.1.2), there are sufficiently many subdivisions so that the total curvature $T_\kappa(P^k)$ can be small enough. In particular, by subdivision we can obtain $T_\kappa(P^k) \leq 2\pi$. Consequently, $T_\kappa(\overline{P^k})$ is less than or equal to 4π and

then each $\overline{P^k}$ is unknotted by the Fary-Milnor Theorem (Theorem 2.3.1). □

2.3.2 Global Arguments for Isotopy

The proof of the existence of the isotopy (Theorem 2.3.5) depends upon Angular Convergence (Theorem 2.1.2) as well as the technique "2D push" [25].

To prove Lemma 2.3.4 below, we use the following spherical triangle inequality.

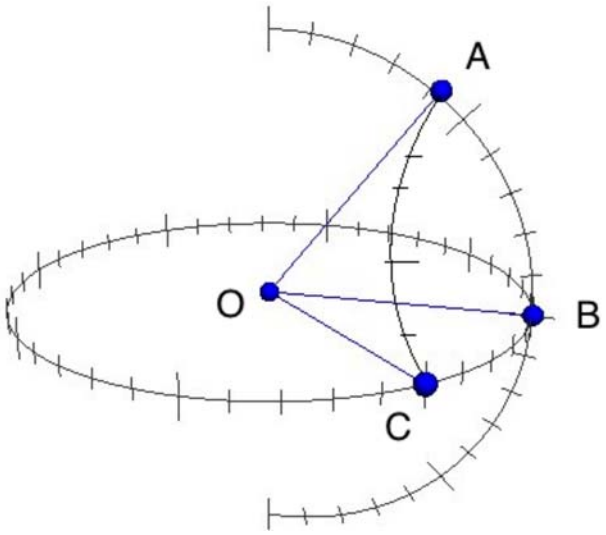

Figure 2.3.1: Spherical triangle $\triangle ABC$

Spherical triangle inequality: Consider Figure 2.3.1, and the three angles $\angle AOB$, $\angle BOC$, and $\angle AOC$, formed by three unit vectors $\overrightarrow{OA}$, $\overrightarrow{OB}$, and $\overrightarrow{OC}$. (Note the common end point O. When we consider angles between vectors that do not share such a common end point, we move the vectors to form a common end point.) Denote the arc length of the curve from A to B as $a(\widehat{AB})$, and similarly for that from B to C as $a(\widehat{BC})$ and that from A to C as $a(\widehat{AC})$. The triangle inequality, $a(\widehat{AB}) \leq a(\widehat{BC}) + a(\widehat{AC})$, of the spherical triangle $\triangle ABC$

provides that

$$\angle AOB \leq \angle BOC + \angle AOC. \tag{2.3.1}$$

It is sufficient here to consider a specialized type of push, designated, below, as a *median push*.

Definition 2.3.3. Assume that triangle $\triangle ABC$ has non-collinear vertices A, B and C. Push a vertex, say B, along the corresponding median of the triangle to the middle point of the side AC. We call this specific kind of "2D push", a median push.

Lemma 2.3.4. [4] If a vertex of a polygon $P = (P_0, P_1, \cdots, P_n)$ in $\mathbb{R}^3$, say P_j (for $j = 1, 2, \cdots, n-1$), undergoes the median push, then the total curvatures of the new open PL curves formed during the push remain the same or decrease, while the trace of the push for P_j remains within the triangle $\Delta P_{j-1}P_jP_{j+1}$. (This holds not only for the median push, but also for any push with a trace lying on the interior of a triangle indicated in Definition 2.3.3.)

Proof. Consider Figure 2.3.2, which illustrates a non-planar polygonal curve in $\mathbb{R}^3$. For $\triangle P_{j-1}P_jP_{j+1}$, consider the median having P_j as an endpoint and denote an arbitrary interior point of that median by P_j'. Suppose that P_j is pushed to P_j' by the median push. Then the exterior angles affected by this push are a, b and

[4] The paper [1] gives a similar result which compares the curvatures before and after a triangle is deformed to a line segment by a median push. The lemma here compares the curvatures before and after a triangle is deformed to either another triangle or a line segment by a median push.

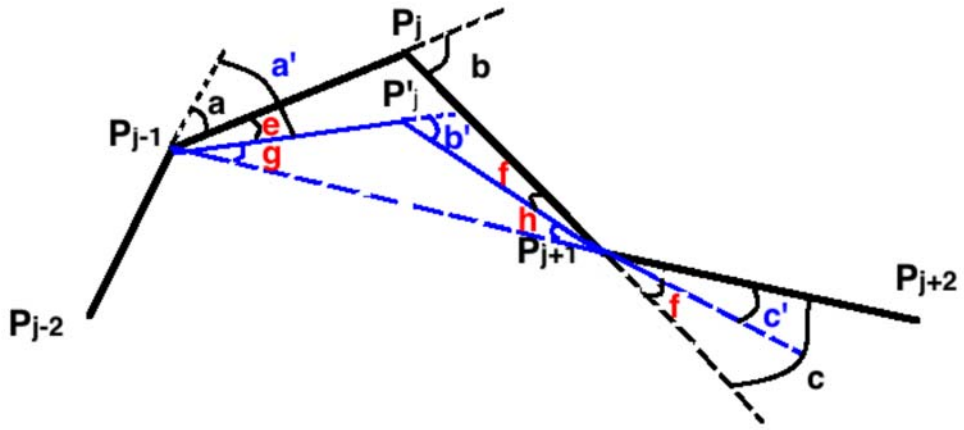

Figure 2.3.2: The change of exterior angles during a push

c. The other angles stay unchanged. So we can compare the total curvatures by comparing $a + b + c$ and $a' + b' + c'$ where a', b' and c' are corresponding angles after the push.

It follows from the Spherical Triangle Inequality 2.3.1 that

$$a' \leq a + e \text{ and } c' \leq f + c,$$

and note that

$$b' = g + h \text{ and } b = e + g + h + f,$$

where a', b' and c' are corresponding exterior angles to a, b and c after the push, and

$$e = \angle P_j P_{j-1} P_{j'}, \quad f = \angle P_j P_{j+1} P_{j'}, \quad g = \angle P_{j'} P_{j-1} P_{j+1} \quad \text{and} \quad h = \angle P_{j'} P_{j+1} P_{j-1}$$

all of which are radians measured between 0 and π. So

$$a' + b' + c' \leq a + e + g + h + f + c \leq a + b + c$$

Therefore the total curvature remains the same or decreases during the median push. □

After i iterations, there are 2^i sub-control polygons, $P^k = (P_{k,0}, \ldots, P_{k,n})$, for $k = 1, \ldots, 2^i$. Denote the convex hull of a sub-control polygon P^k as $\mathbf{CH}(P^k)$. Denote the control polygon as $K = \bigcup_{k=1,\ldots 2^i} P^k$. Let $L = \bigcup_{k=1,\ldots 2^i} \overline{P_{k,0}P_{k,n}}$ be the PL curve formed by connecting the cords from $P_{k,0}$ to $P_{k,n}$, for all $k = 1, \ldots, 2^i$. Theorem 2.3.5 requires that the pipe section Γ_k contains the convex hull $\mathbf{CH}(P^k)$ of P^k. This condition is convenient for establishing theoretical results. But it may require excessively many subdivisions. In the next chapters, we shall develop new proofs to remove this constraint so that the isotopy can be achieved more quickly by subdivision.

Theorem 2.3.5. For $\mathcal{B}$, after sufficiently many subdivisions, the control polygon K, will be ambient isotopic to the corresponding L.

Proof. By convergence in distance [21], take sufficiently many subdivisions such that each convex hull $\mathbf{CH}(P^k)$ of P^k is contained in Γ_k. This strong condition on containing the entire convex hull of each P^k also ensures [8] that each line segment $\overline{P_0^k P_0^{k+1}} \subset \Gamma_k$. Continue, as needed, to subdivide until that each $T_\kappa(P^k) < \pi/2$ to satisfy Lemma 2.2.8 as in the proof of Theorem 2.2.9, so that the union of

the P^k's is simple. Also the convex hulls $\mathbf{CH}(P^k)$ and $\mathbf{CH}(P^{k+1})$, or $\mathbf{CH}(P^k)$ and $\mathbf{CH}(P^{k-1})$, can intersect only the single point where P^k and P^{k+1} or P^{k-1} connect, as P^k and P^{k+1} or P^{k-1} are separated by the normal plane Π except at the point where they connected, by Lemma 2.2.8.

We use median pushes to move vertices of P^k onto $\overline{P_0^k P_0^{k+1}}$. Consider a median push of a vertex other than the end points of P^k. Lemma 2.3.4 implies that the total curvature of P^k remains less than $\pi/2$, and P^k stays inside Γ_k since the convex hull does. So the control polygon remains simple during the push.

A sequence of median pushes will map K to L, while leaving the end points of all sub-control polygons as fixed points. These specific pushes do not produce self-intersections, so this sequence induces an ambient isotopy between K and L [16]. The PL curve L is ambient isotopy to $\mathcal{B}$ [8] and the conclusion now follows from the equivalence relation of ambient isotopy [2]. □

Chapter 3

Construction of Equivalence Relations

In the previous chapter, we proved the existence of ambient isotopies under subdivision, with the possibility of excessively many subdivisions, resulting from the hypothesis of containment of the convex hull of each sub-control polygon within the pipe surface. More aggressive strategies are now shown, relying upon more mathematically sophisticated arguments.

3.1 Motivation

Let $S_r(\mathcal{B})$ be a non-self-intersecting pipe surface for a Bézier curve $\mathcal{B}$. Let Γ_B be the tubular neighborhood bounded by $S_r(\mathcal{B})$. Also suppose $\mathcal{P} = (P_0, P_1, \cdots, P_n)$ is the control polygon. We know that fitting the convex hull of $\mathcal{P}$ inside Γ_B obviously implies that $\mathcal{P}$ is contained inside Γ_B. But the converse is not true, which is shown by the following example.

Consider the following control points:

$$P_0 = (0, 0); P_1 = (1, 1); P_2 = (2, 1); P_3 = (3, 0).$$

The cubic Bézier curve defined by these control points is:

$$\mathcal{B}(t) = [3t, -3t^2 + 3t].$$

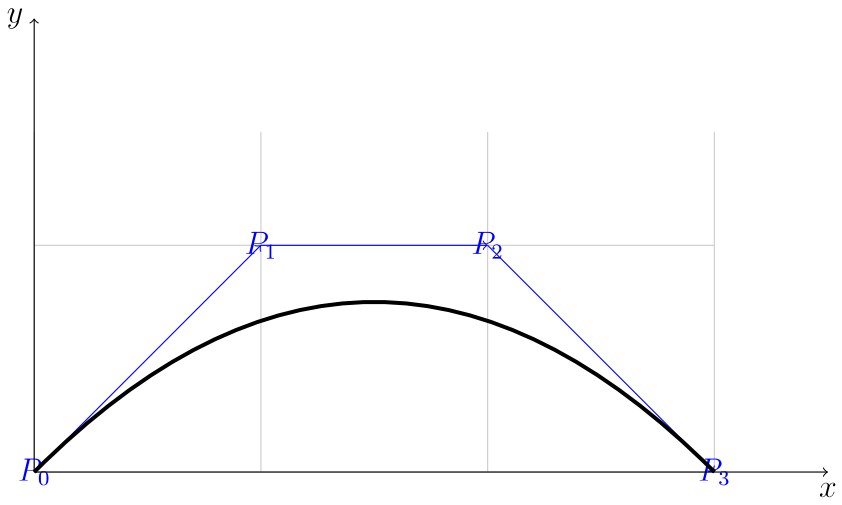

The uniform parametrization of the control polygon is given by

$$\mathcal{P}(t) = \begin{cases} (3t, 3t) & t \in [0, \frac{1}{3}] \\ (3t, 1) & t \in [\frac{1}{3}, \frac{2}{3}] \\ (3t, -3t + 3) & t \in [\frac{2}{3}, 1]. \end{cases} \tag{3.1.1}$$

It follows that

$$\mathcal{B}(t) - \mathcal{P}(t) = \begin{cases} (0, -3t^2) & t \in [0, \frac{1}{3}] \\ (0, -3t^2 + 3t - 1) & t \in [\frac{1}{3}, \frac{2}{3}] \\ (0, -3t^2 + 6t - 3) & t \in [\frac{2}{3}, 1]. \end{cases} \tag{3.1.2}$$

By computation, we have,

$$\max_{t\in[0,1]} |\mathcal{B}(t) - \mathcal{P}(t)| = \frac{1}{3}. \tag{3.1.3}$$

Now, we construct a non-self-intersecting pipe surface of radius r for $\mathcal{B}$ such that $\mathcal{P}$ fits inside the surface. In order to for $\mathcal{P}$ to be contained inside, we set $r > \frac{1}{3}$.

Consider the curvature of $\mathcal{B}$:

$$\kappa(t) = \frac{||\mathcal{B}'(t) \times \mathcal{B}''(t)||}{||\mathcal{B}'(t)||^3} = \frac{18}{||(3, -6t+3)||^3}.$$

In order to prevent self-intersections, we set [8]

$$r < \min_{t\in[0,1]} \frac{1}{\kappa(t)} = \frac{3}{2}.$$

So we take an arbitrary value in $(\frac{1}{3}, \frac{3}{2})$, say

$$r = \frac{1}{3} + 0.1.$$

Then the non-self-intersecting pipe surface $S_r(\mathcal{B})$ of radius r is shown in Figure 3.1.1, in which $\mathcal{P}$ fits inside.

Now consider the line segment $\overline{P_0P_1}$. Note $(\frac{3}{2}, 0) \in \overline{P_0P_1}$. Consider the distance between $(\frac{3}{2}, 0)$ and $\mathcal{B}$. Computation shows that the minimum is $\frac{3}{4}$ obtained between $(\frac{3}{2}, 0)$ and $(\frac{3}{2}, 1)$, and the line segment connecting $(\frac{3}{2}, 0)$ and $(\frac{3}{2}, 1)$ is normal to $\mathcal{B}$, which implies that the minimal distance between the point $(\frac{3}{2}, 0)$ and $\mathcal{B}$ is $\frac{3}{4}$. But $\frac{3}{4} > r$. So the point $(\frac{3}{2}, 0)$ lies outside of the non-self-intersecting

pipe surface, and hence $\overline{P_0P_1}$ does not fit inside the non-self-intersecting pipe surface, as Figure 3.1.1 shows.

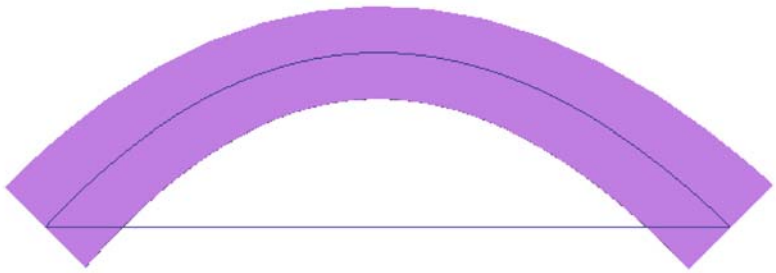

Figure 3.1.1: Pipe, curve and line segment

In order to remove the constraint of fitting convex hulls inside non-self-intersecting pipe sections, we shall explicitly define the ambient isotopy between two curves. There are two consequences:

(1) Theoretically, we shall present two criteria (*Hypotheses 1, 2*) to ensure the ambient isotopy between a PL curve and a C^2 curve connected at the end points;

(2) Practically, we shall optimize the subdivision algorithm so that it no longer relies upon containment of the convex hull within a pipe section (as in Theorem 2.3.5), but has the weaker hypothesis of containment of the subdivided control polygon within the pipe section.

Recall that Theorem 2.2.9 shows the existence of a homeomorphism between $\mathcal{B}$ and the control polygon, which is a necessary condition for the isotopy. The ambient isotopy is explicitly constructed.

In Section 3.2, we shall explicitly construct a homeomorphism between two curves satisfying certain assumptions, with reliance upon several geometric lemmas proven

here. In Section 3.3, we shall extend this result on homeomorphism to exhibit an ambient isotopy.

3.2 Construction of Homeomorphism

Let L be an open, compact, simple PL curve and C be an open, compact, simple, regular, C^2 polynomial curve of degree n in $\mathbb{R}^3$. Let

$$L(t) : [0,1] \to \mathbb{R}^3 \text{ and } C(t) : [0,1] \to \mathbb{R}^3$$

be the corresponding parameterizations of L and C. We will construct a homeomorphism between L and C (Equation 3.2.2), when $L(0) = C(0),\ L(1) = C(1)$, that is, $L \cup C$ forms a closed curve[5].

Denote the disc of radius r centered at $C(t)$ and normal to C as $D_r(t)$. Since C is a compact, simple, regular, and C^2 curve, there exists a non-self-intersecting pipe section (Remark 2.2.6) of radius r formed by these discs, denoted as Γ, that is, $\Gamma = \bigcup_{t\in[0,1]} D_r(t)$. Denote the interior as $\text{int}(\Gamma)$, and the boundary as $\partial\Gamma$. Note that the boundary $\partial\Gamma$ consists of the non-self-intersecting pipe surface (Definition 2.2.5) and the end discs $D_r(0)$ and $D_r(1)$.

Definition 3.2.1. Define $\theta(t) : [0,1] \to [0,\pi]$ by

$$\theta(t) = \eta(C'(t), L'(t)),$$

where the function $\eta(\cdot,\cdot)$ was previously given in Definition 1.1.3.

[5]Any pairwise disjoint simple open curves in $\mathbb{R}^n$ are trivially ambient isotopic.

The following *Hypotheses 1* and *2* will play a central role in establishing the desired homeomorphism between L and C.

Hypothesis 1: $L \setminus \{L(0), L(1)\} \subset \text{int}(\Gamma)$; and

Hypothesis 2: $T_\kappa(L) + \max_{t\in[0,1]} \theta(t) < \frac{\pi}{2}$.

Lemma 3.2.2. Suppose L is a sub-control polygon and C is the corresponding Bézier sub-curve. Then *Hypotheses 1* and *2* can be achieved by subdivision.

Proof. By the convergence in Hausdorff distance under subdivision [21], sufficiently many subdivision iterations will produce a control polygon that fits inside a non-self-intersecting pipe surface. Furthermore, by the Angular Convergence (Theorem 2.1.2) and Lemma 2.2.7, possibly more subdivisions will ensure that each sub-control polygon lies in the corresponding non-self-intersecting pipe section, satisfying *Hypothesis 1*. Denote the number of subdivision iterations to achieve this by ι_1.

By the Angular Convergence (Theorem 2.1.2), $T_\kappa(L)$ converges to 0 under subdivision. Because the discrete derivative of the control polygon converges to the derivative of the Bézier curve [6] under subdivision, $\theta(t)$ converges to 0 for each $t \in [0, 1]$. So *Hypothesis 2* can be achieved by sufficiently many subdivision iterations, denoted by ι_2. (The details to find ι_1 and ι_2 appear in Section 4.2.2.) □

Remark 3.2.3. When we later explicate the number of subdivisions, we shall show that the sufficient number of subdivisions for *Hypothesis 2* is at most one more than that for a weaker condition $T_\kappa(L) < \frac{\pi}{2}$. (Remark 4.2.7 in Section 4.2.2)

Remark 3.2.4. To motivate these hypotheses, we present the case of a Bézier curve. Consider L to be a sub-control polygon and C to be the corresponding sub-curve. *Hypothesis 1* will ensure that L lies inside a non-self-intersecting pipe section, while *Hypothesis 2* will ensure a local homeomorphism between L and C. In particular, *Hypotheses 1* and *2* will be sufficient for us to establish the one-to-one correspondence using normal discs of C.

***Hypotheses 1* and *2* are assumed in the rest of the section.**

Define a function $\tilde{L}(t) : [0, 1] \to L$ by letting

$$\tilde{L}(t) = D_r(t) \cap L, \tag{3.2.1}$$

where $D_r(t)$ is the normal disc of C at t.

Define a map $h : C \to L$ for each $p \in C$ by setting

$$h(p) = \tilde{L}(C^{-1}(p)). \tag{3.2.2}$$

We shall show that h is a homeomorphism. The subtlety here is to demonstrate the one-to-one correspondence by showing each normal disc of C intersects L at a single point (which will be the main goal of the following), and intersects C at a single point (which will be easy), under the assumption of *Hypotheses 1* and *2*.

3.2.1 Outline of the Proof

For each $t_0 \in [0, 1]$, the associated normal disc is denoted as $D_r(t_0)$. Following is the sketch of a proof that $D_r(t_0)$ intersects L at a single point. (See Figure 3.2.1.)

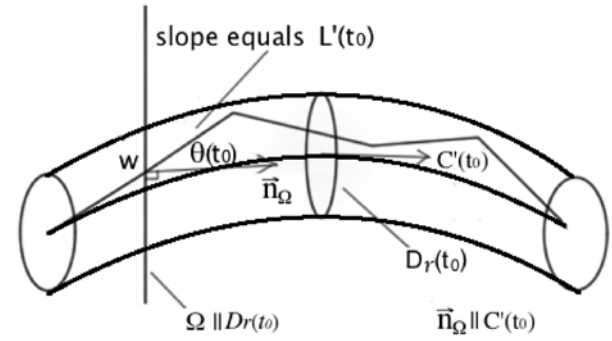

Figure 3.2.1: Each normal disc intersects L at a single point

(i) *The essential initial steps are to select a non-vertex point of L (denoted as w), a plane (denoted as Ω), and an angle (denoted as $\theta(t_0)$):*

(a) Define w and Ω: Pick a line segment of L whose slope is equal to $L'(t_0)$, denoted as ℓ. Choose an interior point of ℓ, denoted as w. Let Ω be the plane that contains w and is parallel to $D_r(t_0)$. (We use w to define two sub-curves of L, a 'left' sub-curve which terminates at w, denoted as L_l, and a 'right' sub-curve which begins at w, denoted as L_r.)

(b) Consider $\eta(C'(t_0), L'(t_0)) = \theta(t_0)$ (Definition 3.2.1). Since Ω is parallel to $D_r(t_0)$, a normal vector of Ω, denoted by $\overrightarrow{n}_\Omega$ has the same direction as $C'(t_0)$ and $\eta(\overrightarrow{n}_\Omega, \ell) = \eta(C'(t_0), L'(t_0)) = \theta(t_0)$.

Remark: Since $\eta(\overrightarrow{n}_\Omega, \ell) = \theta(t_0)$, *Hypothesis 2* implies that $T_\kappa(L) + \eta(\overrightarrow{n}_\Omega, \ell) = T_\kappa(L) + \theta(t_0) < \frac{\pi}{2}$. Since w is an interior point of ℓ, the angle determined by Ω and L_l, and the angle determined by Ω and L_r, have the same measure $\theta(t_0)$, as shown in Figure 3.2.2. So we obtain the similar inequalities $T_\kappa(L_l) + \theta(t_0) < \frac{\pi}{2}$ and $T_\kappa(L_r) + \theta(t_0) < \frac{\pi}{2}$, which will be crucial.

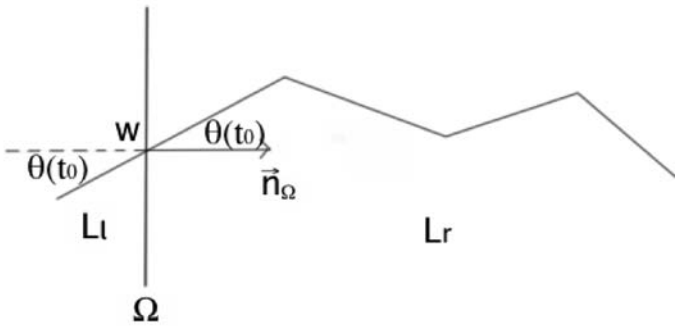

Figure 3.2.2: Similar angles $\theta(t_0)$

(ii) Prove, by *Hypothesis 2*, that $\Omega \cap L_r = w$. Similarly, show that $\Omega \cap L_l = w$. So $\Omega \cap L = w$. (Lemma 3.2.6)

(iii) Prove that any plane parallel to Ω intersects L at no more than a single point. (Lemma 3.2.7)

(iv) Since $D_r(t_0) \parallel \Omega$, it will follow that $D_r(t_0)$ intersects L in, at most, a single point. Show, using *Hypothesis 1*, that $D_r(t_0)$ must intersect L, and hence $D_r(t_0) \cap L$ is a single point. (Lemma 3.2.8)

3.2.2 Preliminary Lemmas for Homeomorphisms

In order to work with total curvatures of PL curves, an extension of the spherical triangle inequality [27], given in Lemma 3.2.5, will be useful, similar to previous usage by Milnor [1]. Lemma 3.2.5 below follows easily from Inequality 2.3.1.

Lemma 3.2.5. Suppose that $\overrightarrow{v}_1, \overrightarrow{v}_2, \ldots, \overrightarrow{v}_m$, where $m \in \{3, 4, \ldots\}$, are nonzero vectors, then

$$\eta(\overrightarrow{v}_1, \overrightarrow{v}_m) \leq \eta(\overrightarrow{v}_1, \overrightarrow{v}_2) + \eta(\overrightarrow{v}_2, \overrightarrow{v}_3), + \ldots, + \eta(\overrightarrow{v}_{m-1}, \overrightarrow{v}_m). \tag{3.2.3}$$

Now, we adopt the notation shown in Figure 3.2.1 and formalize the proof outlined in Section 3.2.1. We assume that the sub-curve on the right hand side of Ω in Figure 3.2.2 is L_r, and the other one is L_l, where we denote the set of ordered vertices of L_r as

$$\{v_0, v_1, \ldots, v_n\},$$

with $v_0 = w$.

By Definition 3.2.1, we have $\theta(t_0) \leq \max_{t\in[0,1]} \theta(t)$. It is trivially true that $T_\kappa(L_r) \leq T_\kappa(L)$, so that with *Hypothesis 2:* $T_\kappa(L) + \max_{t\in[0,1]} \theta(t) < \frac{\pi}{2}$, we have

$$T_\kappa(L_r) + \theta(t_0) \leq T_\kappa(L) + \max_{t\in[0,1]} \theta(t) < \frac{\pi}{2}. \tag{3.2.4}$$

The statement and proof of Lemma 3.2.6 depend upon the point w chosen in Step 1 of the Outline presented in Section 3.2.1. There, the point w was defined as an *interior point* of a line segment ℓ of L, so that w is precluded from being a vertex of the original PL curve L.

Lemma 3.2.6. The plane Ω intersects L only at the single point w.

Proof. Here we prove $\Omega \cap L_r = w$. A similar argument will show $\Omega \cap L_l = w$.

The oriented initial line segment of L_r is $\overrightarrow{wv_1}$ which lies on ℓ. So

$$\eta(\overrightarrow{n}_\Omega, \overrightarrow{wv_1}) = \eta(\overrightarrow{n}_\Omega, \ell) = \theta(t_0) < \frac{\pi}{2}.$$

For a proof by contradiction, assume that Ω intersects L_r at some point u other than w. The possibility that $\overrightarrow{wv_1} \subset \Omega$ is precluded by $\theta(t_0) < \pi/2$, so the plane Ω intersects $\overrightarrow{wv_1}$ only at w. So $u \notin \overrightarrow{wv_1}$.

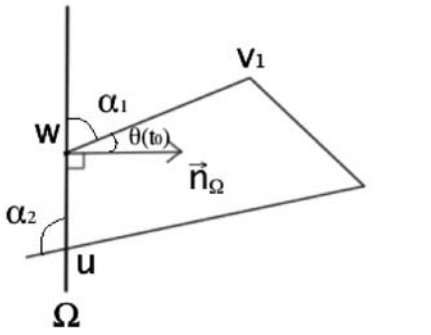

Figure 3.2.3: The intersection u generates a closed PL curve

Denote the sub-curve of L_r from w to u as $L(wu)$. Then, since $u \notin \overrightarrow{wv_1}$, the union, $L(wu) \cup \overrightarrow{uw}$, forms a closed PL curve, as Figure 3.2.3 shows. By Fenchel's theorem we have

$$T_\kappa(L(wu) \cup \overrightarrow{uw}) \geq 2\pi. \tag{3.2.5}$$

Denote the exterior angle of the PL curve $L(wu) \cup \overrightarrow{uw}$ at w as α_1 (Figure 3.2.3), that is,

$$\alpha_1 = \eta(\overrightarrow{uw}, \overrightarrow{wv_1}).$$

By Inequality 2.3.1,

$$\alpha_1 = \eta(\overrightarrow{uw}, \overrightarrow{wv_1}) \leq \eta(\overrightarrow{uw}, \overrightarrow{n}_\Omega) + \eta(\overrightarrow{n}_\Omega, \overrightarrow{wv_1}).$$

Since $\overrightarrow{uw} \subset \Omega$, we have that $\eta(\overrightarrow{uw}, \overrightarrow{n}_\Omega) = \frac{\pi}{2}$. Note also that $\eta(\overrightarrow{n}_\Omega, \overrightarrow{wv_1}) = \theta(t_0)$. So

$$\alpha_1 \leq \frac{\pi}{2} + \theta(t_0).$$

Denote the exterior angle of the PL curve $L(wu) \cup \overrightarrow{uw}$ at u as α_2. Note $\alpha_2 \leq \pi$, according to the definition of exterior angles. So

$$T_\kappa(L(wu) \cup \overrightarrow{uw}) = \alpha_1 + T_\kappa(L(wu)) + \alpha_2 \leq \frac{\pi}{2} + \theta(t_0) + T_\kappa(L(wu)) + \pi.$$

It follows from Inequality 3.2.5 that

$$\frac{\pi}{2} + \theta(t_0) + T_\kappa(L(wu)) + \pi \geq 2\pi,$$

so

$$T_\kappa(L(wu)) + \theta(t_0) \geq \frac{\pi}{2}. \tag{3.2.6}$$

By $L(wu) \subset L_r$, we have

$$T_\kappa(L_r) + \theta(t_0) \geq T_\kappa(L(wu)) + \theta(t_0) \geq \frac{\pi}{2}.$$

But this contradicts Inequality 3.2.4. □

Lemma 3.2.7. Any plane parallel to Ω intersects L at no more than a single point.

Proof. Suppose $\tilde{\Omega}$ is a plane parallel to Ω. If $\tilde{\Omega} \cap L = \emptyset$, then we are done, so we

assume that $\tilde{\Omega} \cap L \neq \emptyset$. If $\tilde{\Omega} = \Omega$, then Lemma 3.2.6 applies, so we also assume that $\tilde{\Omega} \neq \Omega$, implying that $w \notin \tilde{\Omega}$.

Consider two closed half-spaces $\mathbb{H}_l$ and $\mathbb{H}_r$ such that $\mathbb{H}_l \cup \mathbb{H}_r = \mathbb{R}^3$ and $\mathbb{H}_l \cap \mathbb{H}_r = \Omega$. Since $\Omega \cap L_l = \Omega \cap L_r = w$ and $L = L_l \cup L_r$ is simple (Section 3.2), we can assume that $L_l \subset \mathbb{H}_l$ and $L_r \subset \mathbb{H}_r$.

Suppose without loss of generality that $\tilde{\Omega} \subset H_r$, as shown in Figure 3.2.4. Then since $L_l \subset \mathbb{H}_l$ and $\mathbb{H}_l \cap \mathbb{H}_r = \Omega \neq \tilde{\Omega}$, we have $\tilde{\Omega} \cap L_l = \emptyset$. Since we assumed $\tilde{\Omega} \cap L \neq \emptyset$, it follows that $\tilde{\Omega} \cap L_r \neq \emptyset$. Now, it suffices to show that $\tilde{\Omega} \cap L_r$ is a single point.

Since L_r is compact and oriented, let $\tilde{w}$ denote the first point of L_r, at which $\tilde{\Omega}$ intersects L_r. Since $\tilde{\Omega} \parallel \Omega$ and $\tilde{\Omega} \neq \Omega$, we have $\tilde{w} \neq w$. We shall show that $\tilde{\Omega} \cap L_r = \tilde{w}$.

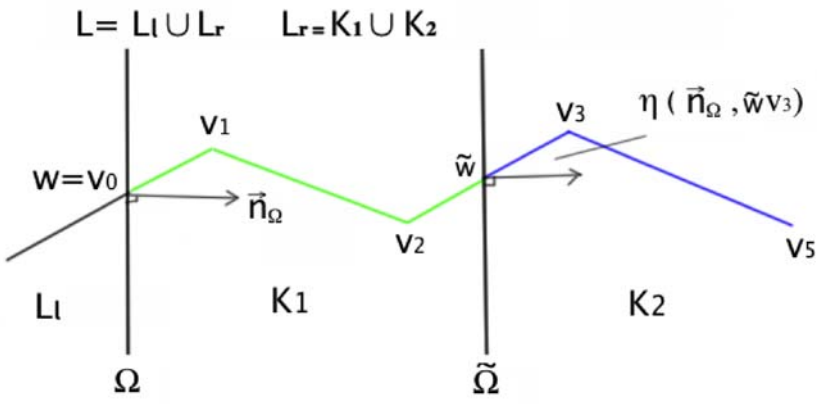

Figure 3.2.4: A parallel plane intersecting L

Denote the sub-curve of L_r from its initial point v_0 to $\tilde{w}$ as K_1, and the sub-curve from $\tilde{w}$ to its end point v_n as K_2, as shown in Figure 3.2.4. Since $\tilde{w}$ is the first

intersection point of $\tilde{\Omega} \cap L_r$, but K_1 ends in $\tilde{w}$, then it is clear that $\tilde{\Omega} \cap K_1$ contains only $\tilde{w}$. Then in order to show $\tilde{\Omega} \cap L_r = \tilde{w}$, it suffices to show that $\tilde{\Omega} \cap K_2 = \tilde{w}$.

If $\tilde{w} = v_n$, then it is the degenerate case: $K_2 = \tilde{w}$, and we are done. Otherwise, there is a vertex v_k for some $k \in \{1, \ldots, n\}$ such that $\overrightarrow{\tilde{w}v_k}$ is the non-degenerate initial segment of K_2, where $\tilde{w} \neq v_k$. Now we shall establish the inequality:

$$T_\kappa(K_2) + \eta(\overrightarrow{n}_\Omega, \overrightarrow{\tilde{w}v_k}) < \frac{\pi}{2},$$

to guarantee a single point of intersection, similar to arguments previously given in Lemma 3.2.6. To this end, we use Inequality 2.3.1 to note that

$$\eta(\overrightarrow{n}_\Omega, \overrightarrow{\tilde{w}v_k}) \leq \eta(\overrightarrow{n}_\Omega, \overrightarrow{v_0v_1}) + \eta(\overrightarrow{v_0v_1}, \overrightarrow{\tilde{w}v_k}) = \theta(t_0) + \eta(\overrightarrow{v_0v_1}, \overrightarrow{\tilde{w}v_k}). \tag{3.2.7}$$

The proof will be completed if we can show that

$$T_\kappa(K_2) + \theta(t_0) + \eta(\overrightarrow{v_0v_1}, \overrightarrow{\tilde{w}v_k}) < \frac{\pi}{2}. \tag{3.2.8}$$

Case1: The intersection $\tilde{w}$ is not a vertex, that is, $\tilde{w} \neq v_{k-1}$. Then $\tilde{w}$ is an interior point of $\overrightarrow{v_{k-1}v_k}$, and hence $T_\kappa(K_1) = \eta(\overrightarrow{v_0v_1}, \overrightarrow{v_1v_2}) + \ldots + \eta(\overrightarrow{v_{k-2}v_{k-1}}, \overrightarrow{v_{k-1}\tilde{w}})$, and $\eta(\overrightarrow{v_{k-1}\tilde{w}}, \overrightarrow{\tilde{w}v_k}) = 0$. By Lemma 3.2.5,

$$\eta(\overrightarrow{v_0v_1}, \overrightarrow{\tilde{w}v_k}) \leq \eta(\overrightarrow{v_0v_1}, \overrightarrow{v_1v_2}) + \ldots + \eta(\overrightarrow{v_{k-2}v_{k-1}}, \overrightarrow{v_{k-1}\tilde{w}}) + \eta(\overrightarrow{v_{k-1}\tilde{w}}, \overrightarrow{\tilde{w}v_k}) = T_\kappa(K_1).$$

So

$$T_\kappa(K_2) + \theta(t_0) + \eta(\overrightarrow{v_0v_1}, \overrightarrow{\tilde{w}v_k}) \leq T_\kappa(K_2) + \theta(t_0) + T_\kappa(K_1).$$

We also have

$$T_\kappa(L_r) = T_\kappa(K_1) + \eta(\overrightarrow{v_{k-1}\tilde{w}}, \overrightarrow{\tilde{w}v_k}) + T_\kappa(K_2) = T_\kappa(K_1) + T_\kappa(K_2),$$

since $\eta(\overrightarrow{v_{k-1}\tilde{w}}, \overrightarrow{\tilde{w}v_k}) = 0$. Furthermore,

$$T_\kappa(K_2) + \theta(t_0) + \eta(\overrightarrow{v_0v_1}, \overrightarrow{\tilde{w}v_k}) \leq T_\kappa(L_r) + \theta(t_0),$$

which is less than $\frac{\pi}{2}$, by Inequality 3.2.4.

Case2: The intersection $\tilde{w}$ is a vertex, that is, $\tilde{w} = v_{k-1}$, then $T_\kappa(K_1) = \eta(\overrightarrow{v_0v_1}, \overrightarrow{v_1v_2}) + \ldots + \eta(\overrightarrow{v_{k-3}v_{k-2}}, \overrightarrow{v_{k-2}\tilde{w}})$. By Lemma 3.2.5,

$$\begin{aligned}
&\eta(\overrightarrow{v_0v_1}, \overrightarrow{\tilde{w}v_k}) \\
&\leq \eta(\overrightarrow{v_0v_1}, \overrightarrow{v_1v_2}) + \ldots + \eta(\overrightarrow{v_{k-3}v_{k-2}}, \overrightarrow{v_{k-2}\tilde{w}}) + \eta(\overrightarrow{v_{k-2}\tilde{w}}, \overrightarrow{\tilde{w}v_k}) \\
&\leq T_\kappa(K_1) + \eta(\overrightarrow{v_{k-2}\tilde{w}}, \overrightarrow{\tilde{w}v_k}).
\end{aligned}$$

So

$$T_\kappa(K_2) + \theta(t_0) + \eta(\overrightarrow{v_0v_1}, \overrightarrow{\tilde{w}v_k}) \leq T_\kappa(K_2) + \theta(t_0) + T_\kappa(K_1) + \eta(\overrightarrow{v_{k-2}\tilde{w}}, \overrightarrow{\tilde{w}v_k}).$$

But by the definition of the total curvature for a PL curve,

$$T_\kappa(K_2) + T_\kappa(K_1) + \eta(\overrightarrow{v_{k-2}\tilde{w}}, \overrightarrow{\tilde{w}v_k}) = T_\kappa(L_r).$$

So

$$T_\kappa(K_2) + \theta(t_0) + \eta(\overrightarrow{v_0v_1}, \overrightarrow{\tilde{w}v_k}) \leq T_\kappa(L_r) + \theta(t_0),$$

which is less than $\frac{\pi}{2}$, by Inequality 3.2.4.

So Inequality 3.2.8 holds, which is an inequality analogous to Inequality 3.2.4. If in the proof of Lemma 3.2.6, we change Ω to $\tilde{\Omega}$, L_r to K_2 and $\theta(t_0)$ to $\eta(\overrightarrow{n}_\Omega, \overrightarrow{\tilde{w}v_k})$, then a similar proof of Lemma 3.2.6 will show that $\tilde{\Omega} \cap K_2 = \tilde{w}$. This completes the proof. □

Lemma 3.2.8. For an arbitrary $t_0 \in [0, 1]$, the disc $D_r(t_0)$ intersects C at a unique point, and also intersects L at a unique point.

Proof. First, we have $C(t_0) \in D_r(t_0) \cap C$. If there is an additional point, say $C(t_1) \in D_r(t_0) \cap C$ where $t_1 \neq t_0$, then we have that $C(t_1) \neq C(t_0)$ because C is simple (Section 3.2) and hence $D(t_1) \neq D(t_0)$. Since also $C(t_1) \in D_r(t_1)$, we have that $C(t_1) \in D_r(t_0) \cap D_r(t_1)$. But this contradicts the non-self-intersection of Γ. So $D_r(t_0) \cap C$ must be a unique point.

Now, we show that $D_r(t_0) \cap L \neq \emptyset$. If $t_0 = 0$ or $t_0 = 1$, then since $L(0) \in D_r(0)$ and $L(1) \in D_r(1)$, we have that $D_r(t_0) \cap L \neq \emptyset$.

Otherwise if $t_0 \in (0, 1)$, then assume to the contrary that $D_r(t_0) \cap L = \emptyset$. Since

$L \subset \Gamma$ by *Hypothesis 1*, the contrary assumption implies that $L \subset \Gamma \setminus D_r(t_0)$. Because C is an open curve (Section 3.2), we have that $D_r(0) \neq D_r(1)$. So $\Gamma \setminus D_r(t_0)$ consists of two disconnected components, but this implies that L is disconnected, which is a contradiction. So

$$D_r(t_0) \cap L \neq \emptyset. \tag{3.2.9}$$

Since $D_r(t_0) \parallel \Omega$ (as discussed in Section 3.2.1), Lemma 3.2.7 implies that the plane containing $D_r(t_0)$ intersects L at no more than a single point, which, of course, further implies that $D_r(t_0)$ intersects L at no more than a single point. This plus Inequality 3.2.9 shows that $D_r(t_0) \cap L$ is a single point.

If $D_r(t_0) \cap L = D_r(t_1) \cap L$ for some $t_1 \neq t_0$, then $D_r(t_0)$ and $D_r(t_1)$ intersect, which contradicts the non-self-intersection of Γ. So there is an one-to-one correspondence between the parameter t and the point $D_r(t) \cap L$ for $t \in [0, 1]$, which shows the uniqueness. □

The function $\tilde{L}(t) : [0, 1] \to L$ is defined by Equation 3.2.1

$$\tilde{L}(t) = D_r(t) \cap L.$$

Lemma 3.2.9. The map $\tilde{L}(t)$ is well defined, one-to-one and onto.

Proof. It is well defined by Lemma 3.2.8. Suppose $\tilde{L}(t_1) = \tilde{L}(t_2)$, then we have $D_r(t_1) \cap L = D_r(t_2) \cap L$ which is not empty by Lemma 3.2.8. So $D_r(t_1) \cap D_r(t_2) \neq \emptyset$. Since Γ is non-self-intersecting, it follows that $D_r(t_1) = D_r(t_2)$. Since C is simple,

if $D_r(t_1) = D_r(t_2)$, then $t_1 = t_2$. Thus $\tilde{L}$ is one-to-one. Since $L \subset \Gamma$, each point of L is contained in some disc $D_r(t)$. So $\tilde{L}$ is onto. □

Lemma 3.2.10. The map $\tilde{L}(t)$ is continuous.

Proof. Let $\Gamma_{t_1t_2}$ be the portion[6] of Γ corresponding to $[t_1, t_2]$, that is

$$\Gamma_{t_1t_2} = \bigcup_{t\in[t_1,t_2]} D_r(t).$$

Suppose that $s \in [0, 1]$ is an arbitrary parameter. Then by Lemma 3.2.9, there is a unique point $q \in L$ such that $q = \tilde{L}(s) = D_r(s) \cap L$. We shall prove the continuity of $\tilde{L}(t)$ at s in terms of the definition of continuity, that is, for $\forall\epsilon > 0$, there exists a $\delta > 0$ such that $|t - s| < \delta$ implies $||\tilde{L}(t) - \tilde{L}(s)|| < \epsilon$.

Note that $D_r(s)$ divides Γ into Γ_{0s} and Γ_{s1}. Since C is an open curve, it follows that $D_r(0) \neq D_r(1)$, and that Γ_{0s} and Γ_{s1} intersect at only $D_r(s)$. By Lemma 3.2.8, $D_r(s) \cap L$ is a single point, so L is divided by $D_r(s)$ into two subcurves, denoted as K_1 and K_2, that is $K_1 \subset \Gamma_{0s}$ and $K_2 \subset \Gamma_{s1}$, as shown in Figure 3.2.5.

Case1: The parameter s is such that $s \neq 0$ and $s \neq 1$. Consider Γ_{s1} first. Since K_2 is oriented, we can let v be the first vertex of K_2 that is nearest (in distance along K_2) to q. For any $0 < \epsilon < ||\overline{qv}||$, let $q' \in \overline{qv}$ such that $||\overline{qq'}|| = \epsilon$. By Lemma 3.2.9, $q' = \tilde{L}(\tau) = D_r(\tau) \cap L$ for some $\tau \in (s, 1]$.

First, note $\overline{qq'} \cap \text{int}\Gamma_{s\tau} \neq \emptyset$. To verify this, observe $\overline{qq'} \subset \overline{qv} \subset K_2 \subset \Gamma_{s1}$ and $\Gamma_{s1} = \Gamma_{s\tau} \cup \Gamma_{\tau 1}$, so $\overline{qq'} \subset \Gamma_{s\tau} \cup \Gamma_{\tau 1}$. If $\overline{qq'} \cap \text{int}\Gamma_{s\tau} = \emptyset$, then the segment $\overline{qq'}$ is

[6] If $t_1 = t_2$, then $\Gamma_{t_1t_2}$ is a single disc.

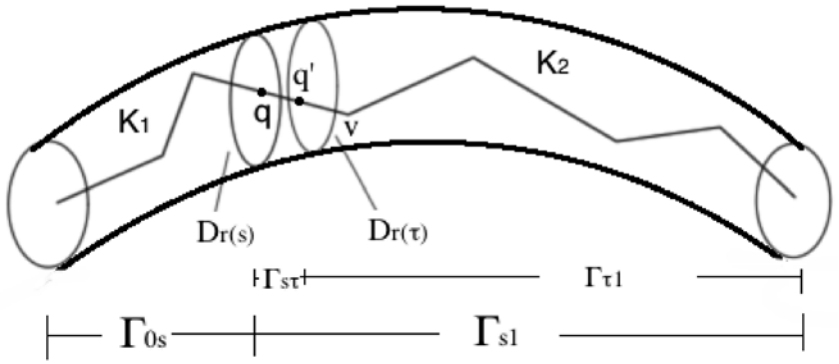

Figure 3.2.5: If $|s-\tau| < \delta$, then $||q-q'|| < \epsilon$

contained in $D_r(s) \cup \Gamma_{\tau 1}$ which is disconnected. This implies $\overline{qq'}$ is disconnected, which is a contradiction.

Secondly, note that the subset $\Gamma_{s\tau}$ of a non-self-intersecting pipe section is connected (since C is C^1), and $\overline{qq'}$ is a line segment jointing the end discs of $\Gamma_{s\tau}$, and has intersections with the interior of $\Gamma_{s\tau}$. This geometry implies that

$$\overline{qq'} \subset \Gamma_{s\tau}. \tag{3.2.10}$$

Let $\delta = \tau - s$. For an arbitrary $t \in (s, s+\delta) = (s, \tau)$, Inclusion 3.2.10 implies that $\tilde{L}(t) = D_r(t) \cap \overline{qq'}$. Since neither $\tilde{L}(t) \neq q$ or $\tilde{L}(t) \neq q'$, it follows that $\tilde{L}(t) \in \text{int}(\overline{qq'})$. So

$$||\tilde{L}(t) - \tilde{L}(s)|| < ||\overline{qq'}|| = \epsilon.$$

This shows the right-continuity. We similarly consider the Γ_{0s} and obtain the left-continuity.

Case2: The parameter s is such that $s = 0$ or $s = 1$. We similarly obtain the right-continuity if $s = 0$, or the left-continuity if $s = 1$. □

Theorem 3.2.11. If L and C satisfy *Hypotheses 1* and *2*, then the map h defined by Equation 3.2.2 is a homeomorphism.

Proof. By Lemma 3.2.9, $\tilde{L}(t)$ is one-to-one and onto. By Lemma 3.2.10, $\tilde{L}(t)$ is continuous. Since $\tilde{L}$ is defined on a compact domain, it is a homeomorphism. Note that C is simple and open, so $C(t)$ is one-to-one, and it is obviously onto. The map $C(t)$ is continuous and defined on a compact domain, so $C(t)$ a homeomorphism. Since h is a composition of C^{-1} and $\tilde{L}$, h is a homeomorphism. □

Remark 3.2.12. A natural expectation for defining a homeomorphism between simple curves C and L would be by $f(p) = L(C^{-1}(p))$. An easy method to extend f to a homotopy is the straight-line homotopy. However, we could not establish that a straight-line homotopy based upon f would also be an isotopy, where it would be necessary to show that each pair of line segments generated is disjoint. Our definition of h (Equation 3.2.2) was strategically chosen so that this isotopy criterion is easily established, as the normal discs are already pairwise disjoint.

3.3 Construction of Ambient Isotopy

Note that L and C fit inside a non-self-intersecting pipe section (Remark 2.2.6) Γ of C. For a similar problem, an explicit construction has appeared [37, 41]. The following proof of Lemma 3.3.3 is a simpler version of a previous proof

[37, Corollary 4]. The construction here relies upon some basic properties of convex sets, which are repeated here. For clarity, the complete proof of Lemma 3.3.3 is given here.

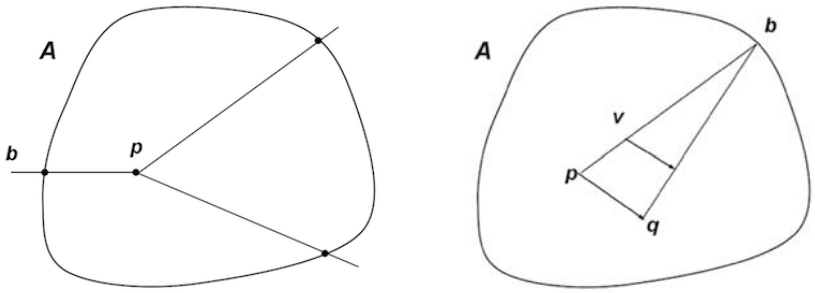

(a) Rays outward (b) Variant of a push

Figure 3.3.1: A convex set and a map defined on it

Lemma 3.3.1. [37, Lemma 6] Let A be a compact convex subset of $\mathbb{R}^2$ with non-empty interior. For each point $p \in int(A)$ and $b \in \partial A$, the ray going from p to b only intersects ∂A at b (See[7] Figure 3.3.1(a).)

Lemma 3.3.2. [37, Lemma 7] Let A be a compact convex subset of $\mathbb{R}^2$ with non-empty interior and fix $p \in int(A)$. For each boundary point $b \in \partial A$, denote by $[p, b]$ the line segment from p to b. Then $A = \bigcup_{b \in \partial A} [p, b]$.

Lemma 3.3.3. There is an ambient isotropy between L and C with compact support of Γ, leaving $\partial\Gamma$ fixed.

Proof. We consider each normal disc $D_r(t)$ for $t \in [0, 1]$. Let $p = D_r(t) \cap C$ and $q = h(p)$ with h defined by Equation 3.2.2, then define a map $F_{p,q} : D_r(t) \to D_r(t)$

[7]The Images in Figure 3.3.1 were created by L. E. Miller [41] and are used, here, with permission.

such that it sends each line segment $[p, b]$ for $b \in \partial D_r(t)$, linearly onto the line segment $[q, b]$ as Figure 3.3.1(b) shows. The two previous lemmas (Lemma 3.3.1 and Lemma 3.3.2), will yield that $F_{p,q}$ is a homeomorphism, leaving $\partial D_r(t)$ fixed [41, Lemma 4.4.6].

In order to extend $F_{p,q}$ to an ambient isotopy, define $H : D_r(t) \times [0, 1] \to D_r(t)$ [41, Corollary 4.4.7] by

$$H(v, s) = \begin{cases} (1 - s)p + sq & \text{if } v = p \\ F_{p,(1-s)p+sq}(v) & \text{if } v \neq p, \end{cases}$$

where $F_{p,(1-s)p+sq}$ is a map on $D_r(t)$ analogous to $F_{p,q}$, sending each line segment $[p, b]$ for $b \in \partial D_r(t)$, linearly onto the line segment $[(1 - s)p + sq, b]$.

It is a routine [41, Corollary 4.4.7] to verify that $H(v, s)$ is well defined on the compact set $D_r(t)$, continuous, one-to-one and onto, leaving $\partial D_r(t)$ fixed. We define an ambient isotopy $T_t : \mathbb{R}^2 \times [0, 1] \to \mathbb{R}^2$ on the plane containing $D_r(t)$ by

$$T_t(v, s) = \begin{cases} H(v, s) & \text{if } v \in D_r(t) \\ v & \text{otherwise.} \end{cases}$$

We then define $T : \mathbb{R}^3 \times [0, 1] \to \mathbb{R}^3$ by

$$T(v, s) = \begin{cases} T_t(v, s) & \text{if } v \in D_r(t) \\ v & \text{otherwise.} \end{cases}$$

The fact that the normal discs $D_r(t)$ are disjoint ensures that T is an ambient isotopy [41, Corollary 4.4.8], with compact support of Γ, leaving $\partial\Gamma$ fixed. $\square$

Now we apply this result to a simple, regular, composite, C^1 Bézier curve $\mathcal{B}$ and the control polygon $\mathcal{P}$. As discussed previously, there exists a non-self-intersecting pipe surface [8] of radius r for $\mathcal{B}$, denoted as $S_{\mathcal{B}}(r)$. Denote the non-self-intersecting pipe section determined by $S_{\mathcal{B}}(r)$ as $\Gamma_{\mathcal{B}}$. Also, for each sub-control polygon of $\mathcal{B}$, there exists a corresponding non-self-intersecting pipe sections. Denote the non-self-intersecting pipe section corresponding to the kth control polygon as Γ_k.

Theorem 3.3.4. For any Bézier curve $\mathcal{B}$, sufficiently many subdivisions can be taken so that each sub-control polygon P^k will satisfy *Hypotheses 1* and *2*. Consequently, there will be an ambient isotropy between $\mathcal{B}$ and $\mathcal{P}$ with compact support of $\Gamma_{\mathcal{B}}$, leaving $\partial\Gamma_{\mathcal{B}}$ fixed.

Proof. By Lemma 3.2.2, *Hypotheses 1* and *2* can be achieved by subdivision. Now consider each sub-control polygon P^k satisfying *Hypotheses 1* and *2*, and the corresponding Bézier sub-curves B^k. Use Lemma 3.3.3 to define an ambient isotopy $\Psi_k : \mathbb{R}^3 \times [0,1] \to \mathbb{R}^3$ between B^k and P^k, for each $k \in \{1, 2, \ldots, 2^i\}$. Define $\Psi : \mathbb{R}^3 \times [0,1] \to \mathbb{R}^3$ by the composition

$$\Psi = \Psi_1 \circ \Psi_2 \circ \ldots \circ \Psi_{2^i}.$$

Note that Ψ_k fixes the complement of $\text{int}(\Gamma_k)$, and $\text{int}(\Gamma_k) \cap \text{int}(\Gamma_{k'}) = \emptyset$ for all $k \neq k'$. So the composition Ψ is well defined. Since each Ψ_k is an ambient isotopy, the composition Ψ is an ambient isotopy between $\mathcal{B}$ and $\mathcal{P}$ with compact support of $\Gamma_{\mathcal{B}}$, leaving $\partial\Gamma_{\mathcal{B}}$ fixed. □

Chapter 4

Algorithms and Applications

Now we are poised to establish closed-form formulas to compute the number of subdivision iterations for achieving topological equivalence and isotopic equivalence. As Bézier curves are fundamental representations for geometric modeling, we shall discuss some applications in visualization.

4.1 Sufficient Subdivision Iterations for Homeomorphisms

From the previous sections we know that the homeomorphism and isotopy are obtained by subdivision iterations based on two criteria:

(i) Angular Convergence; and

(ii) convergence in distance.

So the speed of achieving these topological characteristics is determined by the Angular Convergence rate and the convergence rate in distance, which are both exponential. In this section, we further find a numerical lower bound of subdivision iterations to achieve these properties.

Definition 4.1.1. Let P denote a control polygon of a Bézier curve, and let P_x denote an ordered list of all of x-coordinates of P (with similar meaning given to P_y for the y-coordinates and to P_z for the z-coordinates). Let

$$\| \triangle_2 P_x \|_\infty = \max_{0<m<n} |P_{m-1,x} - 2P_{m,x} + P_{m+1,x}|$$

be the maximum absolute second difference of the x-coordinates of control points, (with similar meanings for the y and z coordinates) . Let

$$\Delta_2 P = (\| \triangle_2 P_x \|_\infty, \| \triangle_2 P_y \|_\infty, \| \triangle_2 P_z \|_\infty),$$

(i.e.) a vector with 3 values.

Definition 4.1.2. The **parameter measure distance**[8] [21] between a Bézier curve $\mathcal{B}$ and the control polygon $l(P, i)$ generated by i subdivisions is given by

$$\max_{t\in[0,1]} ||l(P, i)(t) - \mathcal{B}(t)||.$$

Lemma 4.1.3. The parameter measure distance between the Bézier curve and its control polygon after ith-round subdivision is bounded by

$$\frac{1}{2^{2i}} N_\infty(n) ||\Delta_2 P||, \tag{4.1.1}$$

[8]The paper [21] uses 'distance', but we adopt this terminology 'parameter measure distance' instead.

where

$$N_\infty(n) = \frac{\lfloor n/2 \rfloor \cdot \lceil n/2 \rceil}{2n}.$$

Proof. A published lemma [21, Lemma 6.2] proves a similar result restricted to scalar valued polynomials. We consider coordinate-wise and apply this result to the x, y, and z coordinates respectively, so that the distance of the x-coordinates of the Bézier curve and its control polygon after ith-round subdivision is bounded by

$$\frac{1}{2^{2i}} N_\infty(n) \parallel \Delta_2 P_x \parallel_\infty,$$

with similar expressions for the y and z coordinates. Taking the Euclidean norm of the indicated three x, y and z bounds yields Equation 4.1.1, an upper bound of the distance between the Bézier curve and its control polygon after the ith subdivision. □

For convenience, denote the above bound in distance as:

$$B_{dist\_P}(i) := \frac{1}{2^{2i}} N_\infty(n) ||\Delta_2 P||. \tag{4.1.2}$$

Lemma 4.1.4. After i subdivision iterations, the distance between $l'(P, i)$ and $\mathcal{B}'$ is bounded by $B'_{dist\_P}(i)$, where

$$B'_{dist\_P}(i) := \frac{1}{2^{2i}} N_\infty(n-1) ||\Delta_2 P'||, \tag{4.1.3}$$

and P' that consists of $n-1$ control points is the control polygon of $\mathcal{B}'$.

Proof. The derivative $(l'(P,i))$ of the control polygon P is identical to another PL curve. The PL curve is the control polygon $(l(P',i))$ of the Bézier curve's first derivative [6, Lemma 6]. That is, $l'(P,i) = l(P',i)$. Since (Lemma 4.1.3)

$$\max_{t\in[0,1]} ||l(P',i)(t) - \mathcal{B}'(t)|| \leq B'_{dist\_P}(i),$$

we have

$$\max_{t\in[0,1]} ||l'(P,i)(t) - \mathcal{B}'(t)|| \leq B'_{dist\_P}(i). \tag{4.1.4}$$

□

4.1.1 Number of Subdivisions for Small Exterior Angles

Assume ν is a small measure of angle between 0 and π. We shall find how many subdivisions will generate a control polygon such that the measure α of each exterior angle satisfies

$$\alpha < \nu. \tag{4.1.5}$$

Recall the proof of Angular Convergence (Theorem 2.1.2). Consider two arbitrary consecutive derivatives $u_i = l'(P,i)(t_m)$ and $v_i = l'(P,i)(t_{m-1})$ and the corresponding exterior angle α. Recall that in Section 2.1 we had Inequality 2.1.5:

$$1 - \cos(\alpha) \leq \frac{2||v_i - u_i||}{||u_i||}.$$

Recall the proof of Lemma 2.1.1 where Inequality 2.1.2 is:

$$||u_i - v_i||$$

$$\leq ||l'(P,i)(t_m) - \mathcal{B}'(t_m)|| + ||\mathcal{B}'(t_m) - \mathcal{B}'(t_{m-1})|| + ||\mathcal{B}'(t_{m-1}) - l'(P,i)(t_{m-1})||,$$

and Inequality 2.1.4 is

$$||\mathcal{B}'(t_m) - \mathcal{B}'(t_{m-1})|| \leq \sup_{[0,1]} ||\mathcal{B}''(t)|| \cdot |t_m - t_{m-1}| = \frac{\gamma}{n2^i},$$

where $\gamma = \sup_{[0,1]} ||\mathcal{B}''(t)||$. Combining the above inequalities yields

$$1 - \cos(\alpha) \leq \frac{2(||l'(P,i)(t_m) - \mathcal{B}'(t_m)|| + ||\mathcal{B}'(t_{m-1}) - l'(P,i)(t_{m-1})|| + \gamma/(n2^i))}{||u_i||}.$$

Using Lemma 4.1.4 we get

$$1 - \cos(\alpha) \leq \frac{2(2B'_{dist\_P}(i) + \gamma/(n2^i))}{||u_i||}. \tag{4.1.6}$$

Let $\sigma = \min\{||\mathcal{B}'(t)|| : t \in [0,1]\}$. The regularity of $\mathcal{B}$ ensures that $\sigma > 0$ and the continuity of $\mathcal{B}'$ on the compact interval $[0,1]$ ensures that the minimum exists. Recall $u_i = l'(P,i)(t_m)$ for some $t_m \in [0,1]$. So it follows from Inequality 4.1.4 that

$$||\mathcal{B}'(t_m)|| - ||u_i|| \leq B'_{dist\_P}(i).$$

Solving the inequality we get

$$||u_i|| \geq ||\mathcal{B}'(t_m)|| - B'_{dist\_P}(i) \geq \sigma - B'_{dist\_P}(i).$$

In order to have $u_i \neq 0$, it is sufficient to perform enough subdivisions such that

$$||u_i|| \geq \sigma - B'_{dist\_P}(i) > 0,$$

that is $B'_{dist\_P}(i) < \sigma$. By the definition (Equation 4.1.3) of $B'_{dist\_P}(i)$ we set,

$$\frac{1}{2^{2i}} N_\infty(n-1) \parallel \triangle_2 P' \parallel < \sigma.$$

Therefore for $B'_{dist\_P}(i) < \sigma$, it suffices to have[9]

$$i > \frac{1}{2}\log(\frac{N_\infty(n-1) \parallel \triangle_2 P' \parallel}{\sigma}) = N_1. \tag{4.1.7}$$

It is worth noting that N_1 is a subdivision number depending on variables P', n and σ.

After the i subdivision iterations, whenever $i > N_1$, then $B'_{dist\_P}(i) < B'_{dist\_P}(N_1)$, because $B'_{dist\_P}(i)$ is a strictly decreasing function (Equation 4.1.3). So it follows from Inequality 4.1.6 that whenever $i > N_1$,

$$1 - \cos(\alpha) \leq \frac{2(2B'_{dist\_P}(i) + \gamma/(n2^i))}{|\sigma - B'_{dist\_P}(i)|} \leq \frac{2(2B'_{dist\_P}(i) + \gamma/(n2^i))}{\sigma - B_{dist\_P}(N_1)}.$$

To obtain $\alpha < \nu$ (Inequality 4.1.5), it suffices to have that $1 - cos(\alpha) < 1 - cos(\nu)$.

[9]Throughout this thesis, we use log for $\log_2$.

Since $B'_{dist\_P}(i)$ converges to 0 as $i \to \infty$ (Equation 4.1.4), we can choose i large enough so that

$$1 - \cos(\alpha) \leq \frac{2(2B'_{dist\_P}(i) + \gamma/(n2^i))}{\sigma - B'_{dist\_P}(N_1)} < 1 - \cos(\nu). \tag{4.1.8}$$

The second inequality of Inequality 4.1.8 implies that

$$2B'_{dist\_P}(i) + \frac{\gamma}{n2^i} < \frac{1}{2}(1 - \cos(\nu))(\sigma - B'_{dist\_P}(N_1)).$$

We could solve the above inequality for i, but we can avoid this complicated computation by noting that $2B'_{dist\_P}(i)$ is much smaller than $\frac{\gamma}{n2^i}$ when i is large. (Note that $\gamma = \sup_{[0,1]} ||\mathcal{B}''(t)||$. If $\gamma = 0$, then the Bézier curve would be a straight line segment. We exclude this trivial case and assume that $\gamma > 0$.)

So let $2B'_{dist\_P}(i) < \frac{\gamma}{n2^i}$, that is

$$i > \log(\frac{2nN_\infty(n-1) \parallel \triangle_2 P' \parallel}{\gamma}) = N_2. \tag{4.1.9}$$

So for $i > N_2$ we get

$$2B'_{dist\_P}(i) + \frac{\gamma}{n2^i} < 2\frac{\gamma}{n2^i}.$$

Then we consider

$$2\frac{\gamma}{n2^i} < \frac{1}{2}(1 - \cos(\nu))(\sigma - B'_{dist\_P}(N_1)). \tag{4.1.10}$$

Solving Inequality 4.1.10 we get

$$\frac{1}{2^i} < \frac{n}{4\gamma}(1-\cos(\nu))(\sigma - B'_{dist\_P}(N_1))$$

and

$$i > \log(\frac{1}{\frac{n}{4\gamma}(1-\cos(\nu))(\sigma - B'_{dist\_P}(N_1))}).$$

To simplify this expression, let

$$c_{\mathcal{B}} = \frac{1}{\frac{n}{4\gamma}(\sigma - B'_{dist\_P}(N_1))},$$

which is a constant for a given $\mathcal{B}$, and

$$f(\nu) = \frac{c_{\mathcal{B}}}{1-\cos\nu}. \tag{4.1.11}$$

Then, we have

$$i > \log(f(\nu)).$$

Theorem 4.1.5. Given any $\nu > 0$, there exists an integer $N(\nu)$ defined by

$$N(\nu) = \max\{N_1, N_2, \log(f(\nu))\} \tag{4.1.12}$$

where N_1, N_2 and $f(\nu)$ are given by Equations 4.1.7 4.1.9 and 4.1.11 respectively, such that each exterior angle is less than ν, whenever $i > N(\nu)$.

Proof. It follows from the definitions of N_1, N_2 and $f(\nu)$ and the analysis in this section. □

It is worth noting that $N(\nu)$ is a logarithmic function depending on an upper bound variable ν as well as several other parameters including γ, σ, $N_\infty(n)$ and $\triangle_2 P'$.

4.1.2 Sufficient subdivision iterations for homeomorphisms

For a regular Bézier curve $\mathcal{B}$ of degree 1 or 2, the control polygon is trivially[10] ambient isotopic to $\mathcal{B}$. We consider $n \geq 3$.

Given any $\nu > 0$, Theorem 4.1.5 shows that there exists an integer $N(\nu)$, such that each exterior angle is less than ν after $N(\nu)$. Furthermore, there is an explicit closed formula to compute $N(\nu)$.

Theorem 4.1.6. There exists a positive integer, $N(\frac{\pi}{n-1})$ for $n > 2$, where $N(\frac{\pi}{n-1})$ is defined by Equation 4.1.12, such that after $N(\frac{\pi}{n-1})$ subdivisions, each sub-control polygon will be simple.

Proof. By Theorem 4.1.5, after $N(\frac{\pi}{n-1})$ subdivisions, each exterior angle is less than $\frac{\pi}{n-1}$. Since each sub-control polygon has a $n-1$ exterior angles, the total curvature of each sub-control polygon is less than π. Lemma 2.2.1 implies that this is a sufficient condition for each sub-control polygon being simple.

□

[10]For degree 1, both the curve and the polygon are either a point or a line segment. For degree 2, there are three points. The curve and the polygon are planar and open (otherwise the curve is not regular).

While existence of sufficiently many iterations for the control polygon to fit inside the pipe $S_r(\mathcal{B})$ has been established, it remains of interest to bound the number of subdivisions that are sufficient for this containment. Define $N'(r)$ by

$$N'(r) = \frac{1}{2}\log(\frac{N_\infty(n)||\Delta_2 P||}{r}), \tag{4.1.13}$$

where r is the radius of a non-self-intersecting pipe surface for $\mathcal{B}$. Thus we have $B_{dist\_P}(i) < r$ whenever $i > N'(r)$, by the definition of $B_{dist\_P}(i)$ (Equation 4.1.2) and Equation 4.1.13.

Lemma 4.1.7. The control polygon generated by i subdivisions, where $i > N'(r)$ with $N'(r)$ being given by Equation 4.1.13, satisfies

$$\max_{t\in[0,1]} ||\mathcal{B}(t) - l(P,i)(t)|| < r,$$

and therefore fits inside the non-self-intersecting pipe surface of radius r for $\mathcal{B}$.

Proof. By Lemma 4.1.3, $\max_{t\in[0,1]} ||\mathcal{B}(t) - l(P,i)(t)|| \leq B_{dist\_P}(i)$. Then this lemma follows from the definition of $N'(r)$ given by Equation 4.1.13. □

While Theorem 4.1.6 addresses each sub-control polygon, Theorem 4.1.8 has the stronger result that the union of all these sub-control polygons remains simple.

Theorem 4.1.8. Take any $N \geq \max\{N(\frac{\pi}{2(n-1)}), N'(r)\}$, where $N(\cdot)$ is defined by Equations 4.1.12 and $N'(r)$ is given by Equation 4.1.13. Then after the Nth subdivision, the control polygon will be simple.

Proof. The inequality $N \geq N'(r)$ implies that the control polygon generated after the Nth subdivision lies inside the pipe. The inequality $N \geq N(\frac{\pi}{2(n-1)})$ ensures that the total curvature of its each sub-control polygon is less than $\frac{\pi}{2}$. These two conditions are sufficient conditions for the control polygon to be simple (The proof of Theorem 2.2.9). □

4.2 Subdivision Iterations for Ambient Isotopies

Recall that the ambient isotopy given by Theorem 2.3.5 relies upon the containment of convex hulls by a non-self-intersecting pipe surface, while the ambient isotopy defined by Theorem 3.3.4 does not require this containment. We shall find the lower bounds of subdivision iterations for these two cases respectively.

4.2.1 Number of Subdivisions for Isotopy with Convex Hulls

Now we consider how many subdivision iterations are need to achieve the ambient isotopy defined by Theorem 2.3.5. In order to generate a control polygon ambient isotopic to $\mathcal{B}$, sufficiently small total curvatures and sufficiently small distance between the control polygon and $\mathcal{B}$ are enough. Small total curvatures are provided by taking $N(\frac{\pi}{2(n-1)})$ (Equation 4.1.12) subdivisions. So here we consider the number of subdivisions to ensure the distance criteria.

The following lemma from the paper [17] indicates the distance of any two consecutive vertices of control polygons converges to 0 under subdivision.

Lemma 4.2.1. [17, Lemma 2.5] For any two consecutive vertices R and Q of the corresponding control polygon after i subdivision iterations we have

$$||R - Q|| \leq \frac{M}{2^i}$$

where $M = \max_{j\in\{1,2,\cdots,n\}}\{||P_j - P_{j-1}||\}$, P_j and P_{j-1} are two connected control points of the initial control polygon before performing subdivision.

Lemma 4.2.2. The convex hull $\mathbf{CH}(P^k)$ of each sub-control polygon P^k will be contained in the corresponding non-self-intersecting pipe section Γ_k after the ith subdivision, where i is large enough such that $\frac{Mn}{2^i} < \frac{r}{2}$. That is

$$i > \log(\frac{2Mn}{r}) = \hat{N}. \tag{4.2.1}$$

Proof. Consider the sphere with the center to be the initial control point of the sub-control polygon and radius to be $\frac{r}{2}$. Using Lemma 4.2.1 we get that the distance between the center and any vertex of this sub-control polygon is less than $\frac{Mn}{2^i}$ and hence less than $\frac{r}{2}$ by the hypothesis. So the sphere contains all of the vertices and furthermore its convex hull. By the convex hull property [11] of $\mathcal{B}$, the corresponding sub-curve of $\mathcal{B}$ is contained in the sphere. So the maximal distance between the sub-curve and the boundary of the sphere is less than r. Since the distance between the sub-curve and $S_r(c)$ is r, the sphere lies inside S_r and consequently the convex hull fits inside $S_r(c)$. □

Theorem 4.2.3. There exists a positive integer M, such that after the Mth subdivision, the control polygon will be ambient isotopic to the Bézier curve $\mathcal{B}$. Furthermore, there is an explicit closed formula to compute M.

Proof. Take $M = \max\{N(\frac{\pi}{2(n-1)}), \hat{N}\}$, where $N(\cdot)$ is defined in Equations 4.1.12 and $\hat{N}$ is given by Equations 4.2.1. Then after the Mth subdivision, the control polygon will be ambient isotopic to the Bézier curve $\mathcal{B}$, as follows from the above Lemma 4.2.2 and Theorem 2.3.5. □

4.2.2 Number of Subdivisions for The Isotopy without Convex Hulls

Now we consider sufficient numbers of subdivision iterations to achieve the ambient isotopy defined by Theorem 3.3.4. By Theorem 3.3.4, we shall have a control polygon that satisfies *Hypotheses 1* and *2*. The number of subdivisions for *Hypothesis 1* is given by Lemma 4.1.7. To obtain the number of subdivisions for *Hypothesis 2*, we consider the following lemmas, for which we let $\mathcal{P}'(t) = l'(P, i)(t)$ (the first derivative of the control polygon $\mathcal{P}$), and denote the angle between $\mathcal{B}'(t)$ and $\mathcal{P}'(t)$ as $\theta(t)$, for $t \in [0, 1]$.

Lemma 4.2.4. For any $0 < \nu < \frac{\pi}{2}$, let $N(\nu)$ be the value given by Equation 4.1.12, then after $N(\nu)$ subdivisions, we have $\max_{t\in[0,1]} \theta(t) < \nu$.

Proof. Note (similarly as Inequality 2.1.5)

$$1 - \cos(\theta(t)) = 1 - \frac{\mathcal{B}'(t) \cdot \mathcal{P}'(t)}{||\mathcal{B}'(t)|| \cdot ||\mathcal{P}'(t)||}$$

$$= \frac{||\mathcal{B}'(t)|| \cdot ||\mathcal{P}'(t)|| - \mathcal{P}'(t) \cdot \mathcal{P}'(t) + \mathcal{P}'(t) \cdot \mathcal{P}'(t) - \mathcal{B}'(t) \cdot \mathcal{P}'(t)}{||\mathcal{B}'(t)|| \cdot ||\mathcal{P}'(t)||}$$

$$\leq \frac{||\mathcal{B}'(t)|| - ||\mathcal{P}'(t)||}{||\mathcal{B}'(t)||} + \frac{||\mathcal{B}'(t) - \mathcal{P}'(t)||}{||\mathcal{B}'(t)||} \leq \frac{2||\mathcal{B}'(t) - \mathcal{P}'(t)||}{\sigma},$$

where $\sigma = \min\{||\mathcal{B}'(t)|| : t \in [0,1]\}$ (Recall $\sigma > 0$.) By Inequality 4.1.4

$$\max_{t\in[0,1]} ||\mathcal{B}'(t) - \mathcal{P}'(t)|| \leq B'_{dist\_P}(i),$$

we have

$$1 - \cos(\theta(t)) \leq \frac{2B'_{dist\_P}(i)}{\sigma}.$$

Recalling Inequality 4.1.8 (Note that Inequality 4.1.8 is valid for $i > N(\nu)$), as

$$\frac{2(2B'_{dist\_P}(i) + \gamma/(n2^i))}{\sigma - B'_{dist\_P}(N_1)} < 1 - \cos(\nu),$$

we get

$$1 - \cos(\theta(t)) \leq \frac{2B'_{dist\_P}(i)}{\sigma}$$

$$< \frac{2(2B'_{dist\_P}(i) + \gamma/(n2^i))}{\sigma - B'_{dist\_P}(N_1)} < 1 - \cos(\nu).$$

So $\cos(\theta(t)) > \cos(\nu)$. Note that $0 \leq \theta(t) \leq \pi$, and $0 < \nu < \frac{\pi}{2}$ by the hypothesis. Since $\cos x$ for $x \in [0, \frac{\pi}{2}]$ is monotonically decreasing, we have $\theta(t) < \nu$. This is true for all $t \in [0,1]$, so $\max_{t\in[0,1]} \theta(t) < \nu$. □

Lemma 4.2.5. Performing $N(\frac{\pi}{2n})$ subdivisions will yield a control polygon $\mathcal{P}$ with each sub-control P^k satisfying *Hypothesis 2*:

$$T_\kappa(P^k) + \max_{t\in[0,1]} \theta(t) < \frac{\pi}{2}.$$

Proof. Recall that $N(\frac{\pi}{2n})$ given by Equation 4.1.12 is a sufficient number of subdivisions to produce $\mathcal{P}$ such that all exterior angles are less than $\frac{\pi}{2n}$, as shown by Theorem 4.1.5. Note that each P^k has $n-1$ exterior angles. So after $N(\frac{\pi}{2n})$ subdivisions, we have

$$T_\kappa(P^k) < \frac{\pi(n-1)}{2n}.$$

By Lemma 4.2.4, after $N(\frac{\pi}{2n})$ subdivisions, we also have $\max_{t\in[0,1]} \theta(t) < \frac{\pi}{2n}$. Finally, after $N(\frac{\pi}{2n})$ subdivisions, we obtain

$$T_\kappa(P^k) + \max_{t\in[0,1]} \theta(t) < \frac{\pi(n-1)}{2n} + \frac{\pi}{2n} = \frac{\pi}{2}.$$

□

Let

$$N^\star = \max\{N(\frac{\pi}{2n}), N'(r)\}, \tag{4.2.2}$$

where r is the radius of $S_r(\mathcal{B})$, $N(\cdot)$ is defined by Equations 4.1.12 and $N'(r)$ is given by Equation 4.1.13.

Theorem 4.2.6. Performing $N^\star$ or more subdivisions, where $N^\star$ is given by Equation 4.2.2, will produce an ambient isotopic $\mathcal{P}$ for $\mathcal{B}$.

Proof. By Lemma 4.1.7 *Hypothesis 1* is satisfied after $N'(r)$ subdivisions. By Lemma 4.2.5, *Hypothesis 2* is satisfied after $N(\frac{\pi}{2n})$ subdivisions. Then Theorem 3.3.4 can be applied to draw the conclusion. □

Before formulating *Hypothesis 2*, we considered $T_\kappa(P^k) < \frac{\pi}{2}$, as a more natural criterion, but we could not establish the results based on this weaker condition. However, *Hypothesis 2* uses just one more subdivision than the weaker condition, as shown below.

Remark 4.2.7. The sufficient number of subdivisions for *Hypothesis 2* is at most one more than that for the weaker condition $T_\kappa(P^k) < \frac{\pi}{2}$.

Proof. By the above proof of Lemma 4.2.5 we know that $N(\frac{\pi}{2(n-1)})$ subdivisions are sufficient to guarantee $T_\kappa(P^k) < \frac{\pi}{2}$, while $N(\frac{\pi}{2n})$ subdivisions are sufficient to obtain $T_\kappa(P^k)+\max_{t\in[0,1]}\theta(t) < \frac{\pi}{2}$. The function $N(\cdot)$ is given by Equation 4.1.12, that is,

$$N(\nu) = \max\{N_1, N_2, \log(f(\nu))\},$$

where N_1 and N_2 are constants for a given $\mathcal{B}$, and the function $f(\cdot)$ is defined by Equation 4.1.11:

$$f(\nu) = \frac{c_{\mathcal{B}}}{1-\cos\nu},$$

where $c_{\mathcal{B}}$ is a constant. Note that,

$$N(\frac{\pi}{2(n-1)}) = \max\{N_1, N_2, \log(f(\frac{\pi}{2(n-1)}))\}$$

and

$$N(\frac{\pi}{2n}) = \max\{N_1, N_2, \log(f(\frac{\pi}{2n}))\}.$$

To compare $N(\frac{\pi}{2(n-1)})$ with $N(\frac{\pi}{2n})$, we consider

$$\log(f(\frac{\pi}{2n})) - \log(f(\frac{\pi}{2(n-1)})) = \log \frac{f(\frac{\pi}{2n})}{f(\frac{\pi}{2(n-1)})} = \log \frac{1-\cos(\frac{\pi}{2(n-1)})}{1-\cos(\frac{\pi}{2n})}.$$

As before, we consider only $n \geq 3$ and the expression inside the logarithm as the function:

$$\frac{1-\cos(\frac{\pi}{2(x-1)})}{1-\cos(\frac{\pi}{2x})}.$$

Since its derivative is negative for $x \geq 3$, we have that

$$\log(f(\frac{\pi}{2n})) - \log(f(\frac{\pi}{2(n-1)})) \leq \log \frac{1-\cos(\frac{\pi}{2(3-1)})}{1-\cos(\frac{\pi}{2\cdot 3})} \approx 0.78.$$

This implies that

$$N(\frac{\pi}{2n}) - N(\frac{\pi}{2(n-1)}) < 1,$$

for any $n \geq 3$. □

Remark 4.2.8. Theorem 4.2.3 gives the number ($N = \max\{N(\frac{\pi}{2(n-1)}), \hat{N}\}$) of subdivision for an ambient isotopy with convex hulls, while Theorem 4.2.6 provides the number ($N^\star = \max\{N(\frac{\pi}{2n}), N'(r)\}$) for an ambient isotopy without convex hull. Note first by the above Remark 4.2.7 that $N(\frac{\pi}{2n})$ is at most one more than $N(\frac{\pi}{2(n-1)})$. However, observe that $\hat{N} = \log(\frac{2Mn}{r})$ (Equation 4.2.1) and $N'(r) = \frac{1}{2}\log(\frac{N_\infty(n)||\Delta_2 P||}{r})$ (Equation 4.1.13). It is a tedious but elementary exercise to show that $\hat{N}$ is much larger than $N'(r)$, especially when n is large. So in many cases, especially for high degree Bézier curves, N (with convex hulls) is much larger than $N^\star$ (without convex hulls).

4.3 Applications to Visualization and Simulations

Computer-aided geometric design (CAGD) is the process of using computer technology to create and visualize geometric models for iterative design simulations. Bézier curves are particularly popular in computer visualization because of the simplicity of their construction and their capability of approximating complex curves.

4.3.1 Molecular visualization and simulations

An ongoing industrial collaboration [40, 54] models molecular structure (Figure 4.3.1 shows[11] an example) by Bézier curves using the control polygons to approximate the Bézier curves. A fundamental requirement during the approximation is the equivalence under ambient isotopy. Our ambient isotopy theorem

[11] Image credit: http://domino.research.ibm.com/comm/pr.nsf/pages/rscd.bluegenepicaa.html.

serves as a theoretical foundation for this application.

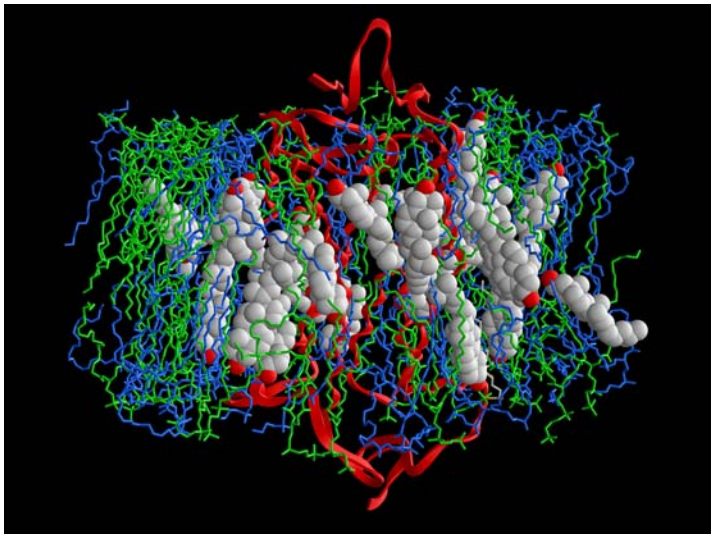

Figure 4.3.1: A molecule in computer visualization

Large molecules may have in excess of ten thousand atoms. Algorithmic efficiency is a practical concern in designing simulation programs. We showed in previous sections that the number of subdivisions to achieve ambient isotopy is based on Angular Convergence (Theorem 2.1.2) and the convergence in terms of distance, and both of the convergence rates are exponential, a promising theoretical indication of efficiency, which will be tested in practical experiments.

4.3.2 Preserving topological integrity during molecular dynamics

For chemical simulations of macro-molecules, the HPC algorithms will produce voluminous numerical data describing how the molecule twists and writhes under local chemical and kinetic changes. These are reflected in changed co-ordinates of the geometric model, called perturbations. To produce a scientifically valid visualization, it is crucial that topological artifacts are not introduced by the

curve approximations used for rendering within the dynamic visualizations of these perturbations [36].

From the proof of ambient isotopy and the algorithm presented in Section 4.1, we have two criteria which jointly guarantee homeomorphism and ambient isotopy:

(1) $\max_{t\in[0,1]} ||\mathcal{B}(t) - \mathcal{P}(t)| < r$, where r is the radius of a non-self-intersecting pipe surface of $\mathcal{B}$.

(2) $T_\kappa(\mathcal{P}) + \max_{t\in[0,1]} \theta(t) < \frac{\pi}{2}$, where $T_\kappa(\mathcal{P})$ is the total curvature of $\mathcal{P}$ and $\theta(t)$ is the exterior angle between $\mathcal{B}'(t)$ and $\mathcal{P}'(t)$.

When static ambient isotopic curves are perturbed, the perturbation may destroy their isotopic equivalence. However, the above two criteria imply: if the perturbed curve remains inside of the non-self-intersecting pipe surface of radius r, and the change of exterior angles is small such the the above (2) is satisfied, then the perturbation does not change the equivalence relation.

Chapter 5

Visualization for Topology Counterexamples

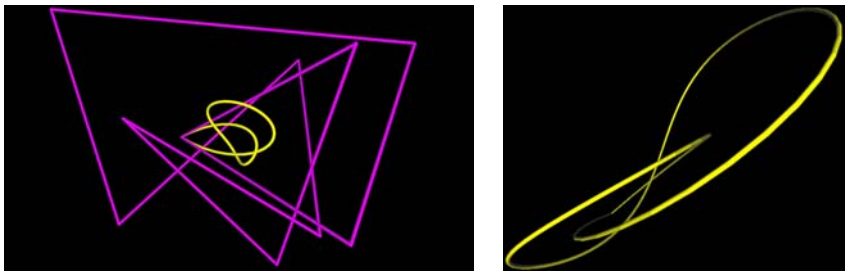

(a) Unknotted **P** with knotted **B** (b) Zoomed-in view of **B**

Figure 5.0.1: Unknotted **P** with knotted **B**

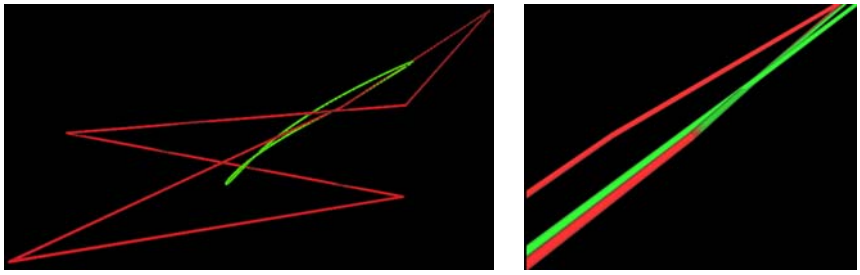

(a) Equilateral **P** vs. Intersecting **B** (b) Zoomed-in intersection

Figure 5.0.2: Equilateral, simple **P** with self-intersecting **B**

This work in Chapter 5, undertaken for this dissertation, has already been published [40]. The ideas presented here from general topology, geometric topology and knot theory are complemented by numeric arguments in a novel integration of the 'pure' field of topology with the 'applied' focus of numerical analysis. Additionally, aspects of computer visualization and graphics were vital to formulating

conjectures, with principles from those disciplines incorporated into the finalized proofs.

5.1 Introduction

We restrict our attention to a closed Bézier curve $\mathbf{B}$ and the associated closed control polygon $\mathbf{P}$. As $\mathbf{B}$ is created from $\mathbf{P}$, it is natural to ask which topological characteristics are shared by these two curves, particularly as the control polygon often serves as an approximation to the Bézier curve in many practical applications. However, topological differences between a Bézier curve and its control polygon can exist and it is natural to develop counterexamples to show these topological differences. These counterexamples extend beyond related results [23, 31], while we introduce new computational methods to generate additional counterexamples.

In Section 5.2, we present a counterexample of a Bézier curve and its control polygon being homeomorphic, yet not ambient isotopic. To develop this counterexample, we created and used a computer visualization tool, called *Knot_Spline_Vis* [30], to study topological relationships between a Bézier curve and its control polygon. We viewed the images to motivate formal proofs, which also rely on numerical analysis and geometric arguments.

Using the *Knot_Spline_Vis* [30] visualization tool, we viewed many examples where the Bézier curve was simple, while its control polygon was equilateral and simple. It is well-known that a Bézier curve can be self-intersecting even when

its control polygon is simple, but we conjectured that the additional hypothesis of an equilateral control polygon resulted in both curves being simple. While this visual evidence was suggestive, we present a general numerical approach in Section 5.3 that supports a contrary conclusion. This is particularly relevant for computer graphics as a foundation for appropriate approximation over this class of control polygons, even while we have not yet found a theoretical, infinite precision counterexample.

We exhibit the self-intersection by a numerical method, which finds the roots of a system of equations. We freely admit that these roots are not determined with infinite precision, but such calculations on polynomials of degree 6, as used in these examples, typically elude precise calculation. We argue [40] that there are two primary values of our method for these approximated solutions:

(i) as a catalyst to alternative examples that may admit precision calculation and rigorous topological proofs, and

(ii) as having specified digits of accuracy, often of primary interest in computational mathematics.

A legitimate concern is whether the numerical approximation produces coordinates for a 'near' intersection, subject to the accuracy of the floating point computation. We cannot refute that possibility, but we argue that in the context of graphical images, the level of approximation produced is often sufficient. In particular, we have parameters in the code to adjust the number of digits of

accuracy. This level of user-defined precision is often accepted as sufficient for visualization [38]. The user can then set the graphical resolution so that points that are determined to be the same within some acceptable numerical tolerance will also appear within the same pixel.

5.2 Unknotted P with Knotted B

In order to produce a knotted Bézier curve with an unknotted control polygon, we invoked *Knot_Spline_Vis* [30] with an example (Figure 5.2.1) of an unknotted Bézier curve, where the total curvature appeared[12] to be larger than 4π. (The total curvature being larger than 4π is a necessary condition of knottedness.) We

(a) Unknotted **B** & The **P** (b) Zoomed-in View of **B**

Figure 5.2.1: Visual experiments

experimented on this example by moving control points to construct a Bézier curve that visually appeared to be knotted. We then moved control points to unknot the control polygon while keeping the Bézier curve knotted. In the end we obtained a Bézier curve and the control polygon (of degree 10) (Figure 5.0.1(a))

[12]The careful use of 'appeared' throughout this section is to emphasize the approximations inherent in visualization, leaving open the question of corresponding theoretical proofs for examples under infinite precision.

defined by the control points $\{P_0, P_1, \cdots, P_9, P_0\}$ listed below:

$$(-5.9, 4.7, -6.2), (10.3, -1.1, 8.9), (-2.6, -12.4, -6.3), (-10, 7, -0.3),$$

$$(1.9, -12, -0.6), (11.2, 7.5, -7.6), (-15.3, -1.7, -4.1), (-11.7, 20, 3.5),$$

$$(17.9, -1.1, 2.9), (2.9, -13.7, 4.8), (-5.9, 4.7, -6.2).$$

The 3D visualization offers only suggestive evidence that the above Bézier curve is knotted while the control polygon is unknotted. We provide rigorous mathematical proofs of these properties in Sections 5.2.1 and 5.2.2. Generally, proving knottedness or unknottedness can be difficult [26], but is accessible for the counterexample here.

5.2.1 Proofs of the Bézier curve being knotted

We prove that the Bézier curve is a trefoil[13]. We orthogonally project the curve onto x-y plane. We then show, numerically, that there are three self-intersections in the projection and these intersections are alternating crossings in 3D. Since projections preserve self-intersections, this curve can have no more than 3 self-intersections, but these self-intersections in x-y plane are shown to have pre-images that are 3D crossings, so the original curve has no self-intersections.

Since the 2D curve in Figure 5.2.2 has degree 10, we use a numerical method implemented by MATLAB function 'fminsearch' to find the parameters where

[13]A trefoil is a knot with three alternating crossings [2].

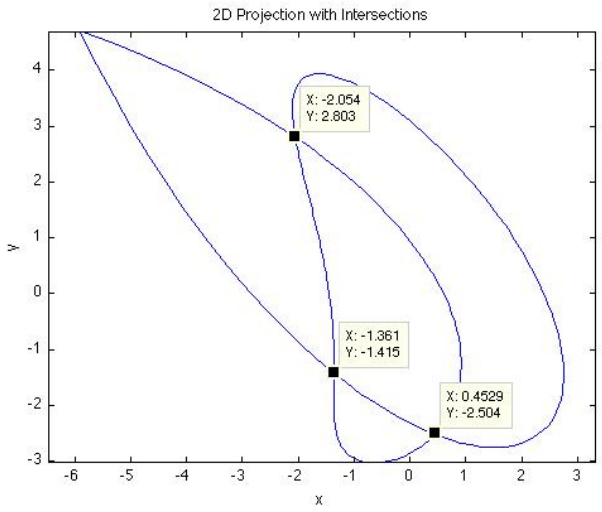

Figure 5.2.2: The 2D projection of the knot

the curve intersects with itself. We provide the numerical codes in Appendix A.1, and we provide the data used to find these parameters in Appendix A.3. The pairs of parameters (labeled in order as $t_1, \ldots, t_6$) of the self-intersections are listed below:

$$[t_1 = 0.0306, t_4 = 0.5573], [t_2 = 0.1573, t_5 = 0.9244], [t_3 = 0.3731, t_6 = 0.9493].$$

Next we prove that these 2D intersections are projections from three alternating crossings in 3D. The above parameters are substituted into the Bézier curve to get pairs of points (numerical codes for this calculation are in Appendix A.2):

$$[\mathbf{B}(t_1) = (-2.0539, 2.8001, -2.6929), \mathbf{B}(t_4) = (-2.0530, 2.7987, -2.0143)],$$

$$[\mathbf{B}(t_2) = (0.4376, -2.5212, -0.0576), \mathbf{B}(t_5) = (-0.4364, -2.5206, -0.5547)],$$

$$[\mathbf{B}(t_3) = (-1.3613, -1.4239, -2.2944), \mathbf{B}(t_6) = (-1.3624, -1.4232, -1.9067)].$$

The alternating crossings follow from comparing the z-coordinates in each pair. Precisely, according to the parameters given above, the tracing of the six points in order is

$$\mathbf{B}(t_1), \mathbf{B}(t_2), \mathbf{B}(t_3), \mathbf{B}(t_4), \mathbf{B}(t_5), \mathbf{B}(t_6),$$

and the crossings at these points are

$$\textit{under}, \textit{over}, \textit{under}, \textit{over}, \textit{under}, \textit{over},$$

allowing the trefoil conclusion.

5.2.2 Proof of the control polygon being unknotted

To prove that the control polygon $P = (P_0, P_1, \cdots, P_9, P_0)$ is an unknot, it is necessary to show that P is simple and unknotted. We directly tested each pair of segments of P for non-self-intersection and those calculations can be repeated by the interested reader. We prove unknottedness using a 3D *push*, as the obvious generalization of a 2D function from low-dimensional geometric topology [25]. We restrict attention to a *median push* (Definition 2.3.3). The full sequence of 5 median pushes is explicated, where the first 4 median pushes are equivalently described by Reidemeister moves [2]. After introducing the pushes, we show that each push is also an ambient isotopy.

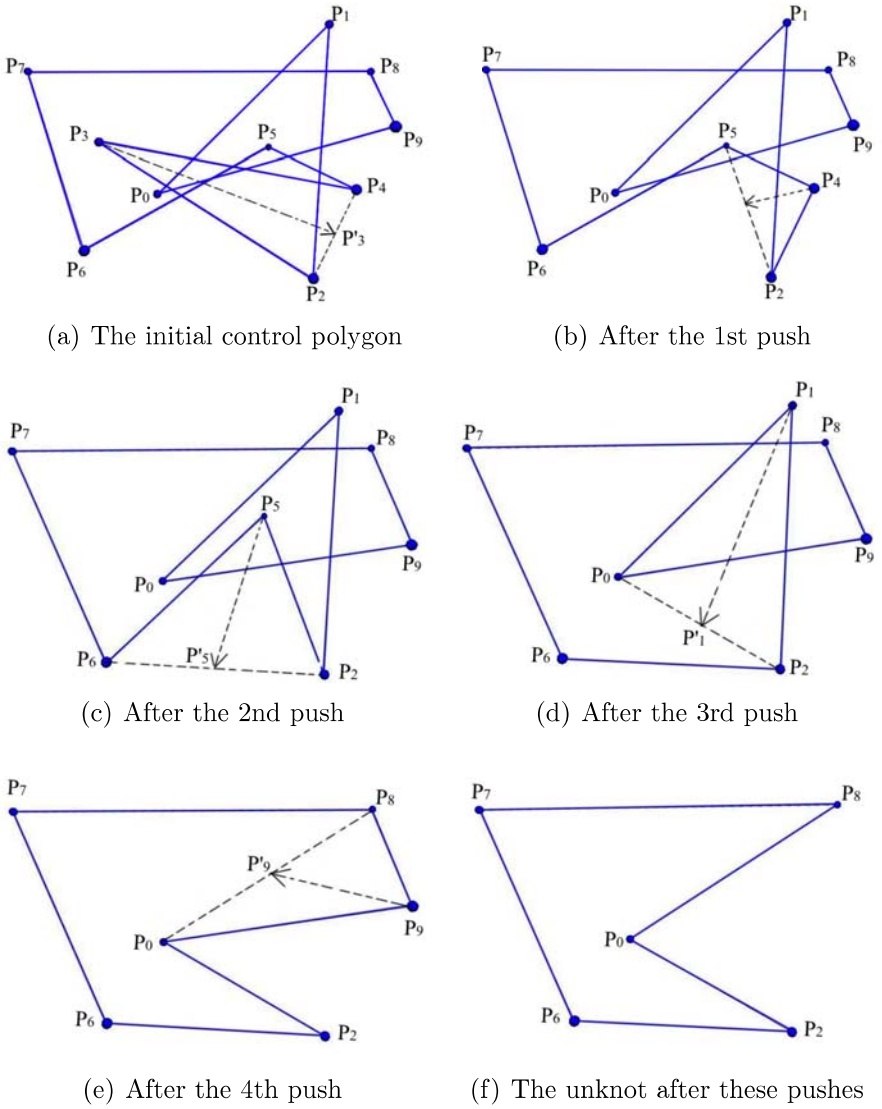

(a) The initial control polygon (b) After the 1st push

(c) After the 2nd push (d) After the 3rd push

(e) After the 4th push (f) The unknot after these pushes

Figure 5.2.3: Pushes and PL curves in 3D

We depict the sequence of pushes used in Figure 5.2.3, showing the 3D graphs of the PL space curves after the median pushes. These graphs show, at each step, which vertex is pushed and its image. For example, in Figure 5.2.3(a), the vertex P_3 is pushed to P_3' and the resultant polygon after this push is shown by Figure 5.2.3(b). Figures 5.2.3(a) 5.2.3(b) 5.2.3(c) and 5.2.3(d) have corresponding Reidemeister moves, as those pushes eliminate at least one crossing.

Using the published notation [2], Figure 5.2.3(a) depicts a Reidemeister move of Type 2b. Similarly, Figure 5.2.3(b) depicts a Reidemeister move of Type 1b; Figure 5.2.3(c) has Type 2b and Figure 5.2.3(d) has a move of Type 2b, followed by a move of Type 1b. The final push to achieve Figure 5.2.3(f) does not correspond to any Reidemeister move as no crossings are changed, but it is included to have a polygon with only five edges, which necessarily must be the unknot [39].

We prove that P is unknotted by showing that P is ambient isotopic to the unknotted PL curve shown in Figure 5.2.3(f). As a sufficient condition, we show that the pushes do not cause intersections [16]. (We gained significant intuition for specifying the sequence of pushes by visual verification with our 3D graphics software capabilities to translate, rotate and zoom the images.) We now present the formal arguments.

Consider Figure 5.2.3(a), where P_3 is pushed to P_3' (the middle point[14] of $\overrightarrow{P_2P_4}$). We show that any segments other than $\overrightarrow{P_2P_3}$ and $\overrightarrow{P_3P_4}$ of P do not intersect the triangle $\triangle P_2P_3P_4$ or the triangle interior.

We parameterize each segment by:

$$\overrightarrow{P_iP_{i+1}} : P_i + (P_{i+1} - P_i)t,\ t \in [0,1]$$

for $i = 0, 1, \cdots, 9$ and let $P_{10} = P_0$. Then the points given by

$$P_3 + a(P_2 - P_3) + b(P_4 - P_3),$$

[14]It is not necessary to push P_3 to the middle point. Any point along $\overrightarrow{P_2P_4}$ would suffice.

for $a, b \geq 0$ and $a+b \leq 1$ are on the $\triangle P_2P_3P_4$ and contained in its interior. Hence $P_i + (P_{i+1} - P_i)t$ intersects $\triangle P_2P_3P_4$ or its interior if and only if

$$P_i + (P_{i+1} - P_i)t = P_3 + a(P_2 - P_3) + b(P_4 - P_3) \tag{5.2.1}$$

has a solution for some $t \in [0, 1]$ and $a, b \geq 0$ and $a + b \leq 1$.

For each $i = 0, 1, \cdots, 9$, we solve Equation 5.2.1 (a system of 3 linear equations) for a, b and t with the above constraints. Calculations show there is no solution for each system, and hence $P_i + (P_{i+1} - P_i)t$ does not intersect $\triangle P_2P_3P_4$ or its interior for each $i = 0, 1, \cdots, 9$. Thus it follows that the push does not cause any intersections.

Similar computations verify that the other pushes do not cause any intersections, thus establishing the ambient isotopy.

5.3 Equilateral, Simple P with Self-intersecting B

We visualized many cases of equilateral control polygons[15] that all had simple Bézier curves. Prompted by this visual evidence, we conjectured that any equilateral control had a simple Bézier curve, where some examples are shown in Figure 5.3.1.

We now present numerical evidence to the contrary. As noted in Section 5.1, the degree 6 polynomials make precise computation difficult, so we do not provide a completely formal proof, independent of numerical methods.

[15]Throughout this section, all control polygons are simple.

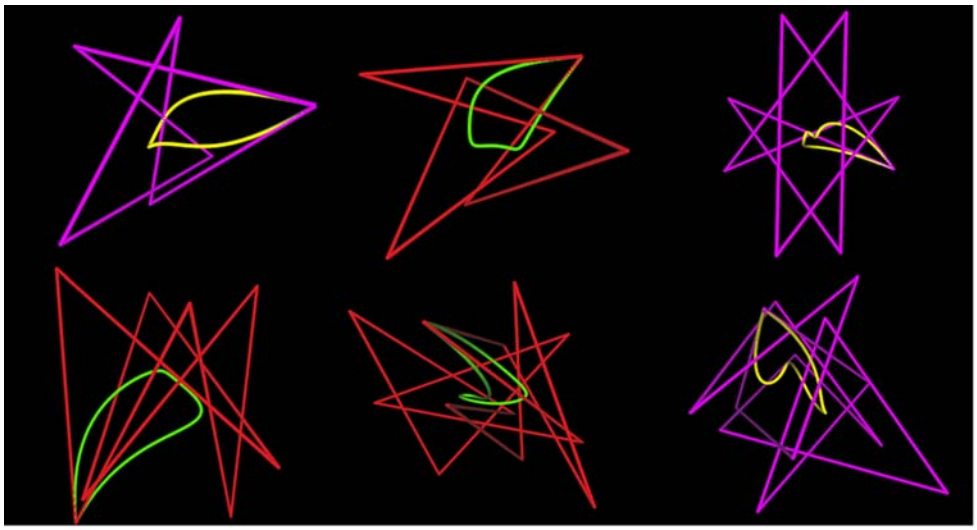

Figure 5.3.1: Simple Bézier curves with equilateral control polygons

5.3.1 Intuitive overview

We created many examples to test and retained only those that satisfy all three criteria listed in Section 5.3.4. We begin the creation of a closed equilateral polygon by setting $P_0 = (0, 0, 0)$. We then take $\{q_0, q_1, \cdots, q_{n-1}\}$ (Equation 5.3.3) from the unit sphere so that

$$P_1 = P_0 + q_0, \quad P_2 = P_1 + q_1, \quad \cdots, \quad P_n = P_{n-1} + q_{n-1}.$$

We ensure that the polygon is closed in Section 5.3.4 item (3).

We consider a sufficient and necessary condition for a Bézier curve being self-intersecting (Equation 5.3.2). Since we want the equilateral polygon to define a Bézier curve that is self-intersecting, we not only select $\{q_0, q_1, \cdots, q_{n-1}\}$ from the unit sphere as above, but also select them such that Equation 5.3.2 is zero for some

parameters s and t. Consequently the set of control points generated determines a closed equilateral control polygon and a self-intersecting Bézier curve.

5.3.2 Necessary and sufficient condition for self-intersection

We rely upon the following published equation [22] for sufficient and necessary conditions for self-intersection of a Bézier curve

$$S(s,t) = \frac{1}{n}\frac{\mathbf{B}(1-s) - \mathbf{B}(t)}{(1-s) - t}, \tag{5.3.1}$$

with the domain $D = \{(s,t) : s + t < 1, s, t \geq 0, (s,t) \neq (0,0)\}$. A Bézier curve defined by $\mathbf{B}(t)$ is self-intersecting if and only if there exist s and t in the domain D such that $S(s,t) = 0$, , with an alternative formulation[16] given by

$$S(s,t) = \frac{1}{n}\sum_{i=0}^{n-1}\sum_{j=0}^{n-1-i}\binom{n-1-i}{j}s^{n-1-i-j}(1-s)^j\sum_{k=0}^{i}\binom{i}{k}(1-t)^{i-k}t^k q_{j+k}, \tag{5.3.2}$$

where

$$q_i = P_{i+1} - P_i \quad for\ i = \{0, 1, \cdots, n-1\}. \tag{5.3.3}$$

5.3.3 A representative counterexample generated

We present a single numerical counterexample, noting that while only one counterexample is presented, the numerical algorithm implemented can be used to

[16] One needs to write out the [22, Equation (6)] to obtain Equation 5.3.2.

find many such examples. We list six distinct control points (the seventh control point is equal to the first control point) that determine an equilateral simple $\mathbf{P}$ and a self-intersecting $\mathbf{B}$ (shown in Figure 5.0.2), as generated by the algorithm described in detail in Section 5.3.4.

$$(0,0,0),(0.0305,0.0810,0.9962),(-0.2074,-0.2671,1.9030),$$

$$(-0.1792,-0.3402,0.9063),(0.0189,0.0782,0.0185),(0.1557,0.2329,-0.9600).$$

We verify that $\mathbf{P}$ is simple by considering all pairwise intersections of the segments of this control polygon. The self-intersection of the Bézier curve occurs at a point that is numerically approximated as

$$[s,t] = [0.2969, 0.0633]$$

where correspondingly,

$$S(s,t) = (-0.0003861, -0.000097, 0.0001462) \approx (0,0,0).$$

The error occurs because of numerical round off on s,t and the control points.

5.3.4 The numerical method for generating counterexamples

We provide the numerical codes and data used in Appendix B. Given a control polygon, we can determine whether a self-intersection of the Bézier curve occurs

by determining whether S (Equation 5.3.2) has a root in D. We consider S as a function $S(s,t,q)$ where $q = \{q_i\}_{i=0}^{n-1}$, so that finding a self-intersecting Bézier curve with an equilateral control polygon is equivalent to determining s, t and q such that the following are satisfied:

(i) $S(s,t,q) = 0$ where $s, t \in D$;

(ii) $||q_i|| = r$ for each $i \in \{0, 1, \cdots, n-1\}$, where $||\cdot||$ is the Euclidean norm;

(iii) $\sum_{i=0}^{n-1} q_i = \sum_{i=0}^{n-1} P_{i+1} - P_i = 0$ since P needs to be closed.

Without loss of generality, we assume $r = 1$, since the value of r can be adjusted by scaling. Throughout the provided codes, n is always the degree of the Bézier curve. We give the code for function S in Appendix B.1, where $[s,t]$ is labeled as u and q as $[a,b,c]$.

The function SF (Appendix B.2) takes parameters for s, t and q and outputs a floating point value. It is designed to be zero if and only if the above three conditions are satisfied simultaneously.

Precisely since q should be taken from the unit sphere, SF assigns a, b, c values given by

$$a = sin(\phi)cos(\theta);$$

$$b = sin(\phi)sin(\theta);$$

$$c = cos(\phi),$$

where ϕ and θ represent input parameters. In order to satisfy Condition (3) above, q_{n-1} is set equal to $-\sum_{i=0}^{n-2} q_i$. But in this way, $||q_{n-1}||$ may fail to be equal to 1. So we include the function F (Appendix B.2) to determine whether $||q_{n-1}|| = 1$. The function is designed to be $F = ||q_{n-1}|| - 1$ such that $||q_{n-1}|| = 1$ if and only if $F = 0$.

Symbolically,

$$SF = ||S|| + ||F||, \tag{5.3.4}$$

where S is given by Equation 5.3.2 and $F = ||q_{n-1}|| - 1$. Having the above three conditions satisfied simultaneously is equivalent to finding input values such that $SF = 0$.

Since $SF \geq 0$, the minimum of SF is 0. The function $SFminimizer$ (Appendix B.3) uses $fminsearch$ (a numerical method integrated in MATLAB) to search for the minimum of SF, while returning this minimum and the corresponding values of s, t and q. Initial values for s, t and q, as provided by the user, greatly influence the results, so we assign $SFminimizer$ randomized initial values K times so that we get K different minimums for different initial values. But no matter which initial values we use, as long as we can get "a" minimum of 0, then we get the equilateral control polygon which determines a self-intersecting Bézier curve. The data of finding the counterexample of Section 5.3.3 is included in Appendix B.4.

Chapter 6

Isotopic Convergence Theorem

In this chapter, we no longer restrict our attention to spline curves, but greatly generalize our previous curve convergence results for parametric curves. Namely, we prove a convergence criterion for successive approximations to eventually yield an ambient isotopic approximation for parametric curves. This work, developed during this dissertation research, has already been published [53].

6.1 Introduction

Curve approximation has a rich history, where the Weierstrass Approximation Theorem is a classical, seminal result [42]. Curve approximation algorithms typically do not include any guarantees about retaining topological characteristics, such as ambient isotopic equivalence. One may easily obtain a sequence of non-trivial knots converging pointwise to a circle, with the knotted portions of the sequence becoming smaller and smaller. These non-trivial knots will never be ambient isotopic to the circle. However, ambient isotopic equivalence is a fundamental concern in knot theory. Moreover, it is a theoretical foundation for curve approximation algorithms in computer graphics and visualization.

So a natural question is what criterion will guarantee ambient isotopic equivalence

for curve approximation? The answer is that, besides pointwise convergence, an additional hypothesis of convergence in total curvature will be sufficient, as we shall prove.

There are three main theorems presented. All have a hypothesis of a sequence of curves converging to another smooth curve $\mathcal{C}$. In Theorem 6.3.5, the elements of the sequence are PL inscribed curves. In Theorems 6.4.2 and 6.6.6, the class of curves is generalized to piecewise C^2 parametric curves, with Theorem 6.4.2 being a technical result about a lower bound for the total curvature of elements in some tail of the sequence. These first two results (Theorems 6.3.5 and 6.4.2) are used to provide the main result Theorem 6.6.6, showing that pointwise convergence and convergence in total curvature over this richer class of piecewise C^2 curves produce a tail of elements that are ambient isotopic to $\mathcal{C}$.

6.2 Preliminaries

Use $\mathcal{C}$ to denote a compact, regular, C^2, simple, parametric, space curve. Let $\{C_i\}_1^\infty$ denote a sequence of piecewise C^2, parametric curves. Suppose all curves are parametrized on $[0,1]$, with $\mathcal{C} = \mathcal{C}(t)$ and $C_i = C_i(t)$ for $t \in [0,1]$. Denote the sub-curve of $\mathcal{C}$ corresponding to $[a,b] \subset [0,1]$ as $\mathcal{C}_{[a,b]}$, and similarly use $C_{i[a,b]}$ for C_i. Denote total curvature as a function $T_\kappa(\cdot)$.

6.2.1 Total curvatures of piecewise C^2 curves

Definition 6.2.1 (Exterior angles of piecewise C^2 curves)**.** For a piecewise C^2 curve $\gamma(t)$, define the exterior angle at some t_i to be the exterior angle formed by $\gamma'(t_i-)$ and $\gamma'(t_i+)$ where

$$\begin{aligned} \gamma'(t_i-) &= \lim_{h\to 0} \frac{\gamma(t_i) - \gamma(t_i - h)}{h} \text{ and} \\ \gamma'(t_i+) &= \lim_{h\to 0} \frac{\gamma(t_i + h) - \gamma(t_i)}{h}. \end{aligned} \tag{6.2.1}$$

Definition 6.2.2 (Total curvatures of piecewise C^2 curves)**.** Suppose that a piecewise C^2 curve $\phi(t)$ is not C^2 at finitely many parameters $t_1, \cdots, t_n$. Denote the sum of the total curvatures of all the C^2 sub-curves as $T_{\kappa 1}$, and the sum of exterior angles at $t_1, \cdots, t_n$ as $T_{\kappa 2}$. Then the total curvature of $\phi(t)$ is $T_{\kappa 1} + T_{\kappa 2}$.

6.2.2 Definitions of convergence

Definition 6.2.3. We say that $\{C_i\}_1^\infty$ converges to $\mathcal{C}$ pointwise if for any $t \in [0, 1]$, and any $\epsilon > 0$, there exists an integer N such that $|C_i(t) - \mathcal{C}(t)| < \epsilon$ for all $i \geq N$.

Remark 6.2.4. The pointwise convergence implies the convergence in Hausdorff distance, by the definition of Hausdorff distance [20].

Definition 6.2.5. We say that $\{C_i\}_1^\infty$ converges to $\mathcal{C}$ in total curvature if for any $\epsilon > 0$, there exists an integer N such that $|T_\kappa(C_i) - T_\kappa(\mathcal{C})| < \epsilon$ for all $i \geq N$. We designate this property as *convergence in total curvature*.

Definition 6.2.6. We say that $\{C_i\}_1^\infty$ uniformly converges to $\mathcal{C}$ in total curvature if for any $[t_1, t_2] \subset [0, 1]$ and $\forall \epsilon > 0$, there exists an integer N such that whenever

$i \geq N$, $|T_\kappa(C_{i[t_1,t_2]}) - T_\kappa(\mathcal{C}_{[t_1,t_2]})| < \epsilon$. We designate this property as *uniform convergence in total curvature.*

Remark 6.2.7. Uniform convergence in total curvature implies convergence in total curvature. However, obviously, the converse is not true.

6.3 Isotopic Convergence of Inscribed PL Curves

We will use the concept of PL inscribed curves as previously defined [1].

Definition 6.3.1. A closed PL curve L with vertices $v_1, v_2, \cdots, v_m$ is said to be inscribed in curve $\mathcal{C}(t)$ if there is a sequence $\{t_j\}_1^m$ of parameter values such that $v_i = \mathcal{C}(t_j)$ for $j = 1, 2, \cdots, m$. We parametrize L over $[0, 1]$, denoted as $L(t)$, by

$$L(t_j) = v_j \ for \ j = 0, 1, \cdots, m$$

and $L(t)$ interpolates linearly between vertices.

The previously established results [1, Theorem 2.2] and [45, Proposition 3.1] showed that a sequence of finer and finer inscribed PL curves will converge in total curvature. The uniform convergence in total curvature follows easily. For the sake of completeness, we present the proof here.

Lemma 6.3.2. For a piecewise C^2 curve $\gamma(t)$ parametrized on $[0, 1]$ (which is regular at all C^2 points), a sequence $\{L_i\}_1^\infty$ of inscribed PL curves can be chosen such that $\{L_i\}_1^\infty$ pointwise converges to γ and uniformly converges to γ in total curvature.

Proof. We first take the end points $\gamma(t_0) = \gamma(0)$ and $\gamma(t_n) = \gamma(1)$. And then select[17] the points where γ fails to be C^2. Denote these points as

$$\{\gamma(t_0), \gamma(t_1), \cdots, \gamma(t_{n-1}), \gamma(t_n)\}.$$

We then compute midpoints: $\gamma(\frac{t_j+t_{j+1}}{2})$ for $j \in \{0, 1, \ldots, n-1\}$ to form L_2 which is determined by vertices:

$$\{\gamma(t_0), \gamma(\frac{t_0+t_1}{2}), \gamma(t_1), \cdots, \gamma(t_{n-1}), \gamma(\frac{t_{n-1}+t_n}{2}), \gamma(t_n)\}.$$

Continuing this process, we obtain a sequence $\{L_i\}_1^\infty$ of inscribed PL curves. Suppose the set of vertices of L_i is $\{v_{i,k} = \gamma(t_{i,k})\}$, for some finitely many parameter values $t_{i,k}$. Use uniform parametrization [6] for L_i such that $v_{i,k} = L_i(t_{i,k})$, and points between each pair of consecutive vertices are interpolated linearly. Note first that this process implies that $\{L_i\}_1^\infty$ pointwise converges to $\mathcal{C}$. For the uniform convergence in total curvature, consider the following:

(i) Consider each t_j where γ fails to be C^2. Denote the parameters of vertices of L_i adjacent to $L_i(t_j)$ as t_{j1}^i and t_{j2}^i, then $\lim_{i\to\infty} t_{j1}^i = \lim_{i\to\infty} t_{j2}^i = t_j$. This implies that the slope of $\overrightarrow{L_i(t_{j1}^i)L_i(t_j)}$ and the slope of $\overrightarrow{L_i(t_{j2}^i)L_i(t_j)}$ go to $\gamma'(t_j-)$ and $\gamma'(t_j+)$ respectively. This shows that

$$\lim_{i\to\infty} \eta(\overrightarrow{L_i(t_{j1}^i)L_i(t_j)}, \overrightarrow{L_i(t_{j2}^i)L_i(t_j)}) = \eta(\gamma'(t_j-), \gamma'(t_j+)).$$

[17] Astute readers will observe that this choice of points is sufficient for this lemma, but not necessary. This choice is for ease of exposition.

(ii) Consider a pair of parameters $t_{i,1}$ and $t_{i,2}$ of any two consecutive vertices of L_i. Denote the corresponding PL curve as $L_{i[t_{i,1},t_{i,2}]}$. Note that the corresponding sub-curve $\gamma_{i[t_{i,1},t_{i,2}]}$ of γ is C^2, since the parameters where γ is not C^2 have been selected as vertices. Provided that $\lim_{i\to\infty} |t_{1,i}-t_{2,i}| = 0$, we have $T_\kappa(L_{i[t_{i,1},t_{i,2}]}) \to T_\kappa(\gamma_{[t_{i,1},t_{i,2}]})$ as $i \to \infty$, as shown in the proof of a theorem already appearing in the literature [1, Theorem 2.2].

By Definition 6.2.2, the immediately previous (i) and (ii) together imply that the total curvature of any sub-curve of L_i converges to the corresponding sub-curve of γ (either C^2 or just piecewise C^2), which is the uniform convergence in total curvature (Definition 6.2.6). □

Since uniform convergence in total curvature implies convergence in total curvature (Definition 6.2.6), the corollary below follows immediately.

Corollary 6.3.3. [1, Theorem 2.2] [45, Proposition 3.1] For $\mathcal{C}$, a sequence $\{L_i\}_1^\infty$ of inscribed PL curves can be chosen such that $\{L_i\}_1^\infty$ converges to $\mathcal{C}$ pointwise and in total curvature.

Lemma 6.3.4. Denote the plane normal to $\mathcal{C}$ at some $t_0 \in (0,1)$ as $\Pi(t_0)$. Consider two sub-curves $\mathcal{C}_{[t_0-u]}$ and $\mathcal{C}_{[t_0+v]}$ for some $u \in (0,t_0)$ and $v \in (t_0,1)$. If both $T_\kappa(\mathcal{C}_{[t_0-u]}) < \frac{\pi}{2}$ and $T_\kappa(\mathcal{C}_{[t_0+v]}) < \frac{\pi}{2}$, then these two sub-curves $\mathcal{C}_{[t_0-u]}$ and $\mathcal{C}_{[t_0+v]}$ are separated by $\Pi(t_0)$ except at $\mathcal{C}(t_0)$.

Proof. Denote the point $\mathcal{C}(t_0)$ as a. Suppose that the conclusion is false, then either $\mathcal{C}_{[t_0-u]}$ or $\mathcal{C}_{[t_0+v]}$ intersects $\Pi(t_0)$ other than at a. Assume without loss of

generality that $\mathcal{C}_{[t_0+v]} \cap \Pi(t_0)$ contains another point, denoted as b. Then the sub-curve $\mathcal{C}_{[t_0+v]}$ and the line segment $\overline{ab}$ form a closed curve $\mathcal{C}_{[t_0+v]} \cup \overline{ab}$. So $T_\kappa(\mathcal{C}_{[t_0+v]} \cup \overline{ab}) \geq 2\pi$ by Theorem 1.1.6.

Denote the exterior angles at a and b as α and β respectively. Then $\alpha = \frac{\pi}{2}$ since $\Pi(t_0)$ is normal to $\mathcal{C}'(t_0)$. By Definition 1.1.3, $\beta \leq \pi$. By Definition 6.2.2 we have

$$T_\kappa(\mathcal{C}_{[t_0+v]} \cup \overline{ab}) = T_\kappa(\mathcal{C}_{[t_0+v]}) + \alpha + \beta \leq T_\kappa(\mathcal{C}_{[t_0+v]}) + \frac{\pi}{2} + \pi.$$

So

$$T_\kappa(\mathcal{C}_{[t_0+v]}) + \frac{\pi}{2} + \pi \geq 2\pi.$$

Therefore

$$T_\kappa(\mathcal{C}_{[t_0+v]}) \geq \frac{\pi}{2},$$

which is a contradiction. □

Theorem 6.3.5 below is restricted to "inscribed PL curves". The general theorem of "piecewise C^2 curves, either inscribed or not" will be established later in Theorem 6.6.6.

Theorem 6.3.5. For any sequence $\{L_i\}_1^\infty$ of inscribed PL curves that pointwise converges to $\mathcal{C}$ and uniformly converges to $\mathcal{C}$ in total curvature, a positive integer N can be found as below such that for all $i > N$, L_i is ambient isotopic to $\mathcal{C}$.

Proof. For $\mathcal{C}$, there is a non-self-intersecting pipe surface[18] of radius r (Remark 2.2.6). Pointwise convergence and the uniform convergence in total curvature imply that there exists a positive integer N such that for an arbitrary $i > N$:

(i) The PL curve L_i lies inside of the pipe surface of radius r; and

(ii) Denote the set of vertices of L_i as $\{v_j\}_{j=0}^{n}$. Suppose the sub-curve of $\mathcal{C}$ between two arbitrary consecutive vertices v_j and v_{j+1} as $\mathcal{A}_j$, for $j = 0, \ldots, n-1$. Then since the total curvature of $\overrightarrow{v_j v_{j+1}}$ is 0, the total curvature of $\mathcal{A}_j$ can be less than $\frac{\pi}{2}$.

Lemma 6.3.4 implies that all such sub-curves $\mathcal{A}_j$ are separated by normal planes except the connection points. The facts about fitting inside a pipe surface and separation by normal planes provide a sufficient condition [8] for L_i being ambient isotopic to $\mathcal{C}$. □

6.4 Pointwise Convergence

Pointwise Convergence provides a lower bound of the total curvatures of approximants (Theorem 6.4.2). The proof relies upon showing this for PL curves first (Lemma 6.4.1). The method used here is related to the previously presented median push (Definition 2.3.3) and Lemma 2.3.4.

Lemma 6.4.1. Let $\{L_i\}_{i=1}^{\infty}$ be a sequence of PL curves parametrized on $[0, 1]$ and L be a PL curve parametrized on $[0, 1]$. If $\{L_i\}_{i=1}^{\infty}$ pointwise converges to L,

[18] Recall that $\mathcal{C}$ is C^2, even while some of the previous results [8] were generalized to piecewise C^2 curves.

then for $\forall \epsilon > 0$, there exists an integer N such that $T_\kappa(L_i) > T_\kappa(L) - \epsilon$ for all $i \geq N$.

Proof. For an arbitrary vertex v of L, suppose $v = L(t_v)$ for some $t_v \in [0, 1]$. Let B_v be a closed ball centered at v. Since L is a compact PL curve, we can choose the radius of B_v small enough such that:

(i) the ball B_v contains only the single vertex v of L; and

(ii) it intersects only the two line segments of L which are connected at v. Denote these intersections as $u = L(t_u)$ and $w = L(t_w)$ for some $t_u, t_w \in [0, 1]$. Then u, w and v together form a triangle $\triangle uvw$.

Let $u_i = L_i(t_u)$, $v_i = L_i(t_v)$ and $w_i = L_i(t_w)$. Denote the exterior angle of the triangle $\triangle uvw$ at v as $\eta(v)$, and correspondingly the exterior angle of $\triangle u_i v_i w_i$ at v_i as $\eta(v_i)$. (Note that $\eta(v)$ is not necessarily equal to the exterior angle of L at v. Similarly for $\eta(v_i)$.) By the pointwise convergence we have that the triangle $\triangle u_i v_i w_i$ converges to $\triangle uvw$. So $\eta(v_i)$ converges to $\eta(v)$. That is, for $\forall \epsilon' > 0$ there exists an N such that $\eta(v_i) > \eta(v) - \epsilon'$ for all $i \geq N$.

Consider the PL sub-curve of L_i lying in B_v and denote its total curvature as $T_\kappa(L_i \cap B_v)$. This PL sub-curve of L_i can be reduced by median pushes to $\triangle u_i v_i w_i$. Lemma 2.3.4 implies that $T_\kappa(L_i \cap B_v) \geq \eta(v_i)$. So for $i \geq N$,

$$T_\kappa(L_i \cap B_v) > \eta(v) - \epsilon'. \tag{6.4.1}$$

Denote the set of vertices of L as V. Then $T_\kappa(L) = \sum_{v\in V} \eta(v)$. Note that $T_\kappa(L_i) \geq \sum_{v\in V} T_\kappa(L_i \cap B_v)$. So Inequality 6.4.1 implies that

$$T_\kappa(L_i) \geq \sum_{v\in V} T_\kappa(L_i \cap B_v) > \sum_{v\in V} \eta(v) - \epsilon' n = T_\kappa(L) - \epsilon' n$$

where n is the number of vertices of L. Let $\epsilon' = \frac{\epsilon}{n}$, then we complete the prove. □

Theorem 6.4.2. If $\{C_i\}_1^\infty$ pointwise converges to $\mathcal{C}$, then for $\forall \epsilon > 0$, there exists an integer N such that $T_\kappa(C_i) > T_\kappa(\mathcal{C}) - \epsilon$ for all $i \geq N$.

Proof. By Lemma 6.3.2, we can use inscribed PL curves to approximate $\{C_i\}_1^\infty$ and $\mathcal{C}$, such that the approximations converge pointwise and in total curvature. Then apply the Lemma 6.4.1 to these inscribed PL curves. Since these inscribed PL curves converge pointwise and in total curvature to $\{C_i\}_1^\infty$ and $\mathcal{C}$ respectively, the desired conclusion follows. □

6.5 Uniform Convergence in Total Curvature

Convergence in total curvature is weaker than uniform convergence in total curvature. But pointwise convergence and convergence in total curvature together imply the uniform convergence, which is shown by Lemma 6.5.1 below.

Lemma 6.5.1. If $\{C_i\}_1^\infty$ converges to a C^2 curve $\mathcal{C}$ pointwise and in total curvature, then $\{C_i\}_1^\infty$ uniformly converges to $\mathcal{C}$ in total curvature.

Proof. Assume not, then there exist a subset $[t_1, t_2] \subset [0, 1]$ and a $\tau > 0$ such that for any integer N, there is a $i \geq N$ such that $|T_\kappa(C_{i[t_1,t_2]}) - T_\kappa(\mathcal{C}_{[t_1,t_2]})| > \tau$,

that is $T_\kappa(C_{i[t_1,t_2]}) > T_\kappa(\mathcal{C}_{[t_1,t_2]}) + \tau$ or $T_\kappa(C_{i[t_1,t_2]}) < T_\kappa(\mathcal{C}_{[t_1,t_2]}) - \tau$. The latter is precluded by Theorem 6.4.2. Therefore

$$T_\kappa(C_{i[t_1,t_2]}) > T_\kappa(\mathcal{C}_{[t_1,t_2]}) + \tau. \tag{6.5.1}$$

Consider the sequence of the sub-curves of $\{C_i\}_1^\infty$ restricted to the complement $[t_1,t_2]^c$ of $[t_1,t_2]$, and denote it as $\{C_{i[t_1,t_2]^c}\}_1^\infty$. By theorem 6.4.2, for $\frac{\tau}{2}$, there exists an integer, say M such that for all $i \geq M$,

$$T_\kappa(C_{i[t_1,t_2]^c}) > T_\kappa(\mathcal{C}_{[t_1,t_2]^c}) - \frac{\tau}{2}. \tag{6.5.2}$$

Note that $T_\kappa(C_i) \geq T_\kappa(C_{i[t_1,t_2]}) + T_\kappa(C_{i[t_1,t_2]^c})$. So Equations 6.5.1 and 6.5.2 imply that there is a $i \geq M$ so that

$$T_\kappa(C_i) \geq T_\kappa(C_{i[t_1,t_2]}) + T_\kappa(C_{i[t_1,t_2]^c}) > T_\kappa(\mathcal{C}_{[t_1,t_2]}) + T_\kappa(\mathcal{C}_{[t_1,t_2]^c}) + \frac{\tau}{2}.$$

Since $\mathcal{C}$ is C^2, $T_\kappa(\mathcal{C}_{[t_1,t_2]}) + T_\kappa(\mathcal{C}_{[t_1,t_2]^c}) = T_\kappa(\mathcal{C})$. Therefore we get

$$T_\kappa(C_i) \geq T_\kappa(\mathcal{C}) + \frac{\tau}{2},$$

which contradicts the convergence in total curvature. □

6.6 Isotopic Convergence

For a C^2 compact curve $\mathcal{C}$, we shall, without loss of generality (Theorem 6.3.5), consider a sequence $\{L_i\}_1^\infty$ of PL curves (instead of piecewise C^2 curves) as its

approximation. We shall divide $\mathcal{C}$ into finitely many sub-curves, and reduce the corresponding sub-curves of L_i to line segments, by median pushes, so as to preserve isotopic equivalence. The line segments generated by the pushes form a polyline. We shall then prove the polyline is ambient isotopic to $\mathcal{C}$.

To get to the major theorem, we need to first establish some preliminary topological results. We use $CH(\cdot)$ to denote the convex hull of a set.

Lemma 6.6.1. Let X and Y be compact subspaces of an Euclidean space $\mathbb{R}^d$. If $X \cap Y = \emptyset$, then Y can be subdivided into finitely many subsets, denoted as $Y_1, \ldots Y_i, \ldots Y_m$ for some $m > 0$, such that $CH(Y_i) \cap X = \emptyset$ for each i.

Proof. Since X is compact, for $\forall y \in Y$, $\inf_{x \in X} ||x - y|| > 0$, and hence $\exists$ an open ball $B_y \subset \mathbb{R}^d$ of y such that $B_y \cap X = \emptyset$. Since Y is compact, among these open balls, there are finitely many, denoted by $B_{y_1}, \cdots, B_{y_m}$ such that $Y \subset \bigcup_{i=1}^{m} B_{y_i}$. Let $Y_i = Y \cap B_{y_i}$ for each $i = 1, \ldots, m$ so that

$$CH(Y_i) = CH(Y \cap B_{y_i}) \subset CH(B_{y_i}) = B_{y_i}.$$

Thus, for each i, we have $CH(Y_i) \cap X = \emptyset$. □

As we mentioned before, for a simple C^2 curve $\mathcal{C}$, there is a non-self-intersecting pipe surface of radius r (Remark 2.2.6). This surface determines a tubular neighborhood [52] of $\mathcal{C}$, denoted as $\Gamma_{\mathcal{C}}$. Denote a sub-curve of $\mathcal{C}$ as $\mathcal{C}^k$, and the corresponding tubular neighborhood of $\mathcal{C}^k$ as Γ^k.

Lemma 6.6.2. The compact curve $\mathcal{C}$ can be divided into finitely many sub-curves, denoted as $\mathcal{C}^1, \ldots, \mathcal{C}^k, \ldots, \mathcal{C}^n$ for some $n > 0$, such that

- $T_\kappa(\mathcal{C}^k) < \frac{\pi}{2}$; and
- $CH(\mathcal{C}^k) \subset \Gamma^k$.

Proof. By Lemma 6.6.1, $\mathcal{C}$ can be partitioned into finitely many non-empty sub-curves, each which is disjoint from $S_r(\mathcal{C})$. Since $\mathcal{C}$, is also of finite total curvature, we can denote these sub-curves as $\mathcal{C}^1, \ldots, \mathcal{C}^k, \ldots, \mathcal{C}^n$ for some $n > 0$, such that for each $k = 1, \cdots, n$, $T_\kappa(\mathcal{C}^k) < \frac{\pi}{2}$ and $CH(\mathcal{C}^k) \cap S_r(\mathcal{C}) = \emptyset$.

Consider $\mathcal{C}^k$ for an arbitrary $k = 1, \ldots, n$ and denote the distinct normal planes at the endpoints of $\mathcal{C}^k$ by Π_1, Π_2, respectively. Denote the closed convex subspace of $\mathbb{R}^3$ that contains $\mathcal{C}^k$ and is bounded by Π_1 and Π_2 as H^k. It is clear that $CH(\mathcal{C}^k) \subset H^k$, but since $CH(\mathcal{C}^k) \cap S_r(\mathcal{C}) = \emptyset$, we have that $CH(\mathcal{C}^k) \subset \Gamma^k$. □

For $k = 1, \ldots, n$, let $[t_{k-1}, t_k]$ be the subinterval whose image is $\mathcal{C}^k$, with corresponding Γ^k. Let ϵ be real valued such that

$$0 < \epsilon < \min_{k \in \{0,\ldots,n\}} \frac{|t_k - t_{k-1}|}{2}.$$

We extend[19] $[t_{k-1}, t_k]$ to $[t_{k-1} - \epsilon, t_k + \epsilon]$, and denote the pipe neighborhood corresponding to the extended subinterval as Γ^k_ϵ, then Γ^k_ϵ only intersects Γ^{k+1}_ϵ and Γ^{k-1}_ϵ for each k.

[19] If $\mathcal{C}$ is open and $t_{k-1} = 0$ or $t_k = 1$, consider $[0, t_k + \epsilon]$ or $[t_{k-1} - \epsilon, 1]$.

For a sequence of PL curves $\{L_i\}_1^\infty$ converging to $\mathcal{C}$ pointwise and in total curvature, denote the sub-curve of L_i corresponding (with the same parameters) to $\mathcal{C}^k$ as L_i^k. Denote the end points of L_i^k by u_i^{k-1} and u_i^k, with the corresponding end points of $\mathcal{C}^k$ by v^{k-1} and v^k.

Lemma 6.6.3. A large positive integer N can be found such that whenever $i \geq N$, for each k, we have

(i) $T_\kappa(L_i^k) < \frac{\pi}{2}$;

(ii) $CH(L_i^k) \subset \Gamma_\epsilon^k$; and

(iii) $|u_i^k - v^k| < \frac{r}{2}$ and $\mu(\overline{u_i^{k-1}u_i^k}, \mathcal{C}^k) < \frac{r}{2}$, where $\mu(\cdot)$ refers to the Hausdorff distance.

Proof. The first condition follows from the uniform convergence in total curvature (Lemma 6.5.1), and the second and third follow from pointwise convergence. □

Lemma 6.6.4. For each $k = 1, \ldots, n$, use median pushes to reduce L_i^k to the line segment $\overline{u_i^{k-1}u_i^k}$. Then during these pushes, L_i remains simple, and hence the resultant PL curve $\bigcup_{k=1}^n \overline{u_i^{k-1}u_i^k}$ is ambient isotopic to the original PL curve L_i.

Proof. Note that the condition (1) in Lemma 6.6.3 implies that $T_\kappa(L_i^{k-1} \cup L_i^k) < \pi$ and $T_\kappa(L_i^k \cup L_i^{k+1}) < \pi$. Lemma 2.2.1 and 2.3.4 show that the pushed L_i^k does not intersect its neighbors L_i^{k+1} or L_i^{k-1}. Since $CH(L_i^k) \subset \Gamma_\epsilon^k$ (Condition (2)), and

Γ_ϵ^k does not intersect Γ_ϵ^j for $j \neq k-1$ or $k+1$, the perturbed L_i^k stays inside Γ_ϵ^k and does not intersect L_i^j for $j \neq k-1$ or $k+1$. Then the conclusion follows. $\square$

For each $k = 1, \ldots, n$, connecting the end points v^{k-1} and v^k of $\mathcal{C}^k$, we obtain the polyline $\bigcup_{k=1}^n \overline{v^{k-1}v^k}$.

Lemma 6.6.5. The polyline $\bigcup_{k=1}^n \overline{v^{k-1}v^k}$ is ambient isotopic to $\bigcup_{k=1}^n \overline{u_i^{k-1}u_i^k}$.

Proof. Perturb u_i^k to v^k. The line segments move linearly from $\overline{u_i^{k-1}u_i^k}$ to $\overline{u_i^{k-1}v^k}$, and from $\overline{u_i^k u_i^{k+1}}$ to $\overline{v^k u_i^{k+1}}$. Since $|u_i^k - v^k| < \frac{r}{2}$ and $\mu(\overline{u_i^{k-1}u_i^k}, \mathcal{C}^k) < \frac{r}{2}$ (Condition (3) in Lemma 6.6.3), the perturbation stays inside Γ_ϵ^k which has a radius r. So during the perturbation, $\overline{u_i^{k-1}, u_i^k}$ and $\overline{u_i^k, u_i^{k+1}}$ do not intersect any line segments of L_i, except their adjacent segments. But note that for each k, $u_i^k, v^k \in \Gamma_\epsilon^k \cap \Gamma_\epsilon^{k+1}$. An easy geometric analysis shows that this restricted area of the perturbation precludes the possibility for $\overline{u_i^{k-1}, u_i^k}$ and $\overline{u_i^k, u_i^{k+1}}$ intersecting their adjacent segments, except, necessarily, at their shared endpoints. So the perturbation does not cause intersections, and hence preserves the ambient isotopy. $\square$

Theorem 6.6.6 (Isotopic Convergence Theorem)**.** If $\{C_i\}_1^\infty$ converges to $\mathcal{C}$ pointwise and in total curvature, then there exists an integer N such that C_i is ambient isotopic to $\mathcal{C}$ for all $i \geq N$.

Proof. For each C_i and $\epsilon > 0$, there exists an inscribed PL curve L_i of C_i such that L_i is sufficiently close (bounded by ϵ) to C_i pointwise and in total curvature

by Lemma 6.3.2, and ambient isotopic to C_i by Theorem 6.3.5. Since ambient isotopy is an equivalence relation [2], we now rely on Theorem 6.3.5 to consider, without loss of generality, a sequence of PL curves $\{L_i\}_1^\infty$ instead of $\{C_i\}_1^\infty$.

Note that $T_\kappa(\mathcal{C}^k) < \frac{\pi}{2}$ and the polyline $\bigcup_{k=1}^n \overline{v^{k-1}v^k}$ lies inside of the tubular neighborhood (since $CH(\mathcal{C}^k) \subset \Gamma_\mathcal{C}$). By the proof of Theorem 6.3.5 we know that these are sufficient conditions for $\mathcal{C}$ being ambient isotopic to $\bigcup_{k=1}^n \overline{v^{k-1}v^k}$. By the equivalence relation of ambient isotopy, Lemma 6.6.5 implies that $\mathcal{C}$ is ambient isotopic to $\bigcup_{k=1}^n \overline{u_i^{k-1}u_i^k}$, and Lemma 6.6.4 further implies that $\mathcal{C}$ is ambient isotopic to L_i. □

6.7 Conceptual Algorithms and Potential Applications

The Isotopic Convergence Theorem has both theoretical and practical applications. Theoretically, it formulates criteria to show the same knot type in knot theory. Practically, it provides rigorous theoretical foundations to extend current algorithms in computer graphics and visualization to much richer classes of curves than the splines already investigated [36], with an example given in Section 6.7.4. The following are the general procedures derived from our Theorem 6.3.5 and Theorem 6.6.6. For a specific problem, further algorithmic development will depend upon characteristics of the class of curves. If the curve is "nice" in the sense that the total curvature and the radius of a pipe surface is easy to compute, then it is easy to develop an algorithm. Such "nice" curves include a rational cubic spline parameterized by arc length, for which the total curvatures can be easily

computed, and the radius of a pipe surface can be found according to an existing result (Remark 2.2.6). Otherwise, for some other curves, the computation of the total curvatures and the radius of a tubular neighborhood may be difficult and is beyond the scope of the details considered here, even while the theorems provide a broad framework within which these subtleties can be considered.

6.7.1 Using PL knots to represent smooth knots

Based on Lemma 6.3.2 and Theorem 6.3.5, a procedure can be designed such that it takes a smooth knot as input and picks finitely many points on it to form an ambient isotopic PL knot. We call this PL knot a *PL representation* of the smooth knot.

Recall that two criteria are sufficient for the isotopy between $\mathcal{C}$ and its inscribed PL curve $\mathcal{L}$:

(i) Each sub-curve of $\mathcal{C}$ which is determined by two consecutive vertices of $\mathcal{L}$ has a total curvature less than $\frac{\pi}{2}$.

(ii) The PL curve $\mathcal{L}$ lies inside of the pipe surface for $\mathcal{C}$ with radius r. (This can be achieved by making the Hausdorff distance between $\mathcal{L}$ and $\mathcal{C}$ less than r.)

The Outline of Forming PL Representations:

(i) Select $\mathcal{C}(0)$ as the initial vertex of $\mathcal{L}$, denoted as v_0.

(ii) Set[20] $\epsilon = 0.1$. Select[21] $t_1 \in [0,1]$ such that $T_\kappa(\mathcal{C}_{[0,t_1]}) = \frac{\pi}{2} - \epsilon$. Let the second vertex of $\mathcal{L}$ be $\mathcal{C}(t_1)$, denoted as v_1.

(iii) Similarly pick t_2 to obtain v_2. Continue until we reach the end point $\mathcal{C}(1)$, denoted as v_n. This process terminates because $\mathcal{C}$ is assumed to be compact. In the end, we obtain an $\mathcal{L}$, and sub-curves of $\mathcal{C}$ with total curvatures being less than $\frac{\pi}{2}$.

(iv) Verify if the Hausdorff distance between $\mathcal{L}$ and $\mathcal{C}$ is less than r; If not, then select midpoints: $\mathcal{C}(\frac{t_j+t_{j+1}}{2})$ for $j \in \{0, 1, \ldots, n-1\}$, denoted as $v_{\frac{2j+1}{2}}$, to form a new inscribed PL curve determined by vertices:

$$\{v_0, v_{\frac{1}{2}}, v_1, v_{\frac{3}{2}}, v_2, \ldots, v_{n-1}, v_{\frac{2n-1}{2}}, v_n\}.$$

(v) Repeat 4 until the Hausdorff distance between $\mathcal{L}$ and $\mathcal{C}$ is less than r. This process of selecting midpoints implies the pointwise convergence. So this process terminates.

6.7.2 Testing isotopic convergence

For a C^2 curve $\mathcal{C}$ and a sequence $\{C_i\}_1^\infty$ of piecewise C^2 curves, where $\{C_i\}_1^\infty$ converges to $\mathcal{C}$ pointwise and in total curvature, we shall design a procedure to determine a positive integer N such that whenever $i \geq N$, C_i is ambient isotopic

[20] This ϵ value is not unique. Many others, for example $\epsilon = 0.01$, also work.

[21] It is not necessary for $T_\kappa(\mathcal{C}_{[0,t_1]})$ to be exactly $\frac{\pi}{2} - \epsilon$. For efficiency, it is fine to end up with a value not equal to $\frac{\pi}{2} - \epsilon$ as long as it is less than $\frac{\pi}{2}$. This aspect will require a subroutine to be developed that will likely vary over the class of curves considered and this detail is beyond the scope of the current investigation.

to $\mathcal{C}$. Use $T_\kappa(\cdot)$ to denote the total curvature, $CH(\cdot)$ the convex hull, and $\mu(\cdot)$ the Hausdorff distance.

The Outline of Testing Isotopic Convergence:

(i) Divide $\mathcal{C}$ into sub-curves $\mathcal{C}^k$ for $k = 1, \cdots, n$ such that

- $T_\kappa(\mathcal{C}^k) < \frac{\pi}{2}$; and
- $CH(\mathcal{C}^k) \subset \Gamma^k$.

(ii) Set $i := 1$.

(iii) Use the above technique to form a *PL Representation* L_i for the piecewise C^2 curve C_i such that L_i is ambient isotopic to C_i.

(iv) Let L_i^k but the sub-curve of L_i corresponding to $\mathcal{C}^k$. Denote the end points of L_i^k as u_i^{k-1} and u_i^k, and the corresponding end points of $\mathcal{C}^k$ as v^{k-1} and v^k.Verify three criteria:

- $T_\kappa(L_i^k) < \frac{\pi}{2}$;
- $CH(L_i^k) \subset \Gamma_\epsilon^k$; and
- $|u_i^k - v^k| < \frac{r}{2}$ and $\mu(\overline{u_i^{k-1}u_i^k}, \mathcal{C}^k) < \frac{r}{2}$.

(v) If these criteria are satisfied, then let $N := i$ and stop. Otherwise let $i := i + 1$ and go to (3).

We know that $\{C_i\}_1^\infty$ pointwise converges to $\mathcal{C}$ and uniformly converges to $\mathcal{C}$ in total curvature (Lemma 6.5.1), so there exists a finite i such that these three criteria are achieved, which means the above process terminates. By Isotopic Convergence Theorem, we obtain the ambient isotopy.

6.7.3 A potential application for molecular simulations

It is often of interest to consider geometric models that are perturbed over time. For chemical simulations of macro-molecules, the algorithms in high performance computing (HPC) environments will produce voluminous numerical data describing how the molecule twists and writhes under local chemical and kinetic changes. To produce a scientifically valid visualization, it is crucial that topological artifacts are not introduced by the visual approximations [36]. A primary distinction between the approximations created here in Section 6.7.1 and those based on Taylor's Theorem [36] is the expression here of the upper bound for total curvature to be less than $\frac{\pi}{2} - \epsilon$.

6.7.4 A representative example of offset curves

Offset curves are defined as locus of the points which are at constant distant along the normal from the generator curves [43]. It is well-known [24, p. 553] that offsets of spline curves need not be splines. They are widely used in various applications, and the related approximation problems were frequently studied. A literature survey on offset curves and surfaces prior to 1992 was conducted by Pham [44], and another such survey between 1992 and 1999 was given by

Maekawa [43]. Here we show a representative example as a catalyst to ambient isotopic approximations of offset curves.

Let $\mathcal{C}(t)$ be a compact, regular, C^2, simple, space curve parametrized on $[a, b]$, whose curvature κ never equals 1. Then define an offset curve by

$$\Omega(t) = \mathcal{C}(t) + N(t),$$

where $N(t)$ is the normal vector at t, for $t \in [a, b]$.

For example, let $\mathcal{C}(t) = (2\cos t, 2\sin t, t)$ for $t \in [0, 2\pi]$ be a helix, then it is an easy exercise for the reader to verify that the above assumptions of $\mathcal{C}$ are satisfied, with $\kappa = \frac{2}{5}$. Furthermore, it is straightforward to obtain the offset curve $\Omega(t) = (\cos t, \sin t, t)$, which is not a spline.

We first show that $\Omega(t)$ is regular. Let $s(t) = \int_a^t |\mathcal{C}'(t)|dt$ be the arc-length of $\mathcal{C}$. Then by Frenet-Serret formulas [4] we have

$$\Omega'(t) = \mathcal{C}'(t) + N'(t)$$

$$= \frac{ds}{dt}T + (-\kappa T + \tau B)\frac{ds}{dt} = (1-\kappa)\frac{ds}{dt}T + \tau\frac{ds}{dt}B,$$

where T and B are the unit tangent vector and binormal vector respectively. Since $T \perp B$, if $(1-\kappa)\frac{ds}{dt} \neq 0$ then $\Omega'(t) \neq 0$. But $(1-\kappa)\frac{ds}{dt} \neq 0$ because $\kappa \neq 1$ and $\mathcal{C}(t)$ is regular by the assumption. Thus $\Omega(t)$ is regular.

Now we define a sequence $\{\Omega_i(t)\}_{i=1}^{\infty}$ to approximate $\Omega(t)$ by setting

$$\Omega_i(t) = \mathcal{C}(t) + \frac{i-1}{i}N(t).$$

It is obvious that $\{\Omega_i(t)\}_{i=1}^{\infty}$ pointwise converges to $\Omega(t)$. For the convergence in total curvature, note that $\lim_{i\to\infty}\Omega_i'(t) = \Omega'(t)$, $\lim_{i\to\infty}\Omega_i''(t) = \Omega''(t)$, and $|\Omega'(t)| \neq 0$ due to the regularity of $\Omega(t)$. Therefore

$$\lim_{i\to\infty}\frac{\Omega_i'(t)\times\Omega_i''(t)}{|\Omega_i'(t)|^3} = \frac{\Omega'(t)\times\Omega''(t)}{|\Omega'(t)|^3}.$$

The convergence in total curvature follows.

Consequently, by[22] the Isotopic Convergence Theorem, we conclude that there exists a positive integer N such that $\Omega_i(t)$ is ambient isotopic to $\Omega(t)$ whenever $i > N$.

[22]Since the example satisfies C^0 and C^1 convergence and the paper [45] shows ambient isotopy under C^0 and C^1 convergence, the ambient isotopy for this example also follows from the previous result [45]. Here our purpose is to use it as a representation to show how the Isotopic Convergence Theorem can be applied.

Chapter 7

Conclusions and Future Work

For simple, regular, C^1, composite Bézier curve $\mathcal{B}$ associated with control polygon $\mathcal{P}$ in $\mathbb{R}^3$, we established:

(i) the *exterior angles* of $\mathcal{P}$ converge to 0 at the rate of $O(\sqrt{\frac{1}{2^i}})$, where i is the number of subdivisions,

(ii) sufficiently many subdivisions produce $\mathcal{P}$ homeomorphic and further ambient isotopic to $\mathcal{B}$.

(iii) closed-form formulas to compute *a priori* sufficient iteration number.

In order to improve computational efficiency, we moved further to construct explicit topological and isotopic equivalence, as discussed in Chapter 3.

Apart from the equivalence, we also investigated the topological differences between a Bézier curve $\mathbf{B}$ and its original control polygon $\mathbf{P}$ before performing subdivisions. We showed counterexamples where $\mathbf{P}$ is unknotted, while $\mathbf{B}$ is knotted, and where $\mathbf{P}$ is equilateral and simple, while $\mathbf{B}$ is self-intersecting. These results are accompanied with knot visualization and numerical analysis.

Finally, we considered C^2 parametric curves and derived the Isotopic Convergence Theorem. It establishes broad criteria for a sequence of piecewise linear curves

to become ambient isotopic to a given smooth curve. In particular, for knots, it provides a method to pick finitely many points from a given knot, and connect these points to form a curve of the same knot type.

This research suggests some topics for continuing investigation[23]:

- Bézier surfaces are also pervasive geometric representations. Designing an appropriate PL structure associated to a Bézier surface and establishing topological and isotopic equivalence may be of interest.

- The examples showing that control polygons whose topological structure is different from the topological structure of the corresponding Bézier curves have large Lipschitz constants (when considered as PL curves). Are such large Lipschitz constants sufficient for these topological differences?

- We may derive an infinite precision proof for a counterexample of the simple, closed equilateral polygon conjecture, where these demands will likely require further, substantive mathematical innovation.

[23]The last two questions were created by an anonymous referee of the Journal of Applied General Topology

Appendix A

Code and Data: Knottedness of the Bézier curve

A.1 Code: Self-intersections of the Projection

The function $C2d(t)$ defines the projection of the Bézier curve.

function [value] = C2d(t)

n=10;

P=zeros(2,11);

P(1,:)= [-5.9, 10.3, -2.6, -10, 1.9, 11.2, -15.3, -11.7, 17.9, 2.9, -5.9];

P(2,:)= [4.7, -1.1, -12.4, 7, -12, 7.5, -1.7, 20, -1.1, -13.7, 4.7];

sum=0; for i=0:n $sum = sum + nchoosek(n,i) * t^i * (1-t)^{(n-i)} * P(1,i+1)$;

end

$v_1 = sum$;

sum=0; for i=0:n $sum = sum + nchoosek(n,i) * t^i * (1-t)^{(n-i)} * P(2,i+1)$; end

$v_2 = sum$;

$value = [v_1, v_2]$;

Use the function 'fminsearch' to find the minimums of $fnS(x)$, the zero mini-

mums and parameters where the zeros occur are what we look for.

function [value] = fnS(x)

$value = norm(C2d(x(1)) - C2d(x(2)), 2);$

function [value] = Smin(s0,t0)

Max=optimset('MaxFunEvals',1e+19);

comb=@(x)fnS(x);

u=[s0,t0];

$[xval, fval] = fminsearch(comb, u, Max)$

A.2 Code: Determining the Crossings

Below is the function of the Bézier curve in 3D.

function [value] = C(t)

n=10;

P=zeros(3,11);

P(1,:)= [-5.9, 10.3, -2.6, -10, 1.9, 11.2, -15.3, -11.7, 17.9, 2.9, -5.9];

P(2,:)= [4.7, -1.1, -12.4, 7, -12, 7.5, -1.7, 20, -1.1, -13.7, 4.7];

P(3,:)= [-6.2, 8.9, -6.3, -0.3, -0.6, -7.6, -4.1, 3.5, 2.9, 4.8, -6.2];

sum=0; for i=0:n $sum = sum + nchoosek(n, i) * t^i * (1 - t)^{(n-i)} * P(1, i + 1);$

end

$v_1 = sum$;

sum=0; for i=0:n $sum = sum + nchoosek(n, i) * t^i * (1 - t)^{(n-i)} * P(2, i + 1)$; end

$v_2 = sum$;

sum=0; for i=0:n $sum = sum + nchoosek(n, i) * t^i * (1 - t)^{(n-i)} * P(3, i + 1)$; end

$v_3 = sum$;

$value = [v_1, v_2, v_3]$;

A.3 Data: Searching the Self-intersections

The initial input $(0.03, 0.55)$ is figured out by the observation and calculations on self-intersections in Figure 5.2.2. Similarly for the others below.

Smin(0.03,0.55)

xval = 0.0306 0.5573

fval = 2.9567e-04

Smin(0.15,0.92)

xval = 0.1573 0.9244

fval = 1.5848e-04

Smin(0.37,0.95)

xval = 0.3731 0.9493

fval = 1.4637e-04

Appendix B

Code and Data for the Counterexamples

Note: The use of adding 1 to the vectors a, b and c is required by MATLAB.

B.1 Code: Equation of Determining Self-intersections

function [value] = S(u,a,b,c)

sum=0; subsum1=0; subsum2=0;

for i=0:n-1

for j=0:n-1-i

for k=0:i $subsum2 = subsum2 + nchoosek(i,k) * (1-u(2))^{(i-k)} * u(2)^k * a(j+k+1)$;

end

$subsum1 = subsum1 + subsum2 * nchoosek(n-1-i,j) * u(1)^{(n-1-i-j)} * (1-u(1))^j$;

end

$sum = sum + subsum1$; end

$v_1 = (1/n) * sum$;

sum=0; subsum1=0; subsum2=0;

for i=0:n-1

for j=0:n-1-i

for k=0: i

$subsum2 = subsum2 + nchoosek(i,k) * (1-u(2))^{(i-k)} * u(2)^k * b(j+k+1)$; end

$subsum1 = subsum1 + subsum2 * nchoosek(n-1-i,j) * u(1)^{(n-1-i-j)} * (1-u(1))^j$;

end

$sum = sum + subsum1$; end

$v_2 = (1/n) * sum$;

sum=0; subsum1=0; subsum2=0;

for i=0:n-1

for j=0:n-1-i

for k=0:i $subsum2 = subsum2 + nchoosek(i,k) * (1-u(2))^{(i-k)} * u(2)^k * c(j+k+1)$;

end

$subsum1 = subsum1 + subsum2 * nchoosek(n-1-i,j) * u(1)^{(n-1-i-j)} * (1-u(1))^j$;

end

$sum = sum + subsum1$; end

$v_3 = (1/n) * sum$;

$value = [v_1, v_2, v_3]$;

B.2 Code: Functions

function [value] = SF(x,n)

q=zeros(3,n); p=zeros(3,n+1);

a=zeros(1,n);b=zeros(1,n);c=zeros(1,n);

$alpha = zeros(1, 2 * n - 2);$

for $i = 1 : 2 * n - 2$

alpha(i)=x(i);

end

for i=1:n-1

$a(i) = sin(alpha(i)) * cos(alpha(n - 1 + i));$

$b(i) = sin(alpha(i)) * sin(alpha(n - 1 + i));$

$c(i) = cos(alpha(i));$

q(:,i)=[a(i),b(i),c(i)];

end

a(n)=0; b(n)=0; c(n)=0;

for i=1:n-1

a(n)=a(n)-a(i); b(n)=b(n)-b(i); c(n)=c(n)-c(i);

q(:,n)=[a(n),b(n),c(n)];

end

u=zeros(1,2); $u = [x(2 * n - 1), x(2 * n)];$

value=abs(F(alpha,n))+norm(S(u,a,b,c),2);

for i=1:n

for j=1:i;

p(:,i+1)=p(:,i+1)+q(:,j);

end

end

p

function [value]=F(alpha,n)

for i=1:n-1

$a(i) = sin(alpha(i)) * cos(alpha(n-1+i)); b(i) = sin(alpha(i)) * sin(alpha(n-1+i)); c(i) = cos(alpha(i));$

end

a(n)=0; b(n)=0; c(n)=0;

for i=1:n-1

a(n)=a(n)-a(i); b(n)=b(n)-b(i); c(n)=c(n)-c(i);

end

$value = abs(a(n)^2 + b(n)^2 + c(n)^2 - 1);$

B.3 Code: Finding the Roots

function [value] = SFminimizer(n,K)

Max=optimset(MaxFunEvals,1e+9);

comb=@(x)SF(x,n);

xval=zeros(2*n,K);

fval=zeros(1,K);

for i=1:K

phi=unifrnd(0,pi,1,n-1); theta=unifrnd(0,2*pi,1,n-1);

s0=unifrnd(0,1); t0=unifrnd(0,1-s0);

x0=[phi,theta,s0,t0];

$[xval(:,i), fval(i)] = fminsearch(comb, x0, Max);$

%make sure $s+t = xval(2*n-1,i) + xval(2*n,i) < 1$ so that $s,t \in D$.

$if\ xval(2*n-1,i) + xval(2*n,i) > 1\ or\ xval(2*n-1,i) + xval(2*n,i) = 1$

fval(i)=1;

else

end

end

%Display the minimums and corresponding s,t and q.

xval fval

%Returns the optimal one.

$[C,I] = min(fval);$

value=[C,I];

B.4 Data: Generating the Counterexamples

The counterexample (Section 5.3.3) uses the second column below for the input parameters.

SFminimizer(6,10)

xval =

Columns 1 through 10

2.1907 0.0867 1.0279 2.4529 0.8294 1.3029 1.0958 0.8502 1.2136 0.3308

2.1572 0.4353 1.9303 0.3841 -0.2788 0.3006 -0.2769 2.8797 3.0782 3.1699

0.0079 3.2225 3.2107 1.8739 3.1482 3.6489 1.3900 0.5959 0.1228 1.8107

0.5496 2.6633 0.2000 1.1955 0.5784 2.0316 1.6273 2.0583 3.1341 1.3276

1.8511 2.9336 1.0424 2.6615 2.3439 1.2207 2.4580 4.3850 0.1877 -0.1146

5.2200 1.2107 7.0598 3.4826 0.3696 0.5633 5.1432 4.2546 3.5523 5.5103

2.7090 4.1128 4.1941 2.3445 2.4291 2.0589 0.4295 2.9467 1.0576 5.9281

0.1954 2.0119 2.2644 7.0575 2.1168 2.3027 1.9744 -0.2264 2.5206 2.4902

0.5312 7.4240 2.2923 5.1205 1.2132 4.0211 3.4493 1.6729 1.7930 5.7145

1.3429 0.8465 1.4447 4.4661 4.0120 1.8860 0.0947 3.9222 5.1409 1.2114

0.5200 0.2969 0.7942 0.7334 0.2149 0.6042 1.3269 0.9360 0.1185 0.0320

0.0054 0.0633 0.2813 0.2543 0.6229 0.4588 0.0165 0.1667 0.5815 0.5970

fval =

Columns 1 through 7

0.0000 0.0000 1.0000 0.2180 0.0001 1.0000 1.0000

Columns 8 through 10

1.0000 0.0001 0.0000

% The corresponding function values of S and F are given:

Svalue = $1.0e-03*$

-0.3861 -0.0970 0.1462

Fvalue =$2.2329e-05$

Bibliography

[1] J. W. Milnor, *On the total curvature of knots*, Annals of Mathematics, Vol. 52: 248-257, 1950

[2] C. Livingston, *Knot Theory*, The Mathematical Association of America, Vol. 24, 1993

[3] M. A. Armstrong, *Basic Topology*, Springer, 1983

[4] M. P. do Carmo, *Differential Geometry of Curves and Surfaces*, Prentice Hall, 1976

[5] C. Apliprantis and O. Burkinshaw, *Problems in Real Analysis*, Academic Press, 1998

[6] G. Morin and R. Goldman, *On the smooth convergence of subdivision and degree elevation for Bézier Curves*, CAGD,Vol. 18: 657-666, 2001

[7] E. L. F. Moore, T. J. Peters and J. A. Roulier, *Preserving computational topology by subdivision of quadratic and cubic Bézier curves*, Computing, Vol. 79(2-4), 317-323, 2007

[8] T. Maekawa, N. M. Patrikalakis, T. Sakkalis and G. Yu, *Analysis and applications of pipe surfaces*, CAGD, Vol. 15(5): 437-458, 1998

[9] M. Stone and T. D. DeRose, *A geometric characterization of parametric cubic curves*, ACM Transactions on Graphics, Vol. 8(3): 147-163, 1989

[10] R. Ait-Haddou and W. Herzog, *Convex subdivision of a Bézier curve*, CAGD, Vol. 19: 663-671, 2002

[11] G. Farin, *Curves and Surfaces for Computer Aided Geometric Design*, Academic Press, 1990

[12] E. Cohen, T. Lyche and R. F. Riesenfeld, *Discrete B-splines and subdivision techniques in computer-aided geometric design*, Computer Graphics Image Process, Vol. 14: 87-111, 1980

[13] M. Neagu, E. Calcoen and B. Lacolle, *Bézier curves: topological convergence of the control polygon*, 6th Int. Conf. on Mathematical Methods for Curves and Surfaces, Vanderbilt, 347-354, 2000

[14] M. Stojanovic, *Algorithms for triangulating polyhedra into a small number of tetrahedra*, Matematicki Vesnik, Vol. 57: 1-9, 2005

[15] L. -E. Andersson, S. M. Dorney, T. J. Peters and N. F. Stewart, *Polyhedral perturbations that preserve topological form*, CAGD, Vol. 12(8): 785-799, 2000

[16] J. W. Alexander and G. B. Briggs, *On types of knotted curves*, Annals of Mathematics, Vol. 28: 562-586, 1926-1927

[17] J. M. Lane and R. F. Riesenfeld, *A theoretical development for the computer generation and display of piecewise polynomial surfaces*, IEEE, Vol. PAMI-2 NO.1, January 1980

[18] J. Peters and X. Wu, *On the optimality of piecewise linear max-norm enclosures based on SLEFES*, International Conference on Curves and Surfaces, Saint-Malo, France, 2002

[19] N. Amenta, T. J. Peters and A. C. Russell, *Computational topology: ambient isotopic approximation of 2-manifolds*, Theoretical Computer Science, Vol. 305: 3-15, 2003

[20] J. Munkres, *Topology* (2nd Ed.), Prentice Hall, 1999

[21] D. Nairn, J. Peters and D. Lutterkort, *Sharp, quantitative bounds on the distance between a polynomial piece and its Bézier control polygon*, CAGD, Vol. 16: 613-631, 1999

[22] L. -E. Andersson, T. J. Peters and N. F. Stewart, *Selfintersection of composite curves and surfaces*, CAGD, Vol. 15: 507-527, 1998

[23] J. Bisceglio, T. J. Peters, J. A. Roulier and C. H. Sequin, *Unknots with highly knotted control polygons*, CAGD, Vol. 28(3): 212-214, 2011

[24] L. Piegl and W. Tiller, *The NURBS Book* (2nd Ed.), Springer, 1997

[25] R. H. Bing, *The Geometric Topology of 3-Manifolds*, American Mathematical Society, 1983

[26] J. Hass, J. C. Lagarias and N. Pippenger, *The computational complexity of knot and link problems*, Journal of the ACM, Vol. 46(2): 185-221, 1999

[27] M. Reid and B. Szendroi, *Geometry and Topology*, Cambridge University Press, 2005

[28] H. Edelsbrunner and E. P. Mücke, *Simulation of simplicity: a technique to cope with degenerate cases in geometric algorithms*, ACM Transactions on Graphics, Vol. 9(1), January 1990

[29] R. Scharein, *The KnotPlot Site*, `http://www.knotplot.com/`

[30] T. J. Peters and D. Marsh, *Personal Home Page of T. J. Peters*, `www.cse.uconn.edu/`

[31] C. H. Sequin, *Spline knots and their control polygons with differing knottedness*, `www.eecs.berkeley.edu/Pubs/TechRpts/2009`

[32] S. Willard, *General Topology*, Addison-Wesley, 1970

[33] G. Monge, *Application de l'Analys à la Geometrie*, Bachelier, 1850

[34] T. A. Grandine, *Applications of contouring*, SIAM Review, Vol. 42(2): 297-316, June 2000

[35] D. L. Blackmore and T. J. Peters, *Computational topology*, invited chapter in the monograph, in Open Problems in Topology II, Editor: E. Pearl, pp. 491 - 546, Elsevier, 2006

[36] K.E. Jordan, L. E. Miller, E.L.F. Moore, T.J. Peters, and A. Russell, *Modeling time and topology for animation and visualization with examples on parametric geometry*, Theoretical Computer Science 405, pp. 4149, 2008

[37] K. E. Jordan, L. E. Miller, T. J. Peters and A. C. Russell, *Geometric topology and visualizing 1-manifolds*, in Topology-based Methods in Visualization, Editors: V. Pascucci and X. Tricoche and H. Hagen and J. Tierny, New York, Springer, 1 – 12, 2011

[38] K. E. Jordan, R. M. Kirby, C. Silva and T. J. Peters, *Through a new looking glass*: mathematically precise visualization*, SIAM News, Vol. 43(5), pp. 1-3, 2010

[39] C. C. Adams, *The Knot Book: An Elementary Introduction to the Mathematical Theory Of Knots*, American Mathematical Society, 2004

[40] J. Li, T. J. Peters, D. Marsh and K. E. Jordan, *Computational topology counterexamples with 3D visualization of Bézier curves*, Applied General Topology, 2012

[41] L. E. Miller (2009), *Discrepancy and isotopy for manifold approximations*, Ph. D. Thesis, University of Connecticut, U.S.

[42] W. Rudin, *Principles of Mathematical Analysis (3rd. ed.)*, McGraw-Hill, 1976

[43] T. Maekawa, *An overview of offset curves and surfaces*, Computer-Aided Design, Vol. 31: 165173, 1999

[44] B. Pham, *Offset curves and surfaces: a brief survey*, Computer-Aided Design, Vol. 24(4): 223229, 1992

[45] J. M. Sullivan, *Curves of finite total curvature*, in Discrete Differential Geometry, Editors: A. I. Bobenko and J. M. Sullivan and P. Schröder and G. M. Ziegler, pages 137-161. Birkhäuser Basel, 2008

[46] E. Denne and J. M. Sullivan, *Convergence and isotopy type for graphs of finite total curvature*, in Discrete Differential Geometry, Editors: A. I. Bobenko and J. M. Sullivan and P. Schröder and G. M. Ziegler, pages 163-174. Birkhäuser Basel, 2008

[47] R. Gulliver and S. Yamada, *Total curvature of graphs after Milnor and Euler*, Pacific Journal of Mathematics, Vol. 256(2): 317-357, 2012

[48] S. Plantinga and G. Vegter, *Isotopic approximation of implicit curves and surfaces*, Proceedings of the 2004 Eurographics/ACM SIGGRAPH symposium on Geometry processing. ACM, 2004

[49] S. Plantinga and G. Vegter, *Isotopic meshing of implicit surfaces*, The Visual Computer 23.1: 45-58, 2007

[50] L. Lin and C. Yap, *Adaptive isotopic approximation of nonsingular curves: the parameterizability and nonlocal isotopy approach*, Discrete & Computational Geometry 45.4: 760-795, 2011

[51] L. Lin, C. Yap, J. Yu, *Non-local isotopic approximation of nonsingular surfaces*, Computer-Aided Design, 2012

[52] W. M. Hirsch, *Differential Topology*, New York, Springer, 1976

[53] J. Li and T. J. Peters, *Isotopic convergence theorem*, Journal of Knot Theory and Its Ramifications, Vol. 22(3), 2013

[54] J. Li, T. J. Peters, and K. E. Jordan, *Knot visualization experiments for verifiable molecular movies*, In preparation.